POLYMER-PEPTIDE HYBRID ASSEMBLIES: SELF-ASSEMBLY AND COMBINATIVE ASSEMBLY WITH DNA

by

JENNIFER AYERS HALEY

(Under the Direction of Yan Geng)

ABSTRACT

Polymer-Peptide hybrids are a novel class of macromolecules that combine sophisticated functionality of biopolymers with synthetic versatility of synthetic polymers. Initially developed by biochemist for bio-medical applications, polymer-peptide hybrids have recently garnered a lot of attention by material scientists for a diverse range of applications including nanotechnology, photonics as well as traditional bio-medical applications.

In this work, polymer-peptide hybrids were synthesized utilizing a modular grafting procedure in which Cysteine-containing peptides are "clicked" on the hydrophobic segment of the amphiphilic polymer polybutadiene-*block*-poly(ethylene oxide) (PBD-*b*-PEO) via free radical addition of the thiol onto the double bonds. These polymer-peptide hybrids were then applied in two areas of research: tuning amphiphilic block copolymer self-assemblies with grafted charged peptides and combinative self-assembly with DNA. Grafting short charged peptides onto PBD-*b*-PEO results in self-assemblies driven by a combination of hydrophobic association, ionic disturbances and H-bonding. Clustering gene-binding peptides, KWK_n, onto (PBD-*b*-PEO) dramatically

changes the DNA condensation pathway. By varying the grafting density and peptide sequence, precise control over the DNA condensation process can be accomplished

INDEX WORDS: Polymer-Peptide Hybrids, Self-assembly, Polyion Complexes, DNA Condensation

POLYMER-PEPTIDE HYBRID ASSEMBLIES: SELF-ASSEMBLY AND COMBINATIVE ASSEMBLY WITH DNA

by

JENNIFER AYERS HALEY

B.S., Georgia Institute of Technology, 2001

A Dissertation Submitted to the Graduate Faculty of The University of Georgia in Partial Fulfillment of the Requirements for the Degree

DOCTOR OF PHILOSOPHY

ATHENS, GEORGIA

2011

POLYMER-PEPTIDE HYBRID ASSEMBLIES: SELF-ASSEMBLY AND COMBINATIVE ASSEMBLY WITH DNA

by

JENNIFER AYERS HALEY

Major Professor: Yan Geng

Committee: Geert-Jan Boons
Vladimir Popik

Electronic Version Approved:

Maureen Grasso
Dean of the Graduate School
The University of Georgia
May 2011

DEDICATION

The following work is dedicated in memory of my grandfather, Virgil Ayers, and my "other dad" Jimmy Smith, I hope I have made you both proud. I also dedicate this work to my husband, Ryan Haley, and my father, Jeff Ayers, both of you have shaped me into the person I am today.

ACKNOWLEDGEMENTS

To my wonderful husband, Ryan Haley, thank you so much for your love and support as we have both endured the journey to obtain my doctorate. I couldn't have done this without you by my side every step of the way, you knew this was possible even when I was not so sure. You inspire me to be the best person I can be everyday and there are no words to fully express my gratitude. To my father, Jeff Ayers, thank you for always expecting more of me and for encouraging me to fulfill my potential in everything I do. I hope I have finally made you happy by going from a Yellow Jacket to a Bulldog! To my parents, Jeff and Tracy Ayers and Terry and Angie Norton, thanks for the love and support through all the years of school and life in general. To my grandmother, Delores Ayers, and my "other mother", Margaret Smith, you are both so very special to me and I love you both. To my sailing family, thanks for the many weekends of fun and stress relief on the water.

I would like to acknowledge the following people for their help in various ways and in no specific order. My advisor, Dr. Yan Geng, you saw something in me that I didn't see myself and pushed me to take the next step, thanks for guiding me through the last few years. My lab mate, Rong Ju, you are the sister I wish I had and have been more helpful to me than you could ever know. My committee members, Dr. Geert-Jan Boons and Dr. Vladimir Popik, thanks for helping me keep things on track and focused on the end goal. Dr. John Shields thank you for ALL the TEM help and general guidance over the past 5 years. Dr. Steven Foulger and Dr. JoAn Hudson from COMSET, Clemson

University, thank you for the TEM studies. Dr. Jeff Urbauer and Ramona Urbauer, thanks for the use of various equipment vital to my research. Dr. Richard Dluhy for FT-IR studies. Dr. Richard Hubbard, Dr. Greg Wylie, Sara Karlson and Sonja Elkund you have all been there for me and have become great friends. To my 6 A.M. gym friends, especially Bob Windham, thanks for all the stress relieving workouts and morning talks.

TABLE OF CONTENTS

Page

LIST OF TABLES

Page

LIST OF FIGURES

Page

CHAPTER 1

INTRODUCTION AND LITERATURE REVIEW

The term polymer is often used in reference to synthetic polymers, however another realm of polymers of biological origin such as DNA and proteins also exist. For decades the two classes of polymers were typically explored in separate fields of research largely due to the difference in fundamental aspects of the macromolecules. Due to billions of years of chemical evolution, in nature the macromolecules of life such as nuclei acids, proteins, peptides and polysaccharides have acquired almost ideal molecular structure. Meanwhile, synthetic manmade polymers are much simpler in design but are chemically much more diverse. Proteins are capable of self-assembling into highly complex hierarchical structures through a variety of noncovalent forces (hydrogen bonding, hydrophobic interactions and electrostatic interactions) involving both intra- and interchain associations. Incorporation of peptides, the basic unit of proteins, into synthetic polymers has given rise to a new class of hybrid macromolecules, polymer-peptide hybrids, with unprecedented properties[1-5]. Initially utilized in biomedical studies[6-9], polymer-peptide hybrids now include a diverse range of applications in nanotechnology, bio-sensors, artificial enzymes, biometrics, light-harvesting systems, photonics, drug and gene delivery and tissue engineering[10-14]. The increased activities in bio-hybrid materials science can be explained largely due to the development of new synthetic methodologies that allow for the construction of well-defined polymer-protein

hybrid materials[15-18]. Techniques from organic and peptide chemistry, polymer chemistry and molecular biology have enriched the material scientist's toolbox.

1.1 Polymer-Peptide Hybrid Self-assembly

The promise of chemical self-assembly in advancing science and technology is well recognized and vigorously pursued.[1] Amphiphilicity defines one of the most fundamental chemical self-assembly principles in constructing discrete mesostructures, *e.g.* micelles and vesicles, that have long found use in nanotechnology and biomedical applications.[2-7] Amphiphiles, ranging from small surfactants, lipids to macromolecules of block copolymers and polypeptides, are typically composed of two distinct parts – a hydrophobic segment covalently connected to a hydrophilic segment, and their spontaneous association is driven by the hydrophobic effect, *i.e.* aggregation of hydrophobic segments to minimize contact with water.[2-7] Despite the tremendous effort in tailoring the shape, size and properties of amphiphile self-assemblies, their geometry is generally limited to highly symmetric spherical structures, *e.g.* spherical micelles and vesicles, as well as cylinders that have uniform diameters. Self-assembly of amphiphilic block copolymers in aqueous solution can readily be predicted based on simple geometric considerations (volume fractions of comonomers), the hydrophilic/hydrophobic ratios, and environmental properties (solvent, ionic strength, etc).

In order to obtain more sophisticated and complex superstructures it becomes necessary to incorporate additional driving forces for self-assembly such as non-covalent interactions, chirality, and secondary structure effects.[15, 19] By combining features of synthetic polymers (solubility, processability, etc.) with those of biological molecules (secondary structure, functionality, biocompatibility, etc.) self-assembled superstructures

with unprecedented properties can be realized. With a vast array of biological molecules available, *i.e.* lipids, nucleic acids, proteins, peptides and carbohydrates, peptides offer the most versatility in structural and functional diversity due to the availability of 20 natural L-α-amino acids and the ease of synthesis via Solid Phase Peptide Synthesis (SPPS).

Early work in the field of polymer-peptides hybrids began with polymer-*block*-polypeptide hybrids, using polystyrene or polybutadiene as the hydrophobic block and polypeptides – poly(L-glutamate)[20, 21] and poly(isocyano-L-alanine)[5] – as the hydrophilic block. Eventhough self-assembly of these hybrids was mainly driven by hydrophobic aggregation of polystyrene or polybutadiene, the polypeptides introduced interesting properties such as helical superstructures from the chirality of poly(isocyano-L-alanine)[5] and pH dependent helix to coil transition of poly(L-glutamate).[20, 21] Inspired by these studies as well as the recent advancements in polymer synthesis[22-26] and bioconjugation strategies,[1, 15] scientists have rapidly expanded the scope of polymer-peptide hybrids in both synthetic diversity or complexity and applications.

The lowest level of complexity is the incorporation of single amino acids in synthetic polymers in which one amino acid moiety is attached per repeat unit of the synthetic polymer resulting in a synthetic polymer backbone with pendent amino acid side chains. By attaching cysteine to each butadiene unit of the block copolymer PEG-*b*-PBD (poly(ethylene oxide)-*b*-poly(1,2-butadiene)) , Geng and coworkers observed a shift in the radius of curvature from micelles to cylinders with a helical pitch.[27] Further extending the peptide to cysteine-phenylalanine (CF) resulted in the formation of micron-sized vesicles.[27] The observed changes in self-assembly morphology was likely due to a

change in the hydrophilic-hydrophobic ratio as well and the presence of hydrogen bonding within the peptide segments and demonstrate that even at the lowest level of complexity in polymer-peptide hybrids, the elementary driving forces responsible for the folding of proteins are intrinsically programmed in single amino acid moieties and subsequently transferred to the polymer-peptide hybrid.

Expanding the complexity of polymer-peptide hybrids by attaching short sequence-defined peptides to synthetic polymers opens up a new avenue for self-assembly in which the peptide segments encode distinct supramolecular organization into unique and programmable suprastructures. Utilizing peptides capable of forming β-sheets, novel nano-fibers/tapes have been constructed using a variety of peptide architectures, *e.g.* linear $(Thr\text{-}Val)_5$,[28, 29] branched or template pre-organized dimethylglycine-$(Thr\text{-}Val)_2$,[30, 31] and cyclic peptides,[32] conjugated to synthetic homopolymers. While these polymer-peptide hybrids use the peptide to guide the self-assembly, charged peptides such as Glu and Lys can be utilized to form self-assemblies based on electrostatic interactions known as polyion complexes[33] and will be discussed in the next section.

Peptides have also been used to impart biological functionality in polymer self-assemblies. Wooley and co-workers developed micelles decorated with the antimicrobial peptide tritrpticin by conjugating the peptide to the block copolymer poly(acrylic acid)-*b*-polystyrene.[34] The resulting tritrpticin derivatized micelles showed increased antimicrobial activity and decreased cytotoxicity compared to the free peptide and demonstrated the power of clustering biologically active peptides onto the surface of micelles.[35] Kiessling and co-workers utilized a similar strategy to develop a polymer-

peptide hybrid that initially self-assembles into nanofibers presenting the peptide on the surface followed by gel formation.[36] This novel material was able to support the adhesion and proliferation of Embryonic Stem cells in an undifferentiated state. [36]

Although polymer-peptide hybrids emerged nearly 40 years ago, this field of study is still fairly young, as the vast majority of the studies have occurred in the past 10. The above mentioned works are meant to illustrate the diversity in polymer-peptide hybrid architecture as well as self-assembly pathways and applications and is by no means a comprehensive review, the field is to broad to cover everything here.

1.2 Polyion Complexes

The self-assembly of amphiphilic block copolymers is mainly driven by solubility differences between the two blocks. Recently, however, the use of electrostatic interactions for self-assembly has gained increasing attention. In fact, combining polymers of opposite charge and equal chain length has resulted in a new class of supramolecular self-assemblies termed polyion complexes (PICs),[33, 37-39] also known as complex coacervate core micelles (C3Ms),[40-42] block ionomer complex micelles[43, 44] and interpolyelectrolyte complexes (IPEC).[45] No matter the name chosen to describe these micelles, they possess characteristic features such as spontaneous and reversible formation and are responsive to external stimuli, such as pH and ionic strength.

Typically the polymers used in the formation of PICs contain weak polyelectrolyte blocks resulting in micelles that only form in a narrow pH range; above or below the critical pH the micelles dissociate due to one of the polymers suffering from too low a charge density.[46, 47] It is well known that with weak polyelectrolytes, the degree of ionization is related to solution pH. Increasing ionic strength in the solution

tends to decrease the driving force for self-assembly due to screening of the electrostatic interactions, often resulting in swelling as the micelles adopt a looser structure with a decrease in aggregation number.[48-53] Above the critical ionic strength micelles dissociate, however, a few examples of decreasing size upon increasing ionic strength as a result of increasing hydrophobic associations have been reported.[54-56] It is important to note that the critical ionic strength of the solution is dependent on many factors such as the type of oppositely charged species, solution pH, mixing fraction, micellar concentration as well as the valency and type of salt added.[50, 51] Mixing fraction (ratio between the number of positively chargeable units and the total number of chargeable units), or charge neutrality/stoichiometry is crucial for self-assembly to occur; thus for weak polyelectrolytes nearly identical chain length of the chargeable segments is required. Kataoka, who pioneered this field of study in 1995, demonstrated the chain-length dependent recognition where self-assembly was observed only when polyanions and polycations of equal chain length were mixed.[33, 38] Kabanov and Stuart quickly followed suit publishing studies using poly(ethylene oxide)-*b*-poly(sodium methacrylate) with poly(N-ethyl-4-vinyl(pyridinium))[43] and poly((dimethylamino) ethyl methacrylate)-*co*-polyglyceryl methacrylate with polyacrylic acid[40] respectively. Since then numerous studies have been reported using a vast array of polycations and polyanions and have been comprehensively reviewed by Stuart.[57] While spherical micelles are the dominant morphologies, vesicles and other morphologies have been reported and typically require additional driving forces or destabilizing forces, such as hydrophobic interactions,[58-61] metal coordination,[62-64] segregative phase separation within the micellar corona,[65, 66] stiff copolymers[67, 68] or non-stoichiometric conditions.[63, 64, 69]

Kataoka's initial PIC studies involved the complexation of poly(ethylene oxide)-*b*-polylysine (PEO-*b*-PLL) with poly(ethylene oxide)-*b*-polyaspartic acid (PEO-*b*-PAsp) resulting in soluble polyion complex micelles whose size is directly proportional to the ionic block length and requires near identical chain length of the ionic blocks.[38, 70] Mixed PICs in which a block copolymer, PEG-*b*-P(Asp), is combined with a simpler homopolymer, PLL, produces micelles with an average radius of ~ 20nm that is essentially independent of ionic block length. Perhaps the most intriguing feature of the mixed PICs is the ability of micelles to form from unmatched chain lengths. Compared to the block copolymer, the homopolymer is not required to align its chain end to the core/corona interface and thus has a higher freedom in the chain arrangement in the core of the PIC micelle allowing for micelle formation with unmatched chain lengths.[70] PIC micelles are not restricted to synthetic polymers, biomacromolecules such as proteins and DNA can be incorporated into the core of PIC micelles for drug and gene delivery applications.[37, 71]

In addition to micelles, vesicles prepared from amphiphilic block copolymers (polymersomes) are capable of encapsulating biologically relevant substances and have attracted a lot of attention. Polymersomes suffer a few major drawbacks; the hydrophobic nature of the membrane limits its permeability to hydrophilic substances and the harsh preparation conditions (use of organic solvents) can potential hinder the encapsulation of fragile biological molecules. The need for vesicles with simple preparation conditions and tuneable membrane permeability inspired the development of vesicles containing a polyion complex (PIC) membrane, PICsomes.[72] Utilizing a similar approach as with the PIC micelles, Kataoka formed micron-sized vesicles by the addition

of salt (150 mM NaCl) to a mixture of poly(ethylene oxide)-*b*-poly(aspartic acid), PEG-*b*-P(Asp), and poly(ethylene oxide)-*b*-poly((5-aminopentyl)aspartimide), PEG-*b*-P(Asp-AP). It is crucial to note that in the absence of salt PIC micelles were the observed morphology. These novel PICsomes displayed many attractive properties such as permeability to macromolecules with molecular weights up to 70,000 and pH dependent stability.[73] Most recently, nano-PICsomes with unilamellar membranes were discovered when the block polymer-peptide hybrid (PEO-*b*-PAsp) was combined with the oppositely charged homopolymer (PAsp-Ap) in low ionic strength buffer (10 mM phosphate buffer, 0 mM NaCl, pH 7.4).[74] It is hypothesized that a reduction in the PEG weight fraction (f_{eo}) from ~ 15 % in the block aniomer/block catiomer to ~ 8 % in the block aniomer/homocatiomer system and lower ionic strength conditions allow for tighter packing for the transition from micelle to vesicle, prior PIC micelles studies were conducted in 10 mM sodium phosphate buffer.[74] The addition of 150 mM NaCl transformed the Nano-PICsomes into the previously observed micron-sized PICsomes.[74]

Polyion complexation has given rise to a versatile class of supramolecular assemblies with tunable properties and versatile applications.

1.3 DNA Condensation

Polyion complexation has also be used to describe *in-vitro* condensation of DNA[71], where multivalent cations interact electrostatically with the negatively charged backbone of DNA resulting in the collapse of DNA into ordered structures (toroids, rods and spheres) of finite size with ordered DNA packing distinguishing condensation from aggregation. *In-vitro* DNA condensation is the first of many steps toward the development of successful gene delivery vectors. This phenomenal biophysical

transformation was initially studied as a model system to reveal the interactions underlying the gene packaging within cell nuclei, viruses and sperm cells, where genomic DNA is compacted on the order of 10^4-10^6 fold into the virus caspid or sperm head.[75-77] However, more recently the focus has shifted toward the packaging of DNA for gene therapies where the size, shape/morphology and stability of the condensates effect transfection efficiency; thus, compacting DNA into discrete particles with control of size and morphology is crucial for the advancement of gene therapy. To be effective in delivering DNA, gene delivery vectors must have low toxicity, exhibit low levels of antigenicity or complement activation, and protect DNA from degradation.[78, 79] Simultaneously addressing each of these has been one of the major impediments to developing highly effective *in-vivo* gene delivery formulations.

Initial DNA condensing agents, simple natural oligo-amines[76, 77] and multivalent cations[80], have evolved into more complex and sophisticated polymeric cations, such as polylysine (PLL), polyethyleneimine (PEI) and their block copolymers[71, 81]. The nature of the condensing agent, DNA properties such as length, persistence length and topology, as well as solution condition (e.g. DNA concentration and ionic strength) have been shown to effect the resulting size and morphology of DNA condensates.[82, 83] Understanding the factors that govern the size and shape of DNA condensates and ultimately controlling the final morphology, is important for the development of successful artificial gene delivery vectors.

In order for DNA condensation to occur, DNA must overcome unfavorable energetic barriers that prevent self-condensation: hydration entropy, mixing entropy, electrostatic energies and bending energy. Binding of condensing agents to DNA, forces

DNA-bound waters of hydration to rearrange and/or release to the bulk solvent thus increasing the hydration entropy of the system. Hydration entropy is an attractive force that favors the collapse of a DNA polymer in the presence of condensing agents.[84, 85] While hydration entropy increases in the system, mixing entropy decreases upon condensation where DNA excludes solvent in favor of interactions with condensing agents resulting in a demixing of DNA and solvent.[76] Thus mixing entropy favors a homogeneous mixture of DNA, condensing agent and solvent and is a repulsive force that opposes DNA condensation.[84] The predominant energetic force opposing condensation is the electrostatic repulsion between the anionic phosphate groups of the nucleotides. In order for DNA condensation to occur, > 89% of DNA's anionic phosphate groups must be neutralized through the addition of cations with a charge of +3 or greater.[77, 86-91] The last energetic barrier to DNA condensation requires the DNA to be bent or distorted to bring two segments of the same chain in close proximity. This bending energy is directly proportional to the persistence length of DNA and is hypothesized to be a determinant in condensate morphology.[75, 84] Electrostatic interactions between positively charged condensing agents and negatively charged DNA should be stronger than the entropic interactions so the entropy loss can be overcome, and requires multivalent ions with a valence ≥ 3 for DNA condensation to occur. When the electrostatic interactions are strong enough to dominate entropic interactions, DNA collapses into a condensed ordered structure, such as a toroid, rod or occasionally a sphere. The energy penalty associated with sharp bends of most stiff polymers oppose the formation of compact globular structures giving rise to predominately toroid and occasionally rod morphologies.[75, 84] It has been proposed that the bending energies associated with rods and toroids are virtually

isoenergetic even though the bending of DNA to form rods involves abrupt kinking in the DNA, whereas there is a continuous bending of the DNA in toroids.[75] Thus, the favored morphology is largely regulated by kinetics and/or the condensation conditions, ***i.e.*** concentration of DNA, salt or condensing agent, pH, and type of condensing agent.

In-vitro DNA condensation was first demonstrated by Shellman and co-worker in 1976, in which they revealed the *in-vitro* condensation of long T7 phage DNA (160kbp) by trivalent spermidine into compact toroids.[77] In the thirty plus years since that ground breaking discovery, many prominent scientist such as Bloomfield, Baldwin have utilized small multivalent cations, ***e.g.*** spermine, spermidine and hexamine cobalts ($Co(NH_3)_6^{3+}$), to extensively studied the physical interactions that govern the *in-vitro* DNA condensation process.[76, 84, 86, 88] Their results consistently showed that ~ 90% of the DNA phosphate charges need to be neutralized by counterions (with a minimum valence of three to be efficient) in order to induce the collapse of the semi-flexible double stranded DNA which was in accordance to Manning's counterion condensation theory.[91] Toroid formation was later discovered to form via a two-step process, spontaneous nucleation loop formation formation followed by subsequent toroidal growth (continuous winding of DNA strands around the loop) by Hud and Balhorn.[90, 92-94] The thermodynamic and kinetic factors that govern the size and dimension of DNA toroids was also investigated.[95, 96] Rod-like condensates were occasionally observered, however simple cations are not very efficient in inducing and stabilizing sharps bend in the DNA double helix and the resulting in metastable rod-like condensates quickly diminish with time.[89, 95]

The knowledge gained from *in-vitro* condensation of DNA by simple cations provided an important foundation for future research. However, DNA condensation by

such simple and small condensing agents fail to reflect the complex DNA-compaction protein interactions found in most bacteria and eukaroytic cells. Furthermore, their DNA condensates are relatively unstable and are not sufficiently protected against nuclease degradation. Immense effort has been put forth in the last decade into the development of novel and more complex DNA condensing agents. This surge in constructing new DNA condensing agents was largely driven by gene delivery application purposes. Cationic lipids can condense DNA either by encapsulation or electrostatic interactions[97] while neutral or negatively-charged crowding agents (such as PEG) at high concentrations can provoke DNA compaction through an excluded volume mechanism.[98] Synthetic peptides[99, 100] and polymers[101-105] have also been explored for DNA condensation and gene delivery purposes. With a vast array of possible condensing agents and gene delivery vectors now available, synthetic peptides and polymers have recently garnered a lot of attention.

The knowledge that active nucleotide-binding sites of viral capsids and histones typically involve 5 to 20 amino acids, particularly lysine and arginine, inspired the use of small synthetic oligopeptides for *in-vitro* DNA condensation and gene delivery studies. Most of the cationic peptides used for DNA condensation are low molecular weight (LMW) oligolysines, usually containing a minimum of five consecutive lysine residues,[106] which are less toxic than their high molecular weight counterparts. For efficient DNA delivery, oligopeptides with ~ 18 lysine residues are required for sufficient stability of the complexes exposed to *in-vivo* serum and salt conditions.[100, 107] Incorporation of a single tryptophan residue into an oligopeptide of 13-18 lysine residues has been shown to enhance gene delivery up to 3 orders of magnitude relative to

comparable tryptophan free polylyines.[100] Aromatic amino acids, *i.e.* tryphtophan, phenylalanine and tyrosine, are capable of stacking interactions or partial intercalation (the intruding side chain unstacks two adjacent base pairs, but does not itself stack over one base pair in lieu of the displaced base pair) and are common in DNA compaction proteins where kinking of the DNA double helix occurs.[108] Although less frequently studied than lysine, arginine has also been utilized for DNA condensation and gene delivery studies. In addition to a positive charge, arginine possesses a quanidinium group capable of forming bifurcated hydrogen bonds, which can potentially stabilize the peptide-nucleic acid complex.[109]

Short peptide sequences have been shown to be functionally efficient, much less antigentic, and offer great flexibility in design in comparison to whole proteins. Oligopeptides can easily be synthesized via solid phase peptide synthesis (SPPS) readily enabling the tuning of the oligopeptide sequence and thus oligopeptide-DNA complexation. Since oligopeptide are relatively small in size, the mechanism and pathway of their DNA condensation are comparable to the well-established natural oligoamines, *i.e.* they are fairly straightforward to understand. However, small peptides alone lack the sophisticated architectural features of the whole protein, and are not able to provide sufficient stability and protection for adequate delivery of DNA. Intraparticle cross-linking to inhibit premature dissociation of condensing peptides has been shown to increase the stability of DNA complexes therefore increasing transfection efficiency.[110]

Attempting to achieve the more complex and sophisticated interactions observed with DNA compaction proteins, positively charged polymers, such as polylysine (PLL) and polyethyleneimine (PEI), have show superb capability in condensing DNA into

stable, compact structures.[111, 112] Additonally, polymers have demonstrated promising *in-vitro* transfection efficiencies and offer a lot of chemical flexibility in further functionalization for targeted delivery and endosomal escape. Depsite these promising features, polymers suffer a few drawbacks of cytotoxicity related to the excessive exposed positive charges of polymer-DNA complexes and difficulty in obtaining complete charge neutralization without precipitation. Furthermore, the kinetics and thermodynamics of the interactions between long positively charged polymers and DNA are rather complex. Thomas has shown that the mechanism of DNA condensation via oligolysine is drastically different than that by polylysine.[113] The polydispersity that is associated with polymers further complicates the complexation process and leads to significant heterogenicity in the complex structure especially for polylysines and PEI whose polymerization techniques tend to generate ill-defined polymer architecture and wide molecular weight distributions.

Among recent progress, Kataoka and Kabanov have pioneered the use of PEG-containing block copolymers, such as PEG-*block*-polylysine, to complex with DNA into spherical polyion complex micelles (PCM).[44, 71, 81, 114, 115] Micelle formation is driven by the electrostatic interactions between polylysine segments and DNA forming the hydrophobic core. Meanwhile, the hydrophilic PEG blocks form the corona surrounding the DNA complex which mask the excess charge of the complex and significantly improves stability, solubility and biocompatibility. *In-vitro* studies demonstrate that with the PEG corona is largely responsible for significantly reduced cytotoxity compared to using polylysine or PEI alone. Although the pioneer polyion complex micelle studies have demonstrated the promise of block copolymers as synthetic gene vectors, the innate

problems of complex kinetics and thermodynamics of interaction with DNA and heterogenicty associated with long polycations still exist. Promising results from polylysine and PEI have led to the development of a vast array of cationic polymers such as poly(N-alkyl-4-vinylpyridinium) salts,[116] poly(2-dimethylaminoethylmethacrylate),[117, 118] and Pluronics (PEO-*b*-poly(propylene oxide)-*b*-PEO)[119] to name a few. Emerick recently polymerized a pentalysine peptide via ROMP producing an amphiphilic grafted copolymer capable of condensing DNA into compact spherical particles with superior transfection efficiency and cell viability compared to linear polylysine, jetPEI, SuperFect and Lipofectamine 2000.[120] Variations in polymer architecture, *i.e.* linear homopolymer and block copolymer, brush-like, grafted and branched or star-like polymers as well as dendrimers (highly branched polymers) have also been explored for DNA condensation and gene delivery purposes.[121]

In recent years, intensive effort has focused on developing synthetic materials for DNA comelexation and delivery. Few studies however, sought to elucidate the role that DNA itself may play in the condensation process in a systematic manner. From scattered studies in literature, it is known that DNA topology and conformation can certainly be recognized in the complexation process. The topology of plasmid DNA (*i.e.* supercoiled, linear or relaxed circular) and persistence length (double stranded or single stranded) have been shown to affect the morphology of DNA condensates.[89, 122, 123] Condensation of all three forms of plasmid DNA with spermine produced torodial condensates for all topologies of the DNA, however, supercoiled DNA has been shown to produce significant populations of rods instead of toroids.[89] Further studies of supercoiled DNA suggest that the topological constraints caused by the winding of the DNA influence the

ability of the DNA to condense into compact structures. Condensation of supercoiled DNA causes an increase in the torsional free energy of the molecule. It has been predicted that the radius of the toroid formed by the supercoiled DNA will therefore be less than that of linear or relaxed circular DNA.[89] The ability of the supercoiled DNA to bend to a smaller radius than linear DNA implies that the topology of the DNA allows for bending to occur with reduced energetic barriers. An increased propensity for bending over smaller lengths of DNA may also explain the increased formation of rods in a preparation of supercoiled DNA condensates.[89]

Probing the effect of DNA persistence length in DNA condensation is most readily accomplished by using single-stranded DNA. Double-stranded (ds) DNA (persistence length 50 nm or 147 basepairs for B-form)[124-126] can best be described as a worm-like chain that is between a rigid rod and freely-jointed chain and thus is considered to be semi-flexible.[124, 127, 128] However, single stranded (ss) DNA (persistence length 1-3 nm or 3-9 basepairs) is modeled as a freely jointed chain, *i.e.* highly flexible.[129] Few studies have investigated the condensation behavior of ss DNA due to the tendency to form ill-defined aggregates.[130, 131] To date, Perales has the only reported the ordered condensation of plasmid length ss DNA using polylysine.[78] The resulting ssDNA condensates were significantly smaller (10-15 nm spheres were observed) than ds DNA counterparts under the same conditions and the key to condensation as opposed to aggregation was the use of ultra-low salt conditions, *i.e.* water.[78] Perales also showed that delivery of ssDNA to HepG-2 cells was not significantly different than supercoiled or linear ds plasmid DNA.[78]

With advances in polymer synthesis and bioconjugation techniques, polymer-peptides hybrids are gaining increased attention and are used in a diverse array of applications as can be seen by the examples presented here. Although the field of polymer-peptide hybrids is still fairly young it has yet to be exhausted.

1.4 References

1. Lutz, J. F.; Börner, H. G., Modern trends in polymer bioconjugates design. *Progress in Polymer Science* **2008,** 33, (1), 1-39.

2. van Hest, J. C. M., Biosynthetic-synthetic polymer conjugates. *Polymer Reviews* **2007,** 47, (1), 63-92.

3. Borner, H. G.; Schlaad, H., Bioinspired functional block copolymers. *Soft Matter* **2007**.

4. Klok, H. A., Biological–synthetic hybrid block copolymers: combining the best from two worlds. *Journal of Polymer Science Part A: Polymer Chemistry* **2005,** 43, (1), 1-17.

5. Cornelissen, J.; Fischer, M.; Sommerdijk, N.; Nolte, R. J. M., Helical superstructures from charged poly (styrene)-poly (isocyanodipeptide) block copolymers. *Science* **1998,** 280, (5368), 1427.

6. Duncan, R., The dawning era of polymer therapeutics. *Nature Reviews Drug Discovery* **2003,** 2, (5), 347-360.

7. Langer, R.; Tirrell, D. A., Designing materials for biology and medicine. *Nature* **2004,** 428, (6982), 487-492.

8. Veronese, F. M., Peptide and protein PEGylation:: a review of problems and solutions. *Biomaterials* **2001,** 22, (5), 405-417.

9. Zalipsky, S., Chemistry of polyethylene glycol conjugates with biologically active molecules. *Advanced Drug Delivery Reviews* **1995,** 16, (2-3), 157-182.

10. Zhang, S., Fabrication of novel biomaterials through molecular self-assembly. *Nature biotechnology* **2003,** 21, (10), 1171-1178.

11. Tu, R. S.; Tirrell, M., Bottom-up design of biomimetic assemblies. *Advanced drug delivery reviews* **2004,** 56, (11), 1537-1563.

12. Whitesides, G. M., Nanoscience, nanotechnology, and chemistry. *Small* **2005,** 1, (2), 172-179.

13. Goodsell, D. S., *Bionanotechnology: lessons from nature*. Wiley-Liss: 2004.

14. Niemeyer, C. M.; Mirkin, C. A., *Nanobiotechnology: concepts, applications and perspectives*. Vch Verlagsgesellschaft Mbh: 2004.

15. Löwik, D.; Ayres, L.; Smeenk, J.; Van Hest, J., Synthesis of Bio-Inspired Hybrid PolymersUsing Peptide Synthesis and Protein Engineering. *Peptide Hybrid Polymers* **2006**, 19-52.

16. Nicolas, J.; Mantovani, G.; Haddleton, D. M., Living Radical Polymerization as a Tool for the Synthesis of Polymer Protein/Peptide Bioconjugates. *Macromolecular rapid communications* **2007,** 28, (10), 1083-1111.

17. Ratner, B. D.; Bryant, S. J., Biomaterials: where we have been and where we are going. **2004**.

18. Sakiyama-Elbert, S. E.; Hubbell, J. A., Functional Biomaterials: Design of Novel Biomaterials. *Annual Review of Materials Research* **2001,** 31, (1), 183-201.

19. Cornelissen, J. J. L. M.; Rowan, A. E.; Nolte, R. J. M.; Sommerdijk, N. A. J. M., Chiral architectures from macromolecular building blocks. *Chemical reviews* **2001,** 101, (12), 4039-4070.

20. Kukula, H.; Schlaad, H.; Antonietti, M.; Förster, S., The Formation of Polymer Vesicles or Peptosomes" by Polybutadiene-b lock-poly (l-glutamate) s in Dilute Aqueous Solution. *Journal of the American Chemical Society* **2002,** 124, (8), 1658-1663.

21. Chécot, F.; Brûlet, A.; Oberdisse, J.; Gnanou, Y.; Mondain-Monval, O.; Lecommandoux, S., Structure of polypeptide-based diblock copolymers in solution: Stimuli-responsive vesicles and micelles. *Langmuir* **2005,** 21, (10), 4308-4315.

22. Hawker, C. J.; Bosman, A. W.; Harth, E., New polymer synthesis by nitroxide mediated living radical polymerizations. *Chemical Reviews* **2001,** 101, (12), 3661-3688.

23. Wang, J. S.; Matyjaszewski, K., Controlled/" living" radical polymerization. Atom transfer radical polymerization in the presence of transition-metal complexes. *Journal of the American Chemical Society* **1995,** 117, (20), 5614-5615.

24. Matyjaszewski, K.; Xia, J., Atom transfer radical polymerization. *Chemical Reviews* **2001,** 101, (9), 2921-2990.

25. Chiefari, J.; Chong, Y. K.; Ercole, F.; Krstina, J.; Jeffery, J.; Le, T. P. T.; Mayadunne, R. T. A.; Meijs, G. F.; Moad, C. L.; Moad, G., Living free-radical

polymerization by reversible addition-fragmentation chain transfer: the RAFT process. *Macromolecules* **1998,** 31, (16), 5559-5562.

26. Moad, G.; Rizzardo, E.; Thang, S. H., Living radical polymerization by the RAFT process. *Australian journal of chemistry* **2005,** 58, (6), 379-410.

27. Geng, Y.; Discher, D. E.; Justynska, J.; Schlaad, H., Grafting Short Peptides onto Polybutadiene block poly (ethylene oxide): A Platform for Self Assembling Hybrid Amphiphiles. *Angewandte Chemie* **2006,** 118, (45), 7740-7743.

28. Hentschel, J.; Krause, E.; Börner, H. G., Switch-peptides to trigger the peptide guided assembly of poly (ethylene oxide)-peptide conjugates into tape structures. *Journal of the American Chemical Society* **2006,** 128, (24), 7722-7723.

29. Hentschel, J.; Ten Cate, M. G. J.; Börner, H. G., Peptide-guided organization of peptide-polymer conjugates: Expanding the approach from oligo-to polymers. *Macromolecules* **2007,** 40, (26), 9224-9232.

30. Eckhardt, D.; Groenewolt, M.; Krause, E.; Börner, H. G., Rational design of oligopeptide organizers for the formation of poly (ethylene oxide) nanofibers. *Chemical Communications* **2005,** 2005, (22), 2814-2816.

31. Börner, H. G.; Smarsly, B. M.; Hentschel, J.; Rank, A.; Schubert, R.; Geng, Y.; Discher, D. E.; Hellweg, T.; Brandt, A., Organization of self-assembled peptide-polymer nanofibers in solution. *Macromolecules* **2008,** 41, (4), 1430-1437.

32. Ten Cate, M. G. J.; Severin, N.; Börner, H. G., Self-assembling peptide-polymer conjugates comprising (D-alt-L)-cyclopeptides as aggregator domains. *Macromolecules* **2006,** 39, (23), 7831-7838.

33. Harada, A.; Kataoka, K., Formation of polyion complex micelles in an aqueous milieu from a pair of oppositely-charged block copolymers with poly (ethylene glycol) segments. *Macromolecules* **1995,** 28, (15), 5294-5299.

34. Becker, M. L.; Liu, J.; Wooley, K. L., Peptide-polymer bioconjugates: hybrid block copolymers generated via living radical polymerizations from resin-supported peptides. *Chemical communications (Cambridge, England)* **2003**, (2), 180.

35. Becker, M. L.; Liu, J.; Wooley, K. L., Functionalized micellar assemblies prepared via block copolymers synthesized by living free radical polymerization upon peptide-loaded resins. *Biomacromolecules* **2005,** 6, (1), 220-228.

36. Derda, R.; Li, L.; Orner, B. P.; Lewis, R. L.; Thomson, J. A.; Kiessling, L. L., Defined substrates for human embryonic stem cell growth identified from surface arrays. *ACS Chemical Biology* **2007,** 2, (5), 347-355.

37. Harada, A.; Kataoka, K., Novel polyion complex micelles entrapping enzyme molecules in the core: preparation of narrowly-distributed micelles from lysozyme and poly (ethylene glycol)-poly (aspartic acid) block copolymer in aqueous medium. *Macromolecules* **1998,** 31, (2), 288-294.

38. Harada, A.; Kataoka, K., Chain length recognition: core-shell supramolecular assembly from oppositely charged block copolymers. *Science* **1999,** 283, (5398), 65.

39. Harada, A.; Kataoka, K., On-off control of enzymatic activity synchronizing with reversible formation of supramolecular assembly from enzyme and charged block copolymers. *Journal of the American Chemical Society* **1999,** 121, (39), 9241-9242.

40. Stuart, M. A. C.; Besseling, N. A. M.; Fokkink, R. G., Formation of micelles with complex coacervate cores. *Langmuir* **1998,** 14, (24), 6846-6849.

41. Burgh, S.; de Keizer, A.; Stuart, M. A. C., Complex coacervation core micelles. Colloidal stability and aggregation mechanism. *Langmuir* **2004,** 20, (4), 1073-1084.

42. Burgh, S.; Fokkink, R.; Keizer, A.; Stuart, M. A. C., Complex coacervation core micelles as anti-fouling agents on silica and polystyrene surfaces. *Colloids and Surfaces A: Physicochemical and Engineering Aspects* **2004,** 242, (1-3), 167-174.

43. Kabanov, A. V.; Bronich, T. K.; Kabanov, V. A.; Yu, K.; Eisenberg, A., Soluble stoichiometric complexes from poly (N-ethyl-4-vinylpyridinium) cations and poly (ethylene oxide)-block-polymethacrylate anions. *Macromolecules* **1996,** 29, (21), 6797-6802.

44. Kabanov, A. V.; Kabanov, V. A., Interpolyelectrolyte and block ionomer complexes for gene delivery: physico-chemical aspects. *Advanced drug delivery reviews* **1998,** 30, (1-3), 49-60.

45. Gohy, J. F.; Varshney, S. K.; Jérôme, R., Water-Soluble Complexes Formed by Poly (2-vinylpyridinium)-b lock-poly (ethylene oxide) and Poly (sodium methacrylate)-b lock-poly (ethylene oxide) Copolymers. *Macromolecules* **2001,** 34, (10), 3361-3366.

46. Serefoglou, E.; Oberdisse, J.; Staikos, G., Characterization of the soluble nanoparticles formed through coulombic interaction of bovine serum albumin with anionic graft copolymers at low pH. *Biomacromolecules* **2007,** 8, (4), 1195-1199.

47. Weaver, J. V. M.; Armes, S. P.; Liu, S., A Holy Trinity" of Micellar Aggregates in Aqueous Solution at Ambient Temperature: Unprecedented Self-Assembly Behavior from a Binary Mixture of a Neutral-Cationic Diblock Copolymer and an Anionic Polyelectrolyte. *Macromolecules* **2003,** 36, (26), 9994-9998.

48. Park, J. S.; Akiyama, Y.; Yamasaki, Y.; Kataoka, K., Preparation and characterization of polyion complex micelles with a novel thermosensitive poly (2-

isopropyl-2-oxazoline) shell via the complexation of oppositely charged block ionomers. *Langmuir* **2007,** 23, (1), 138-146.

49. Yuan, X.; Yamasaki, Y.; Harada, A.; Kataoka, K., Characterization of stable lysozyme-entrapped polyion complex (PIC) micelles with crosslinked core by glutaraldehyde. *Polymer* **2005,** 46, (18), 7749-7758.

50. Solomatin, S. V.; Bronich, T. K.; Bargar, T. W.; Eisenberg, A.; Kabanov, V. A.; Kabanov, A. V., Environmentally responsive nanoparticles from block ionomer complexes: effects of pH and ionic strength. *Langmuir* **2003,** 19, (19), 8069-8076.

51. Solomatin, S. V.; Bronich, T. K.; Eisenberg, A.; Kabanov, V. A.; Kabanov, A. V., Colloidal stability of aqueous dispersions of block ionomer complexes: effects of temperature and salt. *Langmuir* **2004,** 20, (6), 2066-2068.

52. Jaturanpinyo, M.; Harada, A.; Yuan, X.; Kataoka, K., Preparation of bionanoreactor based on core-shell structured polyion complex micelles entrapping trypsin in the core cross-linked with glutaraldehyde. *Bioconjugate chemistry* **2004,** 15, (2), 344-348.

53. Oh, K. T.; Bronich, T. K.; Bromberg, L.; Hatton, T. A.; Kabanov, A. V., Block ionomer complexes as prospective nanocontainers for drug delivery. *Journal of controlled release* **2006,** 115, (1), 9-17.

54. Voets, I. K.; de Keizer, A.; Stuart, M. A. C.; Justynska, J.; Schlaad, H., Irreversible structural transitions in mixed micelles of oppositely charged diblock copolymers in aqueous solution. *Macromolecules* **2007,** 40, (6), 2158-2164.

55. Ma, R.; Wang, B.; Liu, X.; An, Y.; Li, Y.; He, Z.; Shi, L., Pyranine-induced micellization of poly (ethylene glycol)-block-poly (4-vinylpyridine) and pH-triggered release of pyranine from the complex micelles. *Langmuir* **2007,** 23, (14), 7498-7504.

56. Annaka, M.; Morishita, K.; Okabe, S., Electrostatic self-assembly of neutral and polyelectrolyte block copolymers and oppositely charged surfactant. *The Journal of Physical Chemistry B* **2007,** 111, (40), 11700-11707.

57. Voets, I. K.; de Keizer, A.; Cohen Stuart, M. A., Complex coacervate core micelles. *Advances in colloid and interface science* **2009,** 147, 300-318.

58. Bronich, T. K.; Cherry, T.; Vinogradov, S. V.; Eisenberg, A.; Kabanov, V. A.; Kabanov, A. V., Self-Assembly in Mixtures of Poly (ethylene oxide)-g raft-Poly (ethyleneimine) and Alkyl Sulfates. *Langmuir* **1998,** 14, (21), 6101-6106.

59. Kabanov, A. V.; Bronich, T. K.; Kabanov, V. A.; Yu, K.; Eisenberg, A., Spontaneous formation of vesicles from complexes of block ionomers and surfactants. *Journal of the American Chemical Society* **1998,** 120, (38), 9941-9942.

60. Solomatin, S. V.; Bronich, T. K.; Eisenberg, A.; Kabanov, V. A.; Kabanov, A. V., Nanomaterials from ionic block copolymers and single-, double-, and triple-tail surfactants. *Langmuir* **2007,** 23, (5), 2838-2842.

61. Gohy, J. F.; Mores, S.; Varshney, S. K.; Jérôme, R., Self-Organization of Water-Soluble Complexes of a Poly (2-vinylpyridinium)-b lock-poly (ethylene oxide) Diblock with Fluorinated Anionic Surfactants. *Macromolecules* **2003,** 36, (8), 2579-2581.

62. Sanson, N.; Bouyer, F.; Gérardin, C.; In, M., Nanoassemblies formed from hydrophilic block copolymers and multivalent ions. *Phys. Chem. Chem. Phys.* **2004,** 6, (7), 1463-1466.

63. Bouyer, F.; Gérardin, C.; Fajula, F.; Putaux, J. L.; Chopin, T., Role of double-hydrophilic block copolymers in the synthesis of lanthanum-based nanoparticles. *Colloids and Surfaces A: Physicochemical and Engineering Aspects* **2003,** 217, (1-3), 179-184.

64. Bouyer, F.; Sanson, N.; Destarac, M.; Gérardin, C., Hydrophilic block copolymer-directed growth of lanthanum hydroxide nanoparticles. *New J. Chem.* **2006,** 30, (3), 399-408.

65. Voets, I. K.; Fokkink, R.; Hellweg, T.; King, S. M.; de Waard, P.; de Keizer, A.; Stuart, M. A. C., Spontaneous symmetry breaking: formation of Janus micelles. *Soft Matter* **2008,** 5, (5), 999-1005.

66. Voets, I. K.; de Keizer, A.; de Waard, P.; Frederik, P. M.; Bomans, P. H. H.; Schmalz, H.; Walther, A.; King, S. M.; Leermakers, F. A. M.; Cohen Stuart, M. A., Double Faced Micelles from Water Soluble Polymers. *Angewandte Chemie* **2006,** 118, (40), 6825-6828.

67. Müller, M.; Reihs, T.; Ouyang, W., Needlelike and spherical polyelectrolyte complex nanoparticles of poly (L-lysine) and copolymers of maleic acid. *Langmuir* **2005,** 21, (1), 465-469.

68. Bastardo, L. A.; Iruthayaraj, J.; Lundin, M.; Dedinaite, A.; Vareikis, A.; Makuska, R.; van der Wal, A.; Furó, I.; Garamus, V. M.; Claesson, P. M., Soluble complexes in aqueous mixtures of low charge density comb polyelectrolyte and oppositely charged surfactant probed by scattering and NMR. *Journal of colloid and interface science* **2007,** 312, (1), 21-33.

69. Yan, Y.; Besseling, N. A. M.; de Keizer, A.; Drechsler, M.; Fokkink, R.; Stuart, M. A. C., Wormlike aggregates from a supramolecular coordination polymer and a diblock copolymer. *The Journal of Physical Chemistry B* **2007,** 111, (40), 11662-11669.

70. Harada, A.; Kataoka, K., Effect of charged segment length on physicochemical properties of core-shell type polyion complex micelles from block ionomers. *Macromolecules* **2003,** 36, (13), 4995-5001.

71. Kataoka, K.; Togawa, H.; Harada, A.; Yasugi, K.; Matsumoto, T.; Katayose, S., Spontaneous formation of polyion complex micelles with narrow distribution from antisense oligonucleotide and cationic block copolymer in physiological saline. *Macromolecules* **1996,** 29, (26), 8556-8557.

72. Koide, A.; Kishimura, A.; Osada, K.; Jang, W. D.; Yamasaki, Y.; Kataoka, K., Semipermeable polymer vesicle (PICsome) self-assembled in aqueous medium from a pair of oppositely charged block copolymers: Physiologically stable micro-/nanocontainers of water-soluble macromolecules. *Journal of the American Chemical Society* **2006,** 128, (18), 5988-5989.

73. Kishimura, A.; Liamsuwan, S.; Matsuda, H.; Dong, W. F.; Osada, K.; Yamasaki, Y.; Kataoka, K., pH-dependent permeability change and reversible structural transition of PEGylated polyion complex vesicles (PICsomes) in aqueous media. *Soft Matter* **2008,** 5, (3), 529-532.

74. Anraku, Y.; Kishimura, A.; Oba, M.; Yamasaki, Y.; Kataoka, K., Spontaneous Formation of Nanosized Unilamellar Polyion Complex Vesicles with Tunable Size and Properties. *Journal of the American Chemical Society* **2010,** 132, (5), 1631-1636.

75. Bloomfield, V. A., Condensation of DNA by multivalent cations: considerations on mechanism. *Biopolymers* **1991,** 31, (13), 1471-1481.

76. Bloomfield, V. A., DNA condensation. *Current Opinion in Structural Biology* **1996,** 6, (3), 334-341.

77. Gosule, L. C.; Schellman, J. A., Compact form of DNA induced by spermidine. *Nature* **1976,** 259, (5541), 333-335.

78. Molas, M.; Bartrons, R.; Perales, J. C., Single-stranded DNA condensed with poly--lysine results in nanometric particles that are significantly smaller, more stable in physiological ionic strength fluids and afford higher efficiency of gene delivery than their double-stranded counterparts. *Biochimica et Biophysica Acta (BBA)-General Subjects* **2002,** 1572, (1), 37-44.

79. Rolland, A. P., From genes to gene medicines: recent advances in nonviral gene delivery. *Critical reviews in therapeutic drug carrier systems* **1998,** 15, (2), 143.

80. Hud, N. V.; Downing, K. H., Cryoelectron microscopy of lambda phage DNA condensates in vitreous ice: The fine structure of DNA toroids. *Proceedings of the National Academy of Sciences* **2001,** 98, (26), 14925-14930.

81. Kabanov, A. V.; Vinogradov, S. V.; Suzdaltseva, Y. G.; Alakhov, V. Y., Water-Soluble Block Polycations as Carriers for Oligonucleotide Delivery. *Bioconjugate Chemistry* **1995,** 6, (6), 639-643.

82. Arscott, P. G.; Li, A. Z.; Bloomfield, V. A., Condensation of DNA by trivalent cations. 1. Effects of DNA length and topology on the size and shape of condensed particles. *Biopolymers* **1990,** 30, (5-6), 619-30.

83. Plum, G. E.; Arscott, P. G.; Bloomfield, V. A., Condensation of DNA by Trivalent Cations. II, Effects of Cation Structure. *Biopolymers* **1990,** 30, (5-6), 631-643.

84. Bloomfield, V. A., DNA condensation by multivalent cations. *Biopolymers* **1997,** 44, (3), 269-282.

85. Rau, D. C.; Parsegian, V. A., Direct measurement of the intermolecular forces between counterion-condensed DNA double helices. Evidence for long range attractive hydration forces. *Biophysical journal* **1992,** 61, (1), 246-259.

86. Widom, J.; Baldwin, R. L., Cation-induced toroidal condensation of DNA* 1:: Studies with Co3+ (NH3) 6. *Journal of Molecular Biology* **1980,** 144, (4), 431-453.

87. Wilson, R. W.; Bloomfield, V. A., Counterion-induced condensation of deoxyribonucleic acid. A light-scattering study. *Biochemistry* **1979,** 18, (11), 2192-2196.

88. Arscott, P. G.; Ma, C.; Wenner, J. R.; Bloomfield, V. A., DNA condensation by cobalt hexaammine (III) in alcohol–water mixtures: dielectric constant and other solvent effects. *Biopolymers* **1995,** 36, (3), 345-364.

89. Arscott, P. G.; Li, A. Z.; Bloomfield, V. A., Condensation of DNA by trivalent cations. 1. Effects of DNA length and topology on the size and shape of condensed particles. *Biopolymers* **1990,** 30, (5 6), 619-630.

90. Hud, N. V.; Downing, K. H., Cryoelectron microscopy of phage DNA condensates in vitreous ice: the fine structure of DNA toroids. *Proceedings of the National Academy of Sciences of the United States of America* **2001,** 98, (26), 14925.

91. Manning, G. S., The molecular theory of polyelectrolyte solutions with applications to the electrostatic properties of polynucleotides. *Quarterly reviews of biophysics* **1978,** 11, (02), 179-246.

92. Hud, N. V., Double-stranded DNA organization in bacteriophage heads: an alternative toroid-based model. *Biophysical journal* **1995,** 69, (4), 1355-1362.

93. Hud, N. V.; Downing, K. H.; Balhorn, R., A constant radius of curvature model for the organization of DNA in toroidal condensates. *Proceedings of the National Academy of Sciences of the United States of America* **1995,** 92, (8), 3581.

94. Hud, N. V.; Vilfan, I. D., Toroidal DNA condensates: unraveling the fine structure and the role of nucleation in determining size. *Annu. Rev. Biophys. Biomol. Struct.* **2005,** 34, 295-318.

95. Vilfan, I. D.; Conwell, C. C.; Sarkar, T.; Nicholas, V., Time study of DNA condensate morphology: implications regarding the nucleation, growth, and equilibrium populations of toroids and rods. *Biochemistry* **2006,** 45, (26), 8174-8183.

96. Conwell, C. C.; Nicholas, V., Evidence that both kinetic and thermodynamic factors govern DNA toroid dimensions: effects of magnesium (II) on DNA condensation by hexammine cobalt (III). *Biochemistry* **2004,** 43, (18), 5380-5387.

97. Rädler, J. O.; Koltover, I.; Salditt, T.; Safinya, C. R., Structure of DNA-cationic liposome complexes: DNA intercalation in multilamellar membranes in distinct interhelical packing regimes. *Science* **1997,** 275, (5301), 810.

98. Laemmli, U. K., Characterization of DNA condensates induced by poly (ethylene oxide) and polylysine. *Proceedings of the National Academy of Sciences of the United States of America* **1975,** 72, (11), 4288.

99. Smith, L. C.; Duguid, J.; Wadhwa, M. S.; Logan, M. J.; Tung, C. H.; Edwards, V.; Sparrow, J. T., Synthetic peptide-based DNA complexes for nonviral gene delivery. *Advanced drug delivery reviews* **1998,** 30, (1-3), 115-131.

100. Wadhwa, M. S.; Collard, W. T.; Adami, R. C.; McKenzie, D. L.; Rice, K. G., Peptide-mediated gene delivery: influence of peptide structure on gene expression. *Bioconjugate chemistry* **1997,** 8, (1), 81-88.

101. Wagner, E.; Cotten, M.; Foisner, R.; Birnstiel, M. L., Transferrin-polycation-DNA complexes: the effect of polycations on the structure of the complex and DNA delivery to cells. *Proceedings of the National Academy of Sciences of the United States of America* **1991,** 88, (10), 4255.

102. Choi, Y. H.; Liu, F.; Park, J. S.; Kim, S. W., Lactose-poly (ethylene glycol)-grafted poly-L-lysine as hepatoma cell-targeted gene carrier. *Bioconjugate chemistry* **1998,** 9, (6), 708-718.

103. Mislick, K. A.; Baldeschwieler, J. D.; Kayyem, J. F.; Meade, T. J., Transfection of folate-polylysine DNA complexes: evidence for lysosomal delivery. *Bioconjugate chemistry* **1995,** 6, (5), 512-515.

104. Zauner, W.; Ogris, M.; Wagner, E., Polylysine-based transfection systems utilizing receptor-mediated delivery. *Advanced drug delivery reviews* **1998,** 30, (1-3), 97-113.

105. Wong, S. Y.; Pelet, J. M.; Putnam, D., Polymer systems for gene delivery--Past, present, and future. *Progress in Polymer Science* **2007,** 32, (8-9), 799-837.

106. Gottschalk, S.; Sparrow, J. T.; Hauer, J.; Mims, M. P.; Leland, F. E.; Woo, S. L.; Smith, L. C., A novel DNA-peptide complex for efficient gene transfer and expression in mammalian cells. *Gene therapy* **1996,** 3, (5), 448.

107. McKenzie, D. L.; Collard, W. T.; Rice, K. G., Comparative gene transfer efficiency of low molecular weight polylysine DNA condensing peptides. *The Journal of peptide research* **1999,** 54, (4), 311-318.

108. Pörschke, D.; Ronnenberg, J., The reaction of aromatic peptides with double helical DNA. Quantitative characterisation of a two step reaction scheme. *Biophysical Chemistry* **1981,** 13, (4), 283-290.

109. Mascotti, D. P.; Lohman, T. M., Thermodynamics of oligoarginines binding to RNA and DNA. *Biochemistry* **1997,** 36, (23), 7272-7279.

110. Adami, R. C.; Rice, K. G., Metabolic stability of glutaraldehyde cross linked peptide dna condensates. *Journal of pharmaceutical sciences* **1999,** 88, (8), 739-746.

111. Merdan, T.; Kopeek, J.; Kissel, T., Prospects for cationic polymers in gene and oligonucleotide therapy against cancer. *Advanced drug delivery reviews* **2002,** 54, (5), 715-758.

112. Tang, M. X.; Szoka, F. C., The influence of polymer structure on the interactions of cationic polymers with DNA and morphology of the resulting complexes. *Gene Therapy* **1997,** 4, (8), 823.

113. Nayvelt, I.; Thomas, T.; Thomas, T. J., Mechanistic differences in DNA nanoparticle formation in the presence of oligolysines and poly-L-lysine. *Biomacromolecules* **2007,** 8, (2), 477-484.

114. Katayose, S.; Kataoka, K., Water-soluble polyion complex associates of DNA and poly (ethylene glycol)-poly (L-lysine) block copolymer. *Bioconjugate chemistry* **1997,** 8, (5), 702-707.

115. Kakizawa, Y.; Harada, A.; Kataoka, K., Environment-sensitive stabilization of core-shell structured polyion complex micelle by reversible cross-linking of the core through disulfide bond. *Journal of the American Chemical Society* **1999,** 121, (48), 11247-11248.

116. Kabanov, A. V.; Astafieva, I. V.; Maksimova, I. V.; Lukanidin, E. M.; Georgiev, G. P.; Kabanov, V. A., Efficient transformation of mammalian cells using DNA interpolyelectrolyte complexes with carbon chain polycations. *Bioconjugate chemistry* **1993,** 4, (6), 448-454.

117. Haensler, J.; Szoka Jr, F. C., Polyamidoamine cascade polymers mediate efficient transfection of cells in culture. *Bioconjugate chemistry* **1993,** 4, (5), 372-379.

118. Van de Wetering, P.; Cherng, J. Y.; Talsma, H.; Crommelin, D. J. A.; Hennink, W. E., 2-(Dimethylamino) ethyl methacrylate based (co) polymers as gene transfer agents. *Journal of controlled release* **1998,** 53, (1-3), 145-153.

119. Kabanov, A. V.; Lemieux, P.; Vinogradov, S.; Alakhov, V., Pluronic® block copolymers: novel functional molecules for gene therapy. *Advanced drug delivery reviews* **2002,** 54, (2), 223-233.

120. Breitenkamp, R. B.; Emrick, T., Pentalysine-grafted romp polymers for DNA complexation and delivery. *Biomacromolecules* **2008,** 9, (9), 2495-2500.

121. Kabanov, A. V., Taking polycation gene delivery systems from in vitro to in vivo. *Pharmaceutical Science & Technology Today* **1999,** 2, (9), 365-372.

122. Ma, C.; Bloomfield, V. A., Condensation of supercoiled DNA induced by MnCl2. *Biophysical journal* **1994,** 67, (4), 1678-1681.

123. Böttcher, C.; Endisch, C.; Fuhrhop, J. H.; Catterall, C.; Eaton, M., High-yield preparation of oligomeric C-type DNA toroids and their characterization by cryoelectron microscopy. *Journal of the American Chemical Society* **1998,** 120, (1), 12-17.

124. Smith, S. B.; Cui, Y.; Bustamante, C., Overstretching B-DNA: the elastic response of individual double-stranded and single-stranded DNA molecules. *Science* **1996,** 271, (5250), 795.

125. Marenduzzo, D.; Micheletti, C., Thermodynamics of DNA packaging inside a viral capsid: the role of DNA intrinsic thickness. *Journal of molecular biology* **2003,** 330, (3), 485-492.

126. Murphy, M. C.; Rasnik, I.; Cheng, W.; Lohman, T. M.; Ha, T., Probing single-stranded DNA conformational flexibility using fluorescence spectroscopy. *Biophysical journal* **2004,** 86, (4), 2530-2537.

127. Smith, S. B.; Finzi, L.; Bustamante, C., Direct mechanical measurements of the elasticity of single DNA molecules by using magnetic beads. *Science* **1992,** 258, (5085), 1122.

128. Bustamante, C.; Marko, J. F.; Siggia, E. D.; Smith, S., Entropic elasticity of lambda-phage DNA. *Science (New York, NY)* **1994,** 265, (5178), 1599.

129. Zhang, Y.; Zhou, H.; Ou-Yang, Z. C., Stretching single-stranded DNA: interplay of electrostatic, base-pairing, and base-pair stacking interactions. *Biophysical Journal* **2001,** 81, (2), 1133-1143.

130. Sinsheimer, R. L., A single-stranded deoxyribonucleic acid from bacteriophage [phi] X174+. *Journal of Molecular Biology* **1959,** 1, (1), 43-53, IN6.

131. Lin, H. J.; Chargaff, E., On the denaturation of deoxyribonucleic acid. *Biochimica et biophysica acta* **1966,** 123, (1), 66.

CHAPTER 2

A TWIST ON AMPHIPHILICITY YIELDS STICKY SUPRAMOLECULAR CONES

Haley, J.*; Li, X.*; Schlaad, H.; Ju, R. and Geng Y. *Soft Matter*, **2010**, 6, 2037-2043
*Equal contributors

2.1 Abstract

Amphiphilicity defines one of the most fundamental chemical self-assembly principles in constructing mesostructures that have long found use in nanotechnology and biomedical applications. Traditional amphiphiles are composed of two distinct parts – a hydrophobic segment covalently connected to a hydrophilic segment, and the geometry of the amphiphile self-assembly is generally limited to highly symmetric spherical micelles and vesicles, as well as cylinders. In this study, we present a new twist to the basic hydrophobic-hydrophilic two-part amphiphile design by "mandatory" linking a few disturbing ionic peptides along the hydrophobic segment of an amphiphilic block copolymer. We report that such a twist on Amphiphilicity yields unusual supramolecular cones. These cones demonstrate a surprising stickiness property at the base, which fosters spontaneous higher-order self-assembly. The apex angle, length, as well as the stickiness of the cones can all be tuned by chemical manipulations. Moreover, we reveal the delicate balance of forces that governs the unusual sticky supramolecular cone formation.

2.2 Introduction

The promise of chemical self-assembly in advancing science and technology is well recognized and vigorously pursued.[1] Amphiphilicity defines one of the most fundamental chemical self-assembly principles in constructing discrete mesostructures, *e.g.* micelles and vesicles, that have long found use in nanotechnology and biomedical applications.[2-7] Amphiphiles, ranging from small surfactants, lipids to macromolecules of block copolymers and polypeptides, are typically composed of two distinct parts – a hydrophobic segment covalently connected to a hydrophilic segment, and their

spontaneous association is driven by the hydrophobic effect, *i.e.* aggregation of hydrophobic segments to minimize contact with water.[2-7] Despite the tremendous effort in tailoring the shape, size and properties of amphiphile self-assemblies, their geometry is generally limited to highly symmetric spherical structures, *e.g.* spherical micelles and vesicles, as well as cylinders that have uniform diameters, where radii of curvature are largely determined by their formation mechanisms controlling growth or stacking along the long axis.[8-13] Recent findings demonstrate that the structural anisotropicity between the diameter and length has led cylinders to have unusual properties compared to their spherical counterparts, *e.g.* much prolonged circulation in transport and enhanced mechanical strength.[14, 15] Indeed, shape is well known to have a strong influence on nanomaterial properties, and angular structures may have drastically different properties from the spherical counterparts.[16] However, unlike the highly ordered crystallization process, aggregation of hydrophobic segments of amphiphiles into any angular structures would seem rather unusual.

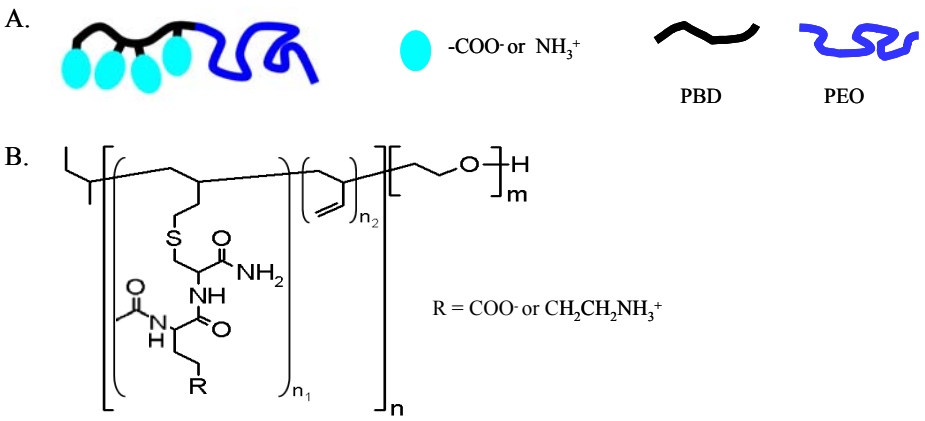

Figure 2.1 Schematic Representation of Polymer-Peptide Hybrid. (A) Schematic representation and (B) the chemical structure of the polymer-peptide hybrid

Another imminent challenge facing amphiphile self-assembly is to advance in the higher hierarchy self-assembly regime.[17, 18] Hierarchy is the hallmark feature used by nature to assemble complex, functional structures, and many technological applications of amphiphile self-assemblies, *e.g.* as templates or scaffolds for nanomaterial synthesis, biomineralization, tissue engineering and lithography,[2-6] require the higher level organization of the primary micelle and vesicle mesostructures. Spontaneous self-assembly of these 'soft' colloids in dilute aqueous solution, however, is rather difficult, as the repulsive solvation force, steric hindrance or electrostatic repulsions would pull them apart into dispersion.[19] The highly symmetric geometry of micelles and vesicles also increases the difficulty in achieving directional and controllable organizations.

Previously, we have controllably tuned amphiphile self-assembly curvature from spherical micelles to cylindrical micelles and vesicles by grafting hydrophobic peptides onto the hydrophobic segment of an amphiphilic block copolymer, where the hydrophobic-hydrophilic two-part nature of the amphiphile has been preserved and the hydrophobic ratio enhanced.[20] Here we present a new twist to the hydrophobic-hydrophilic amphiphile design by "mandatory" linking of a few disturbing ionic peptides along the hydrophobic segment of the amphiphilic block copolymer, Figure 2.1. Ionic groups have high water affinity, and in the past have been generally used as the hydrophiphilic part,[21] or fully neutralized to be included in the hydrophobic part.[22] With highly incompatible ionic groups "mandatory" linked along the hydrophobic segment, such a twist is expected to disturb the overall molecular self-assembly behavior.

2.3 Results and Discussion

In this study, we took a traditional amphiphilic block copolymer – polybutadiene-*block*-poly(ethylene oxide), PBD-*b*-PEO, where PBD is the hydrophobic segment and PEO the hydrophilic segment – and controllably grafted a few ionic amino acids (Glu or Lys), which can dissociate into $–COO^-$ or $–NH_3^+$ ionic side groups respectively, along the hydrophobic PBD segment, Figure 2.1. Thiol-containing cysteine (Cys) was coupled to Glu or Lys as the peptide linker terminus, and the Glu-Cys or Lys-Cys dipeptide was grafted onto the PBD polymer chains *via* a recently developed modular thiol-ene radical addition route.[20] The grafting density, *i.e.* the percentage of the ene double bonds of PBD grafted with the peptides, can be tuned by changing the molar ratio between the reacting thiol groups and the ene double bonds.[20] The grafting route, however, provides no specific control over the grafting location and the peptides are expected to be randomly distributed along the PBD polymer chain. Preliminary studies show that at high grafting densities, where the hydrophobic PBD segment can be completely covered by ionic peptides, the whole polymer-peptide hybrid molecule becomes hydrophilic and simply dissolves in water. Supramolecular self-assembly only proceeds at low grafting densities, where sufficient hydrophobicity has been preserved in the molecule. A low grafting density of 30% was used on two model PBD-*b*-PEO block copolymers – PBD_{14}-*b*-PEO_{93} and PBD_{25}-*b*-PEO_{75} – for this study. The ionization degree of Glu or Lys can be further tuned by adjusting pH or adding salt. Without modification, the PBD_{14}-*b*-PEO_{93} and PBD_{25}-*b*-PEO_{75} amphiphile precursors have the hydrophobic weight fraction $f_{PBD} \sim 0.2$ and 0.3 respectively, and both self-assemble into spherical micelles in aqueous solution,[20] as predicted by their hydrophobic-hydrophilic ratio.[23]

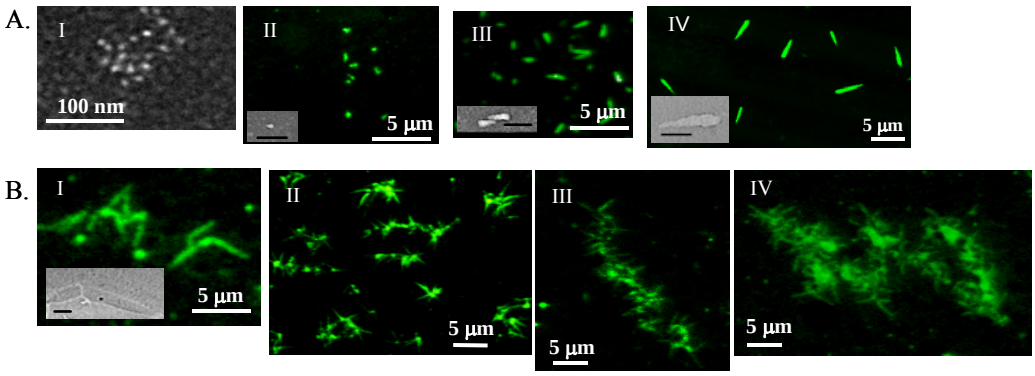

Figure 2.2 Hierarchical self-assembly of Glu grafted PBD_{14}-*b*-PEO_{93} hybrid in water. (A) Supramolecular cone formation and (B) higher-order cone self-assembly. (Scale bars for FM: 5 mm; Inset TEM images: AI, AII 100 nm; AIII, IV and BI 500 nm).

A combination of Fluorescent Microscopy (FM) and Transmission Electron Microscopy was used to study the supramolecular self-assembly behavior in aqueous solution. FM is a reliable visualization technique that can cover a wide range of micron scale structures, whereas TEM compliments FM and reveals nano-scale structural information. Dye labeling in FM is proven to be minimally perturbing to the native supramolecular assembly structures,[24, 25] thus can directly characterize the morphology as well as the dynamics of the structure in solution without sample fixation, providing an equilibrated measurement. TEM, on the other hand, has been widely used on peptide-containing supramolecular self-assembly systems, which are generally stabilized by intermolecular peptide hydrogen bonding for measurement.[5, 6, 10]

Hierarchichical self-assembly of the Glu or Lys grafted to PBD_{14}-*b*-PEO_{93} hybrid is shown in Figure 2.2. Upon dissolution in dilute aqueous solution under neutral pH at 4 ºC, where either Glu or Lys completely ionizes, small namometer conical nuclei that consist of ~ 40 molecules emerged instantaneously, as observed by TEM, Figure 2.2A

(I). The conical nuclei gradually elongated over a week course into microns in length, as consistently observed by both TEM and FM, Figure 2.2A (II –12h, III – 3 days, IV – 7 days). The captured conical nuclei and different conical elongation stages, as well as the notable size-dependent kinetics, all suggest a nucleation-growth self-assembly pathway, rather than an isodesmic route, which would involve an open association process and yield independent association constants regardless of object size.[26, 27] The average apex angle of the supramolecular cones was measured to be around 15º from TEM images, and remained nearly constant throughout the cone growth, whereas the cone base appears to become more ragged and "sticking out" as the cones grow into microns in size. In addition, no significant change in the number of the cones was observed throughout the growth, indicating that the supramolecular cones grow by elongation from the base, *i.e.* depositing of dispersed molecules from the solution onto the cone base. Regardless of the amount of the materials, the supramolecular cones grow into a maximum length of ~ 4 microns, with an estimated aggregation number of ~ 10^5 molecules per cone and further growth appears to be energetically unfavored. The supramolecular cones are highly rigid, exhibiting no thermal fluctuations in solution, probably due to peptide hydrogen bonding within the cone assembly. One should also note that no crystallization is involved in the supramolecular cone formation, as the hybrid molecule is amorphous in nature and Electron Diffraction Analysis further confirmed the non-crystallinity of the cones.

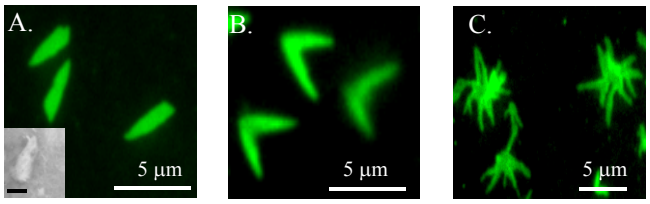

Figure 2.3 Hierarchical self-assembly of the Glu grafted PBD_{25}-*b*-PEO_{75} hybrid in water. Scale bar for inset TEM image: 500 nm

Unlike charged micelles/vesicles, where electrostatic repulsions would prevent further association, such supramolecular cones demonstrate a surprising "stickiness" property at the base and continued to spontaneously self-assemble into higher-hierarchy structures, Figure 2.2B. Initially, dimmers of two cones with their bases adhered to one another started to emerge, as observed by both of FM and TEM, Figure 2.2B (I). More cones joined by the base with time, as directly observed by FM, Figure 2.2B (II). Such large three-dimensional aggregated structures are no longer suitable for TEM studies, but the association of cones at their wider base ends with the tapered apex ends stemming outward is still apparent at the 250 nm resolution of the FM imaging. Spontaneous stringing of cones by the base continued, and long strings of hundreds of cones were eventually formed, Figure 2.2B (III, IV). The final strings of cone assembly are stable in solution (for months) without dissociation.

Cone formation and their spontanteous higher-order self-assembly were also observed for ionic peptide grafted PBD_{25}-*b*-PEO_{75} hybrids in aqueous solution under neutral pH, Figure 2.3. Compared to the PBD_{14}-*b*-PEO_{93} hybrid cones, cones from PBD_{25}-*b*-PEO_{75} hybrid, however, are wider and shorter, with average apex angle of ~ 30º and a maximum length of ~ 3 μm, Figure 2.3A. The wider and shorter PBD_{25}-*b*-PEO_{75}

hybrid cones also appear to have a flatter base. Like PBD_{14}-*b*-PEO_{93} hybrid cones, they continued to spontaneously self-assemble in aqueous solution by sticking their bases together, starting from dimmers to larger clusters, Figure 2.3 B, C. However, instead of elongation into long strings as the PBD_{14}-*b*-PEO_{93} hybrid cones, the wider and shorter PBD_{25}-*b*-PEO_{75} hybrid cones tend to ultimately assemble into more rounded clusters. Such notable differences in the apex angle, length, base stickiness and the higher-order assembly structure between the PBD_{25}-*b*-PEO_{75} and PBD_{14}-*b*-PEO_{93} hybrid cones are likely due the different hydrophobic fraction, f_{PBD}, and the different PBD polymer length of the two amphiphilic block copolymer precursors.

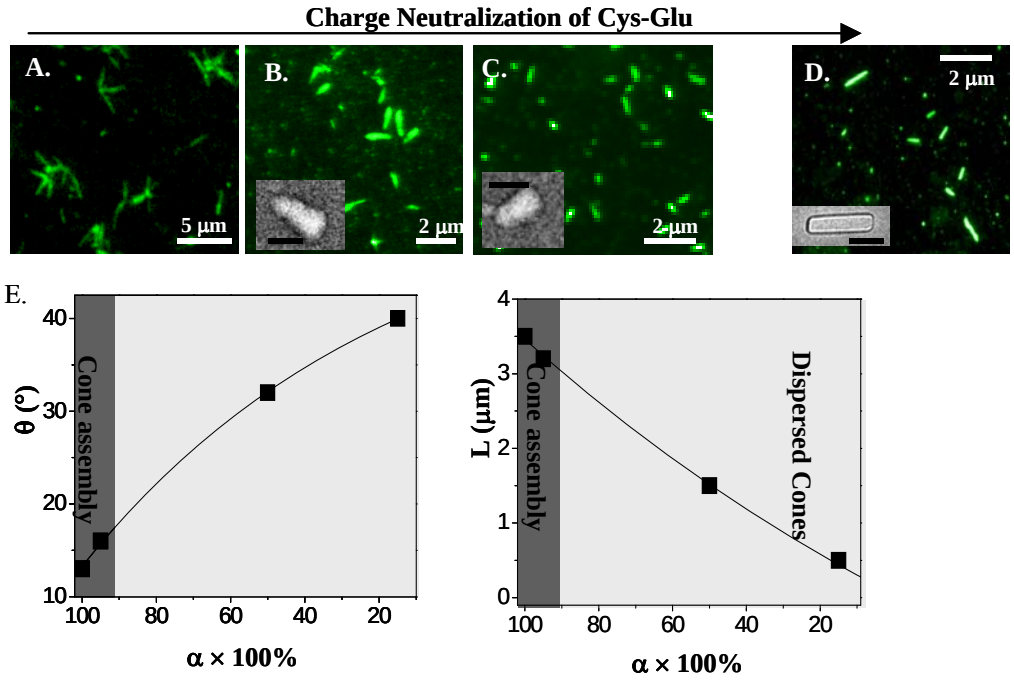

Figure 2.4 Salt and pH Effect on Polymer-Peptide Hybrid Self-assembly. (A-D) Effect of charge neutralization on the polymer-peptide self-assembly behavior; (E) scaling of average cone apex angle (θ) and length (L) with ionization degree α. Scale bars for inset TEM images: 500 nm.

Our preliminary studies show that supramolecular self-assembly only proceeds when sufficient PBD hydrophobicity is preserved, which indicates that the hydrophobic interaction is the driving force for the self-assembly to occur. To elucidate the critical role of the ionic disturbance along the hydrophobic segment in the unusual conical geometry formation, we adjusted the ionization degree of Glu/Lys (α) *via* changing the solution pH or adding salt. Using Glu ($pK_a \sim 4.5$) as an example, the ionization degree α decreases with acidic pH, and the lower the degree of charge led to wider, les punctual and shorter cones, which are also less "sticky" towards further assembly, Figure2.4 (A – pH 6, α 96%; B – pH 4.5, α 50%, C – pH 3.5, α 9%). At pH 6, only small clusters of a few cones were observed, Figure 2.4A, and as the pH gets more acidic, no assembly but dispersed cones were found in solution, Figure 2.4 B, C. Scaling demonstrates that the average cone apex exponentially widens, while the cone length concurrently decays with α, Figure 2.4E. Wider and less sticky cones were also observed for polymer-peptide hybrids with lower grafting density, Figure 2.5. Upon complete charge neutralization of the carboxyl group in Glu, the hybrid molecule no longer assembled into conical geometries but rather traditional cylinders, Figure 2.4D (complete Glu protonation at highly acidic pH 2). Neutral carboxyl or amino groups no longer disturb the hydrophobic PBD backbones, but are rather likely to form hydrogen bonding in the hydrophobic environment. The combination of the enhanced overall hydrophobicity and the stiffening peptide hydrogen bonding may be responsible for shifting the assembly curvature from spheres to cylinders. Such transition from cones to cylinders with charge neutralization, nonetheless, clearly proves that the ionic disturbance along the hydrophobic segment is essential to the formation of the sticky supramolecular cones, and the apex angle, length,

as well as the stickiness of the cones can all be adjusted by the grafting density of the ionic peptides along the PBD backbone and the degree of ionization.

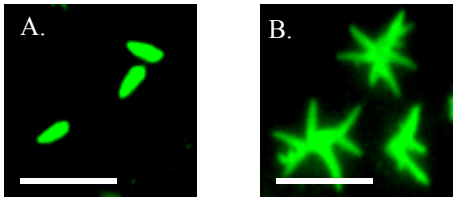

Figure 2.5 Hierarchical self-assembly of 20% Glu-Cys grafted PBD_{14}-*b*-PEO_{93} hybrid in water. (A) Supramolecular cone formation after one week, and (B) higher-order cone assembly at two weeks. Scale bars 5 μm.

Other than hydrophobic interaction and ionic disturbance, the involvement of the peptide hydrogen bonding in the supramolecular cone formation, as indicated by the cone rigidity, is further confirmed by Fourier-Transform Infrared (FT-IR) spectroscopy analysis. A combination of the key Amide I band with the complementary Amide II and Amide III bands of the FT-IR spectra can provide a clear picture on hydrogen bonding and the secondary structure of the peptides.[28-32] Amide I band, the most intense adsorption band in peptides, which is primarily governed by the carbonyl stretching vibrations of the peptide amide backbones and found in the region of 1600-1700 cm^{-1}, is directly related to hydrogen bonding and the conformation of the peptide backbones. Amide II bands (1510-1580 cm^{-1}) mainly derive from N-H bending and the band position is also sensitive to hydrogen bonding. Compared to Amide I and II, Amide III band (1200-1400 cm^{-1}) is much more complex and involves in-phase coupling of N-H bending and C-N stretching. This region, however, provides useful complementary information on peptide secondary structures when combined with Amide I band. A hydrogen-

bonding free, monomeric polymer-peptide sample made in alkaline solution was used as the reference system, and both the reference sample and the supramolecular cone samples were dried for FT-IR analysis. We expect the integrity of these supramolecular cones to be preserved with drying, as TEM images on dried samples showed consistent cone structures as seen for the FM images directly taken in solution. Compared to the indistinguishable wide absorption peak in the Amide I region of the non-hydrogen bonded reference (Figure 2.6A), a distinct Amide I absorption band of the supramolecular cones was observed, Figure 2.6B. Moreover, compared to the 1580 cm^{-1} Amide II band of the non-hydrogen bonding reference (Figure 2.6A), a shift to lower wavenumber of 1560 cm^{-1} was observed for the supramolecular cones, Figure 2.6B. Both evidences consistently support the hydrogen bonding formation of the peptide amide backbones within the cone assemblies.

To further elucidate the amide backbone conformation and the secondary peptide structure within the supramolecular cone assemblies, we have obtained the second derivative spectra of the Amide I band, Figure 2.6C, where the minima represent the individual peaks in the original Amide I band, to expose all the component peaks in the Amide I region.[30] Two characteristic peaks at 1684 and 1650 cm^{-1} were identified, which correlate with the antiparallel β-sheet and random coil conformation respectively.[29] The corresponding absorption peaks at 1240 and 1280 cm^{-1} in the complementary Amide III region, Figure 2.6D, also confirmed the mixture of these two peptide secondary structures.[30, 32, 33]

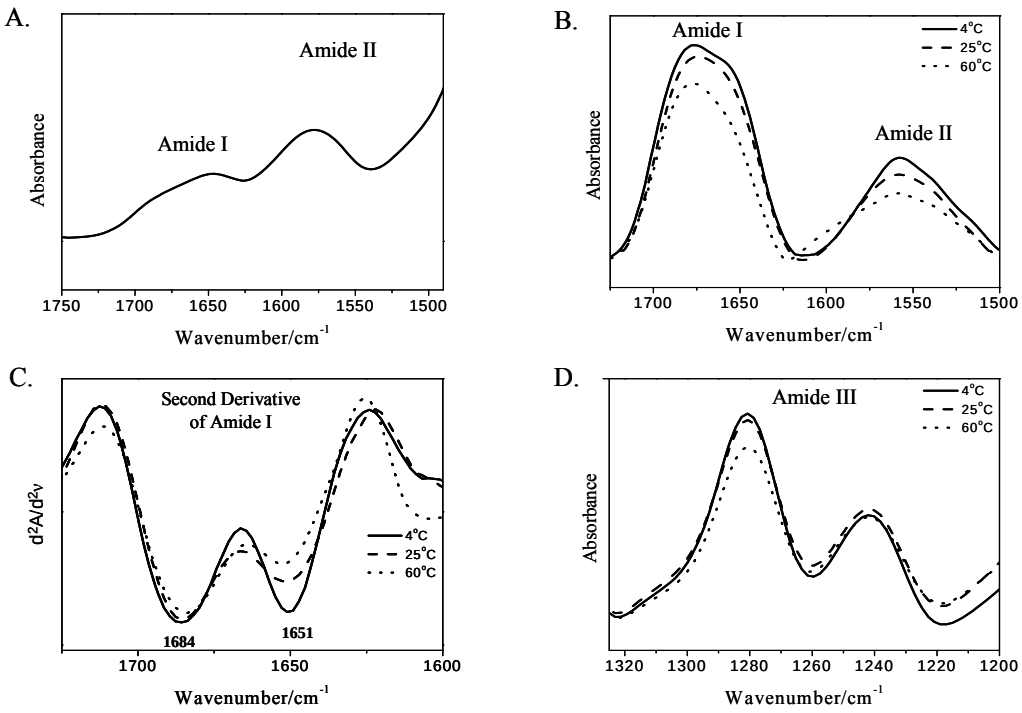

Figure 2.6 FT-IR Spectra of Polymer-Peptide Hybrid Self-assembly. (A) Non-hydrogen bonding polymer-peptide reference sample and (B-D) the spectra of the supramolecular cones formed at different temperatures. B – Amide I andAmide II region; C – Second derivative spectra of Amide I band; D – Amide III region.

To further reveal the role of hydrogen bonding of the peptide hydrogen bonding *versus* the hydrophobic interaction and ionic disturbance in the supramolecular cone formation, we studied the polymer-peptide self-assembly behavior at different temperatures from 4 ºC to 25 ºC and 60 ºC. It is well known that peptide hydrogen bonding quickly melts with raising temperatures, while hydrophobic interaction and ionic disturbance are much less sensitive to temperature changes. As temperature goes up, wider and shorter cones were observed, Figure 2.7. However, the conical geometry can still be formed even at 60 ºC, a sufficiently high temperature for breaking the hydrogen

bonding in many proteins and peptides, Figure 2.7C. The corresponding FT-IR spectra on supramolecular cones formed at different temperatures, Figure 2.6, show clear decreases in amide absorbance, confirming the melting of the peptide hydrogen bonding. This result indicates that the supramolecular cone formation is driven by the hydrophobic interaction, along with the linked ionic disturbance. This is consistent with our preliminary study findings that suggest the hydrophobic interaction is the driving force for self-assembly to occur. Hydrogen bonding from the amide backbones, on the other hand, plays a key factor in stabilizing the cone structure and affecting the geometric parameters (*e.g.* apex angle, length) of the cones.

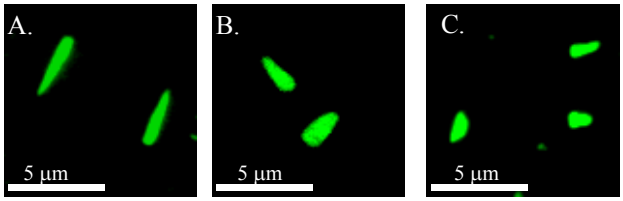

Figure 2.7 Temperature Effect on Supramolecular Cone Assembly. FM images of supramolecular cones at (A) 4°C, (B) 25°C and (C) 60°C

Based on these experimental results, a schematic molecular packing model is proposed in Figure 2.8A. Upon dissolution in water, as a few polymer-peptide hybrid molecules start to nucleate due to the hydrophobic association of the PBD polymer chains, the ionic groups ($–COO^-$ or $–NH_3^+$) that are linked along the PBD chain, however, are highly incompatible with the hydrophobic backbone and would be moving towards water due to their high water affinity. They are likely to gather into a hydrated interface to enclose the aggregated hydrophobic PBD core inside, just like ionic surfactant headgroups,[19] Figure 2.8A. The ionic groups here pack into a conical shape, probably

because the angular cone geometry has a minimal shape factor, $V/A_o h = 1/3$ (V volume; A_o area; h height),[19] that can maximize the volume capacity of a limited surface area. This allows for optimal packing of the bulkier hydrophobic PBD core volume by a limited number of ionic headgroups. The neutral hydrophilic PEO polymer chains, connected to PBD at one end, are likely to segregate around the hydrophobic PBD cone base, shielding it from water. However, considering the sparse density of the PEO polymer chains at the cone base and their floppy nature, any fluctuations can expose the hydrophobic cone base and attract more dispersed polymer-peptide hybrid molecules from water. The hydrophobic PBD segments of those molecules are likely to aggregate on top of the cone base, whereas their linked ionic headgroups pack into a new frustum of the enclosing lateral side, Figure 2.8A (II). The cone growth continues until further packing on top of widened cone base becomes increasingly difficult and no longer energetically favored, Figure 2.8A (III).

While the ionic $-COO^-$ or $-NH_3^+$ side groups of the grafted dipeptides are exposed at the lateral surface, the backbone of some of the dipeptides are able to form antiparallel β-sheet microstructures within the cone assembly, as found in FT-IR studies. In order to produce the planar inter-strand hydrogen bonds between carbonyls and amines found in anti-parallel β-sheets, an interdigitated pattern between dipeptide strands linked to different polymer chains is most likely, Figure 2.8B. The β-sheet peptide backbone microstructures enclosed beneath the ionic lateral surface headgroups are expected to stabilize and stiffen the formed cone assembly.

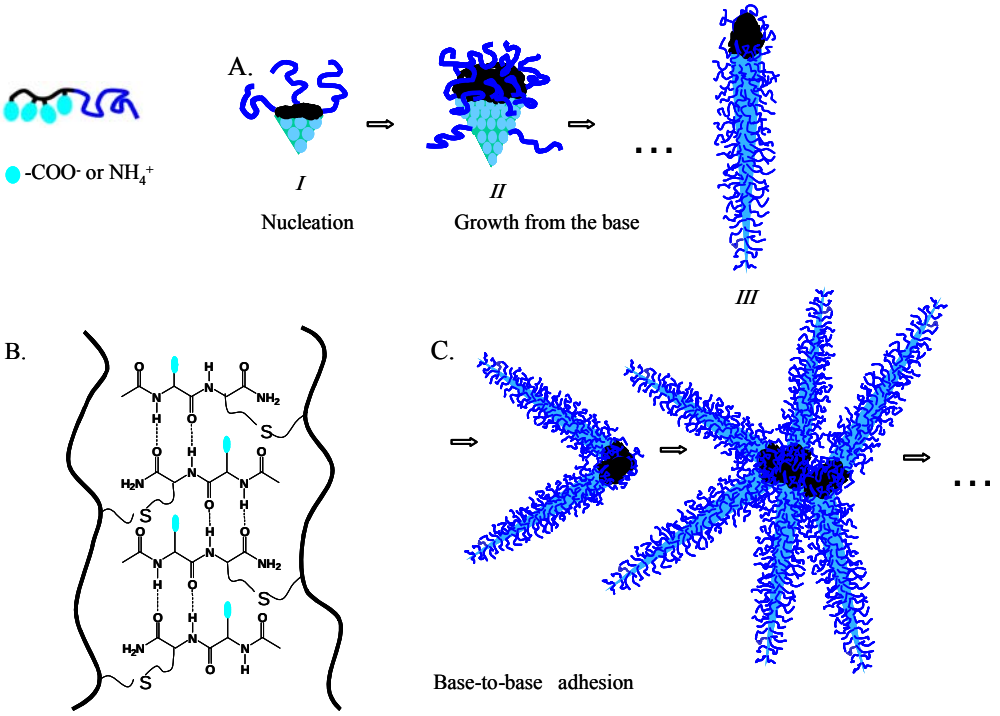

Figure 2.8 Schematic Representation of Supramolecular Cone Formation (A) supramolecular cone formation; (B) antiparallel b-sheet from the peptide amide backbone; and (C) higher-order cone self-assembly.

The hydrophobicity of the cone base also accounts for their base stickiness that fosters the higher-order self-assembly, Figure 2.8C. The cone base-to-base adhesion energy, ΔE_s, can be roughly estimated as $\Delta E_s \sim 2500$ cal mol^{-1} per contact areas (nm^2) based on hydrophobic attraction forces,[34, 35] and only ~ 1 nm^2 contact area would be enough to compensate for the loss of orientational entropy of a rigid cone, $\Delta E_s > T\Delta S > 6$ k_BT,[34] and enables adhesion. As temperature increases, cone assembly was observed to become more difficult, where the entropy barrier increases and larger contact area demanded. From the geometric aspect, compared to wider cones, the needle-like, sharp

cone shape minimizes repulsions between the charged lateral sides and facilitates base contact and cone assembly formation.

2.4 Conclusions

In this study, we report a new twist to amphiphile design, which yields angular supramolecular cone geometry, with a broken symmetry between the apex and the base. Such supramolecular cones demonstrate a surprising stickiness property at their base, which fosters their spontaneous higher-order self-assembly. The apex angle, length, as well as the stickiness of the cones can all be tuned by chemical manipulations. Moreover, we reveal the delicate balance of forces that govern the unusual sticky supramolecular cone formation.

With the "sticky" supramolecular cones, we extend amphiphilicty-based self-assembly to angular geometries, as well as to the higher-hierarchy self-assembly paradigm. The unusual conical geometry, potential peptide functionalization, stickiness, as well as the tuning flexibility of the reported supramolecular cones, will be further explored in the future towards advanced materials applications.

2.5 Experimental

Materials

The amphiphilic diblock copolymer precursors (PBD_{14}-*b*-PEO_{93} and PBD_{25}-*b*-PEO_{75}, subscripts denote the average number of repeating units) with narrow molecular-weight distributions (polydispersity index, PDI ~ 1.05) were prepared by the well established sequential anionic polymerization of buta-1,3-diene and ethylene oxide.[36] The thio-containing cysteine (Cys) terminus was coupled to the ionic amino acid glutamic acid (Glu) or lysine (Lys), using standard Fmoc Solid Phase Peptide Synthesis

procedure with HOBT, HBTU and DIPEA couplings, followed by N-capping with acetylation and C-capping with amidation.[37] The dipeptides of (L,L)-Glu-Cys and (L,L)-Lys-Cys were analyzed by ESI-MS and ^{1}H NMR before grafting. Gly-Cys or Lys-Cys was grafted onto the hydrophobic PBD segment of the amphiphilic block copolymer *via* the free radical addition between the thiol groups and the ene double bonds in PBD.[20]. All chemical and solvents were purchased from Sigma-Aldrich.

Grafting of Gly-Cys or Lys-Cys onto PBD_n-b-PEO_m

The grafting procedure has been published elsewhere, and briefly, the reaction flask containing the polymer PBD_n-*b*-PEO_m, dipeptide, and 2,2 azoisobutyronitrile (AIBN) was degassed for 30 minutes. Dry solvent, 1-methyl-2-pyrrolidone (NMP) was then added. Molar ratio $[C=C]_0/[-SH]_0/[AIBN]_0$ = 1:1.5:0.33 was used to achieve a low grafting density of 30%. The resulting solution was heated to 70ºC and stirred for 48 hours under an argon atmosphere. AIBN was reinjected after 24 hours. After the reaction was complete, excess dipeptide was removed by dialysis. The product was freeze-dried and collected for ^{1}H NMR and Gel Permeation Chromatography (GPC) analysis.

Using Glu-Cys grafted hybrid molecule as an example, in ^{1}H NMR analysis, the characteristic signals of the grafted dipeptide were observed at δ = 1.9 ppm (-C**H**$_3$, a), 2.1-2.3 ppm (-C**H**$_2$-C**H**$_2$-, b) and 4.4-4.6 (-CO-C**H**(R)-NH-, c); the signal of the thioether linkage –CH_2SCH_2- (d) arise at δ ~ 2.7 and 2.9 ppm. Resonances at δ = 4.8-5.6 ppm indicate that the conversion of the PBD double bond did not come to completion. The quantitative analysis of signal intensities relative to that of PEO at δ = 3.6 ppm reveals that the hybrid molecules contains about 4 EC units and 10 unreacted butadiene units.

GPC analysis using NMP as eluent showed a single narrow peak for PBD_{14}-*b*-PEO_{93} precursor (solid line) and the hybrid molecule with Glu-Cys grafts (dashed line) respectively, indicating the narrow polydispersity of the PBD-b-PEO precursor has been preserved during the grafting process

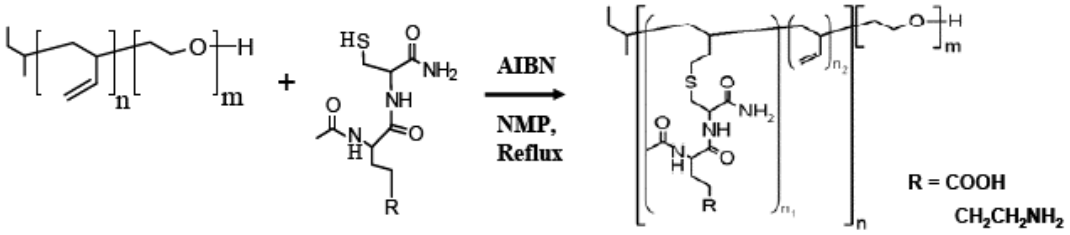

Figure 2.9 Grafting of Cys-containing peptide to PBD-*b*-PEO

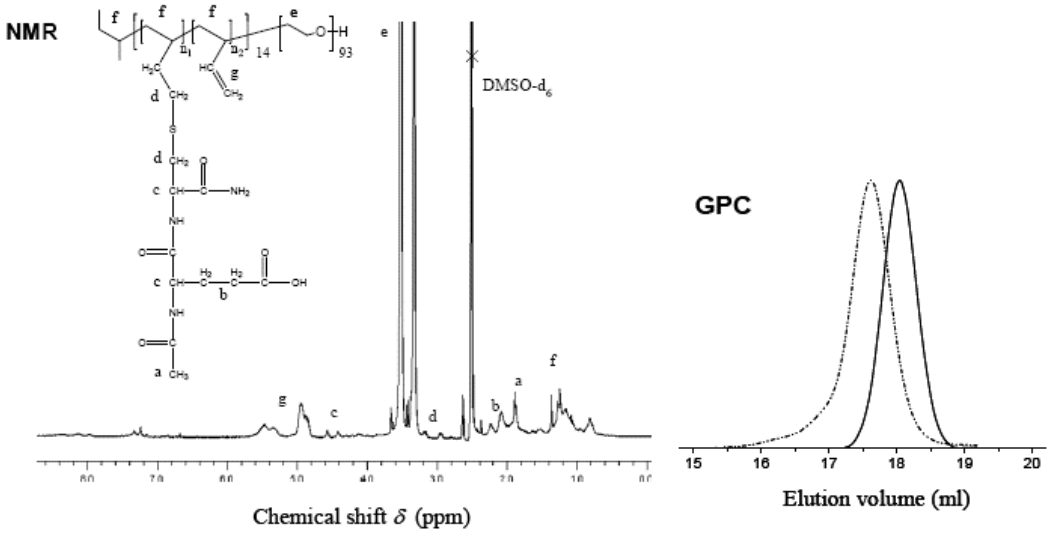

Figure 2.10 Representative ^{1}H NMR and GPC of Polymer-Peptide Hybrid

Fluorescent microscopy imaging

The detailed procedure of using FM to image supramolecular self-assemblies in aqueous solution has been published elsewhere.[20, 24] Briefly, an Olympus IX71 inverted fluorescence microscope with a 60X objective and a Cascade CCD camera was used to

visualize the supramolecular cones at different stages in aqueous solution. A hydrophobic fluorophore dye (PKH 26) was added to the solution, and 2μL sample was used in the chamber formed between the glass slide and cover slip for imaging.

TEM imaging

Images of supramolecular cones were obtained on a FEI TECNAI 20G Transmission Electron Microscope. Typically, 10 μL of supramolecular cone solution is pipetted onto a copper grid with a porous carbon film. A piece of filter paper was then used to quickly remove the liquid. Samples were stained with 2% uranyl acetate for 1 min, followed by removal of the excess liquid with filter paper. The sample grid was put in a desiccator for drying before TEM imaging.

FT-IR spectroscopy studies

FT-IR spectra of supramolecular cones were acquired on a Digilab (Cambridge, MA) FTS-7000 Fourier Transform Infrared spectrometer, equipped with a MCT detector, ZnSe crystal and continuously purging wit dry filtered air. 40 μL of 1 mg/mL supramolecular cone aqueous solution, formed after one week at different temperatures, were applied directly to the crystal and allowed to dry. The non-hydrogen bonded polymer-peptide reference solution was prepared by dissolving 1 mg/mL polymer-peptide hybrid molecules in highly alkaline solution (pH ~11), followed by immediate drying for FT-IR measurement wit no time allowed for self-assembly. Interferograms were collected at 4 cm^{-1} resolution and apodized wit a NB (Norton-Beer) function. Second derivative spectra of Amide I band were obtained with the use of a 9 point Savitsky-Golay algorithm from the Digilab software.

Estimates of the aggregation number of peptide grafted PBD_{14}-b-PEO_{93} conic nuclei and fully grown cones

Assuming the core of the cones is largely made of the aggregated hydrophobic PBD polymer chains (as proposed in Figure 2.8), aggregation number of the initial conical nuclei can roughly be estimated by N = (Mass x N_A)/M_n, where N_A is the Avagadro constant, M_n is the molar mass of the PBD_{14} polymer (M_n ~ 756 g/mol). The mass of the hydrophobic PBD conic core can be calculated as Mass = V x d, where V is the volume and d is the density, which can be approximated by the bulk PBD polymer density (0.89 g/cm^3). The conic core volume V can then be calculated from TEM measurements, V = 1/3 $\pi r^2 h$. For a conic nucleate with ~ 10 nm height and 20º apex angle, V = 1/3 p (10 nm x tan (10º))^2 x 10 nm = 40 nm^3 and the corresponding aggregation number is calculated to be ~ 40 molecules. The aggregation number for a microns-long cone can be estimated in a similar fashion and calculated to be ~ 10^5.

2.6 References

1. Whitesides, G. M.; Mathias, J. P.; Seto, C. T., Molecular self-assembly and nanochemistry: a chemical strategy for the synthesis of nanostructures. *Science* **1991,** 254, (5036), 1312.

2. Wang, X. S.; Wang, H.; Coombs, N.; Winnik, M. A.; Manners, I., Redox-induced synthesis and encapsulation of metal nanoparticles in shell-cross-linked organometallic nanotubes. *J. Am. Chem. Soc* **2005,** 127, (25), 8924-8925.

3. Cui, H.; Chen, Z.; Zhong, S.; Wooley, K. L.; Pochan, D. J., Block copolymer assembly via kinetic control. *Science* **2007,** 317, (5838), 647.

4. Park, M.; Harrison, C.; Chaikin, P. M.; Register, R. A.; Adamson, D. H., Block Copolymer Lithography: Periodic Arrays of~ 1011 Holes in 1? Square Centimeter. *Science* **1997,** 276, (5317), 1401.

5. Hartgerink, J. D.; Beniash, E.; Stupp, S. I., Self-assembly and mineralization of peptide-amphiphile nanofibers. *Science* **2001,** 294, (5547), 1684.

6. Hartgerink, J. D.; Beniash, E.; Stupp, S. I., Peptide-amphiphile nanofibers: a versatile scaffold for the preparation of self-assembling materials. *Proceedings of the National Academy of Sciences of the United States of America* **2002,** 99, (8), 5133.

7. Nowak, A. P.; Breedveld, V.; Pakstis, L.; Ozbas, B.; Pine, D. J.; Pochan, D.; Deming, T. J., Rapidly recovering hydrogel scaffolds from self-assembling diblock copolypeptide amphiphiles. *Nature* **2002,** 417, (6887), 424-428.

8. Zana, R., *Dynamics of surfactant self-assemblies: micelles, microemulsions, vesicles, and lyotropic phases*. CRC: 2005.

9. Wang, X.; Guerin, G.; Wang, H.; Wang, Y.; Manners, I.; Winnik, M. A., Cylindrical block copolymer micelles and co-micelles of controlled length and architecture. *Science* **2007,** 317, (5838), 644.

10. Cornelissen, J.; Fischer, M.; Sommerdijk, N.; Nolte, R. J. M., Helical superstructures from charged poly (styrene)-poly (isocyanodipeptide) block copolymers. *Science* **1998,** 280, (5368), 1427.

11. Kukula, H.; Schlaad, H.; Antonietti, M.; Förster, S., The formation of polymer vesicles or "peptosomes" by polybutadiene-block-poly (L-glutamate) s in dilute aqueous solution. *J. Am. Chem. Soc* **2002,** 124, (8), 1658-1663.

12. Chécot, F.; Lecommandoux, S.; Gnanou, Y.; Klok, H. A., Water Soluble Stimuli Responsive Vesicles from Peptide Based Diblock Copolymers. *Angewandte Chemie* **2002,** 114, (8), 1395-1399.

13. Li, Z.; Kesselman, E.; Talmon, Y.; Hillmyer, M. A.; Lodge, T. P., Multicompartment micelles from ABC miktoarm stars in water. *Science* **2004,** 306, (5693), 98.

14. Geng, Y.; Dalhaimer, P.; Cai, S.; Tsai, R.; Tewari, M.; Minko, T.; Discher, D. E., Shape effects of laments versus spherical particles in ow and drug delivery. *Nat Nanotechnol* **2007**.

15. Dean, J. M.; Verghese, N. E.; Pham, H. Q.; Bates, F. S., Nanostructure toughened epoxy resins. *Macromolecules* **2003,** 36, (25), 9267-9270.

16. Jin, R.; Cao, Y. W.; Mirkin, C. A.; Kelly, K. L.; Schatz, G. C.; Zheng, J. G., Photoinduced conversion of silver nanospheres to nanoprisms. *Science* **2001,** 294, (5548), 1901.

17. Chiruvolu, S.; Walker, S.; Israelachvili, J.; Schmitt, F. J.; Leckband, D.; Zasadzinski, J. A., Higher order self-assembly of vesicles by site-specific binding. *Science* **1994,** 264, (5166), 1753.

18. Wong, G. C. L.; Tang, J. X.; Lin, A.; Li, Y.; Janmey, P. A.; Safinya, C. R., Hierarchical self-assembly of F-actin and cationic lipid complexes: stacked three-layer tubule networks. *Science* **2000,** 288, (5473), 2035.

19. Israelachvili, J. N., *Intermolecular and surface forces.* . Academic Press, London: 1992.

20. Geng, Y.; Discher, D. E.; Justynska, J.; Schlaad, H., Grafting Short Peptides onto Polybutadiene block poly (ethylene oxide): A Platform for Self Assembling Hybrid Amphiphiles. *Angewandte Chemie* **2006,** 118, (45), 7740-7743.

21. Zhang, L.; Eisenberg, A., Aggregates of Polystyrene-b-poly (acrylic acid) Block Copolymers. *Science* **1995,** 268, 23.

22. Harada, A.; Kataoka, K., Chain length recognition: core-shell supramolecular assembly from oppositely charged block copolymers. *Science* **1999,** 283, (5398), 65.

23. Jain, S.; Bates, F. S., On the origins of morphological complexity in block copolymer surfactants. *Science* **2003,** 300, (5618), 460.

24. Discher, D. E.; Eisenberg, A., Polymer vesicles. *Science* **2002,** 297, (5583), 967.

25. Geng, Y.; Ahmed, F.; Bhasin, N.; Discher, D. E., Visualizing worm micelle dynamics and phase transitions of a charged diblock copolymer in water. *J. Phys. Chem. B* **2005,** 109, (9), 3772-3779.

26. Jonkheijm, P.; van der Schoot, P.; Schenning, A.; Meijer, E. W., Probing the solvent-assisted nucleation pathway in chemical self-assembly. *Science* **2006,** 313, (5783), 80.

27. Kentsis, A.; Borden, K. L. B., Physical mechanisms and biological significance of supramolecular protein self-assembly. *Current Protein and Peptide Science* **2004,** 5, (2), 125-134.

28. Krimm, S.; Bandekar, J., Vibrational spectroscopy and conformation of peptides, polypeptides, and proteins. *Adv. Protein Chem* **1986,** 38, (181), 364.

29. Miyazawa, T.; Blout, E. R., The Infrared Spectra of Polypeptides in Various Conformations: Amide I and II Bands1. *Journal of the American Chemical Society* **1961,** 83, (3), 712-719.

30. Singh, B. R., *Infrared Analysis of Peptides and Protiens Principles and Applications*. American Chemical Society: Washington, D.C., 2000; Vol. 750, p 204.

31. Surewicz, W. K.; Mantsch, H. H.; Chapman, D., Determination of protein secondary structure by Fourier transform infrared spectroscopy: a critical assessment. *Biochemistry* **1993,** 32, (2), 389-394.

32. Cai, S.; Singh, B. R., Identification of -turn and random coil amide III infrared bands for secondary structure estimation of proteins. *Biophysical chemistry* **1999,** 80, (1), 7-20.

33. Cai, S.; Singh, B. R., A Distinct Utility of the Amide III Infrared Band for Secondary Structure Estimation of Aqueous Protein Solutions Using Partial Least Squares Methods†. *Biochemistry* **2004,** 43, (9), 2541-2549.

34. Nakata, M.; Zanchetta, G.; Chapman, B. D.; Jones, C. D.; Cross, J. O.; Pindak, R.; Bellini, T.; Clark, N. A., End-to-end stacking and liquid crystal condensation of 6 to 20 base pair DNA duplexes. *Science* **2007,** 318, (5854), 1276.

35. Reynolds, J. A.; Gilbert, D. B.; Tanford, C., Empirical correlation between hydrophobic free energy and aqueous cavity surface area. *Proceedings of the National Academy of Sciences of the United States of America* **1974,** 71, (8), 2925.

36. Forster, S.; Kramer, E., Synthesis of PB- PEO and PI- PEO Block Copolymers with Alkyllithium Initiators and the Phosphazene Base t-BuP4. *Macromolecules* **1999,** 32, (8), 2783-2785.

37. Merrifield, B.; Maat, L., *Life during a golden age of peptide chemistry: the concept and development of solid-phase peptide synthesis*. American Chemical Society Washington, DC: 1993.

CHAPTER 3

COMBINING AND CONTROLING NON-COVALENT FORCES IN MACROMOLECULAR SELF-ASSEMBLY: COMPLEX VESICLES FROM POLYMER-PEPTIDE HYBRIDS

Haley, J.; Ju, R.; Schlaad, H. and Geng Y.
To be submitted to Macromolecules

3.1 Abstract

Mixing oppositely charged polymer-peptide hybrids to combine hydrophobic effect, hydrogen bonding and ionic attraction forces into the self-assembly process results in complex nano-sized vesicles. By varying the grafting density and polymer backbone properties such as vesicle diameter, thickness and permeability can be tuned.

3.1 Introduction

Molecular self-assembly through non-covalent bonding is the cornerstone towards advancing the complexity in structure and function of matter. The heart of the challenge in creating supramolecular assembly is to manipulate molecular design and orchestrate potential non-covalent forces that drive and govern molecular organization, such as hydrophobic effect, electrostatic interactions, hydrogen bonding, π-π stacking, donor-acceptor interactions and metal coordination. Compared to small molecules, macromolecules are not only larger building blocks that are advantageous in scale and dimension, but also flexible in choosing chemical compositions, adjusting molecular size (*e.g.* the molecular weight and chain length of polymers), and generating various molecular shapes and architectures (such as linear, branched, cyclic, comb- and star-shape, *etc*.). With the tremendous advancements in modern polymerization and polymer modification techniques, these features of macromolecules provide great opportunities in molecular programming and integrating various non-covalent forces into self-assembly process.

Over the years, block copolymers have become the fundamental design for polymer self-assembly, where the solubility difference of different blocks in a selective solvent is

the self-assembly driving force. Although many approaches have been developed to modify the polymer self-assembly, such as ionic and pH change, kinetic control and phase manipulation.[1-6] However, the most important aspect of any molecular self-assembly is the non-covalent force that governs the self-assembly process, and in the block copolymer self-assembly, typically only one non-covalent force is involved, i.e. the salvation force. This limits the degree of complexity and sophistication in the structure and function of polymer self-assembly. In nature, many of the macromolecular associations are governed by a combination of non-covalent bonding. For example, in protein-protein association, in many cases, it involves hydrophobic association to shield water and create a hydrophobic microenvironment, and then hydrogen bonding and ionic attractions will also participate to adjust the self-assembly process. It would involve synergistic interplay of multiple non-covalent forces to advance polymer self-assembly.

Among all solvents, water is the exclusive solvent in nature and one of the most important media, especially with the recent increasing awareness in green chemistry and lowering usage in organic solvents. However, water as a highly competitive and disruptive solvent, is also one of the most difficult media for molecular self-assembly. The most effective mechanism for molecular self-assembly is by hydrophobic effect, *i.e.* aggregation of hydrophobic segments to minimize contact with water, which has been commonly used in amphihpilic block copolymers. Our design strategy is to use an amphiphilic block copolymer as a foundation, and then controllably graft peptides along the hydrophobic block, *i.e.* the one responsible for driving molecules to associate, to incorporate other potential non-covalent forces into the self-assembly system, such as

hydrogen bonding, ionic interactions, and π-π stacking. This approach can effectively and flexibly combine and control different forces in macromolecular self-assembly.

Previously, we have developed a modular thiol-ene addition route to graft peptides onto the hydrophobic polybutadiene segment of amphiphilic PBD-b-PEO polymers. By using thiol-containing cysteine amino acid as the peptide linker terminus, target peptide sequences can be grafted along the PBD segment with desired grafting density. In the earlier studies, we have grafted hydrophobic peptides, which enhanced the hydrophobic fraction of the molecule and shifted the self-assembly curvature from spherical micelles to cylindrical micelles and vesicles, as well as promoted helical superstructure formation in the self-assembly. We have also grafted ionic peptides along the hydrophobic PBD segment, and as a result, the ionic disturbance had led to the formation of angular supramolecular cones. In this study, we mix oppositely charged polymer-peptide hybrids to combine hydrophobic effect, hydrogen bonding and ionic attraction forces into the self-assembly process, and we demonstrate the intriguing self-assembly behavior when multiple non-covalent forces interplay .

3.2 Results and Discussion

PBD_{14}-*b*-PEO_{93} was used as the precursor amphihpilic block copolymer, which has a low hydrophobic fraction $f_{PBD} \sim 0.2$. Without any modification, this polymer will self-assemble into spherical micelles in aqueous solution,[7] as predicted by its hydrophobic-hydrophilic ratio[8]. We then grafted Cys-Glutamic acid (GLu) and Cys-Lysine onto PBD_{14}-*b*-PEO_{93} at different grafting density to produce the positively charged polymer-Glu hybrid (PP-Glu) and negatively-charged polymer-Lys hybrid (PP-Lys) respectively, Figure 3.1A. We found that even with just ~25% grafting, i.e. with four peptide grafts,

when mixing two oppositely charged polymer-peptide hybrids, they spontaneously self-assembled into vesicles in water, Figure 3.1B. The average thickness of these vesicles was measured from TEM as ca. 25nm, and the inner diameter as ~ 35nm. This self-assembly behavior is drastically different from PBD-*b*-PEO alone, which would require at least 60% hydrophobicity in order to form vesicles. The formation of the vesicles from mixing oppositely charged polymer-peptide hybrids here must be resulted from the combination of hydrophobic effect with ionic attractions between the carboxyl and amino headgroups, as well as potential hydrogen bonding between the amide backbones of the dipeptides. When grafting density was increased to eight peptide grafts, mixing PP_{14}-8Glu and PP_{14}-8Lys gave rise to thinner and smaller vesicles, Table 3.1. This is probably because the more ionic attractions help tighten the associations between molecules and thus giving rise to a smaller size.

Unlike polyioncomplex vesicles (PICsomes) which require exact length match in order to recognize with each other and self-assembly, these polymer-peptide hybrids can flexibly cross-mix between different numbers of grafts, as long as the total stoichiometry of the oppositely charged peptides are the same. For example, PP_{14}-8Lys can mix with PP_{14}-4Glu, as long as the molarity of PP_{14}-4Glu is twice as the PP_{14}-8Lys, Figure 3.2, Table 3.2. Moreover, polymer-peptide hybrids from different polymer backbones can also be mixed together to generate vesicles. These PP_{14} peptide hybrids can readily mix with oppositely charged PP_{40} based peptide hybrids, Figure 3.2, Table. Vesicles from cross-mixing are notably thicker than the simple direct mixing cases. This is probably due to the packing difficulty and frustration as two different systems trying to manage to

accommodate each other. Uneveness in the vesicle membrane may also be indicating the packing frustration and complex nature of these self-assemblies.

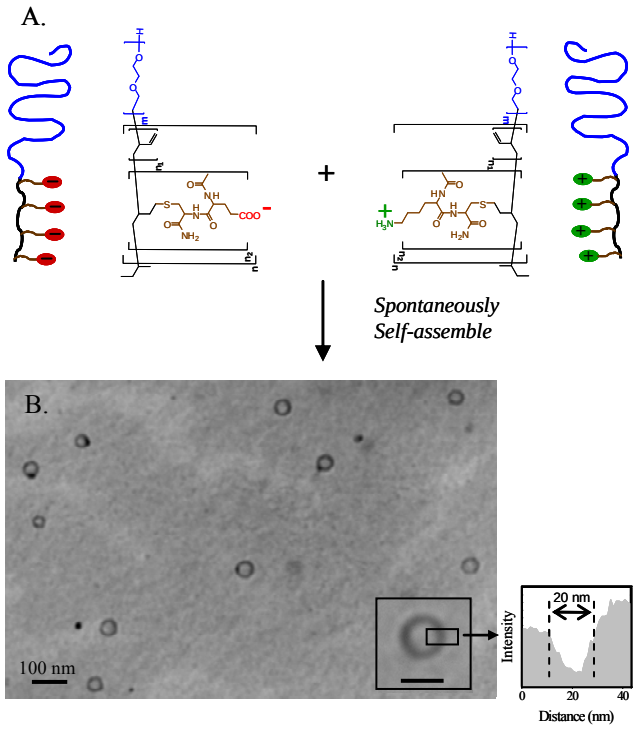

Figure 3.1 Complex Vesicle Formation via Direct Mixing of Polymer-Peptide (PP) Hybrids (A) Schematic representation of polymer-peptide hybrids (PP) and (B) Representative TEM image and intensity profile of Complex vesicles via direct mixing of PP_{14}-8Glu + PP_{14}-8Lys. Inset Scale bar 50 nm

Table 3.1 Complex Vesicle Inner Diameter and Thickness via Direct Mixing

Mixing of PP	Inner Diameter(nm)	Thickness (nm)
PP_{14}-4Glu + PP_{14}-4Lys	35	25
PP_{14}-8Glu + PP_{14}-8Lys	15	20

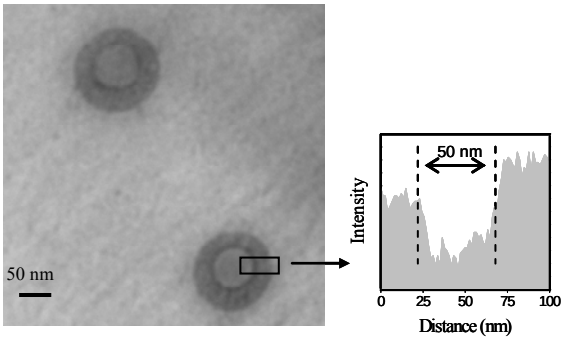

Figure 3.2 Complex Vesicle Formation via Cross Mixing of Polymer-Peptide (PP) Hybrids. Representative TEM image and intensity profile of Complex vesicles via cross mixing of PP_{40}-12Glu + $3PP_{14}$-4Lys

Table 3.2 Complex Vesicle Inner Diameter and Thickness via Cross Mixing

Cross Mixing of PP	Inner Diameter (nm)	Thickness (nm)
PP_{40}-12Glu + **1.5** PP_{14}-8Lys	25	21
PP_{14}-8Glu + PP_{14}-**2** 4Lys	30	30
PP_{40}-12Glu + **3** PP_{14}-4Lys	50	50

The complex vesicle formation must be the result of a combination of hydrophobic effect, ionic attractions and potential hydrogen bonding between the amide backbones of the grafted dipeptides. The critical roles of hydrophobic effect and ionic attractions are relatively apparent. Hydrophobic effect must be crucial to the association of the molecules, otherwise just a few ionic groups in the molecule won't be able to provide substantial binding force to assemble molecules together. In addition, without the hydrophobic effect, such as in PICsomes, in order to form vesicles, it would require a large numbers of ionic moieties compared to PEO. Otherwise, spherical micelles would

form instead of vesicles. The ionic attractions apparently are also critical to the vesicle formation. As we pointed out earlier, the hydrophobic alone in the molecule is too low to form vesicles, but spherical micelles. Other than hydrophobic interaction and ionic attraction, the involvement of the peptide hydrogen bonding in the vesicle is further confirmed by Fourier-transformed Infrared (FT-IR) spectroscopy analysis, Figure 3.3A. A combination of the key Amide I band with the complementary Amide II and Amide III bands of the FT-IR spectra can provide a clear picture on hydrogen bonding and the secondary structure of peptides.[9-13] Amide I band, the most intense absorption band in peptides, which is primarily governed by the carbonyl stretching vibrations of the peptide amide backbones and found in the region of 1600 – 1700cm^{-1}, is directly related to much more complex and involves in-phase coupling of N-H bending and C-N stretching. This region, however, provides useful complementary information on peptide secondary structures when combined with Amide I band. FT-IR absorbance in all regions consistently decreased as temperature was raised from 25ºC to 60ºC, which indicates the formation of amide hydrogen bonding, which weakens with heat and lowers the FT-IR absorbance. From the second derivative of amide I region, where the minima represent the individual peaks in the original Amide I band, two characteristic peaks at 1684 and 1650cm^{-1} were identified, which correlate with the anti-parallel β-sheet and random coil conformation respectively.[10] As we raised the temperature to break the amide hydrogen bonds, mixing the polymer-peptide hybrids could no longer form vesicles, but spherical micelles, Figure 3.3B. This suggests that amide hydrogen bonding also plays a critical role in the vesicle formation. It is likely to form a rigid frame for the vesicles, and once broken, the vesicles will collapse into micelles.

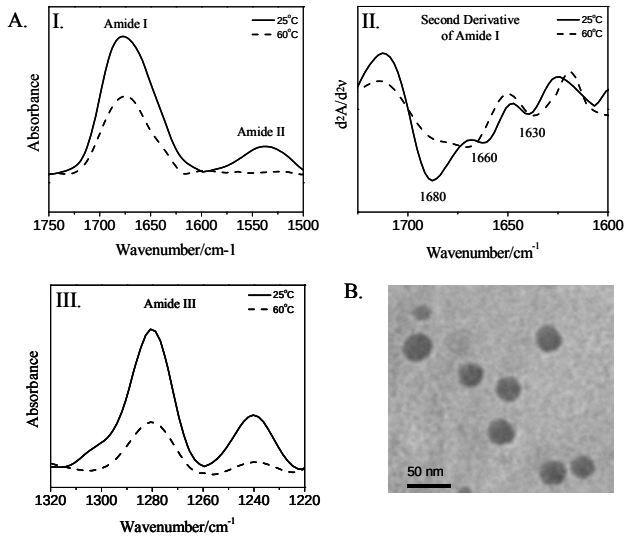

Figure 3.3 Temperature Effect on Hydrogen Bonding in Complex Vesicle Formation (A) FT-IR Spectra of complex vesicles at 25˚C and 60˚C and (B) Representative TEM image of PP_{14}-4Glu + PP_{14}-4Lys self-assembly at 60˚C.

These complex vesicles formed by combining multiple forces are also quite different from the bare PBD-b-PEO vesicles in properties. The membrane of PBD-*b*-PEO vesicles is purely hydrophobic and have low permeability, whereas the existence of ionic pairs within the membrane can probably bring hydration into the membrane, leading to increased permeability. By using a 4000 Dalton Dextrin, we studied the release profile of different vesicles, Figure 3.4. While only near 10% of Dextrin was released from PBD-PEO vesicles, much more substantial profiles were observed in the mixture vesicles, where the more ionic pair density the higher percentage release. This indicates that these mixture vesicles are more permeable than PBD-PEO vesicles, and their permeability can be tuned by adjusting the ionic pair density. This feature can be potentially useful for many applications.

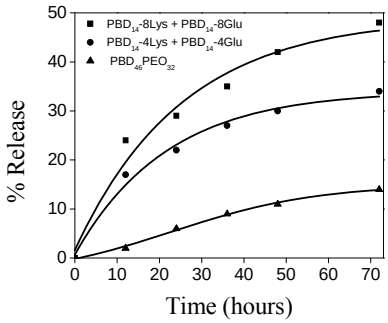

Figure 3.4 Release of FITC Dextran from Complex Vesicles

3.3 Conclusions

In this study, we mixed oppositely charged polymer-peptide hybrids to combine hydrophobic effect, hydrogen bonding and ionic attraction forces into the self-assembly process, and we demonstrated the intriguing self-assembly behavior when multiple non-covalent forces interplay. By varying the grafting density and polymer backbone properties such as vesicle diameter, thickness and permeability can be tuned.

3.4 Experimental

Materials

The amphiphilic diblock copolymer precursors (PBD_{14}-*b*-PEO_{93} and PBD_{40}-*b*-PEO_{62}, subscripts denote the average number of repeating units) with narrow molecular-weight distributions (polydispersity index, PDI ~ 1.05) were prepared by the well established sequential anionic polymerization of buta-1,3-diene and ethylene oxide.[14] The thio-containing cysteine (Cys) terminus was coupled to the ionic amino acid glutamic acid (Glu) or lysine (Lys), using standard Fmoc Solid Phase Peptide Synthesis procedure with HOBT, HBTU and DIPEA couplings, followed by N-capping with

acetylation and C-capping with amidation.[15] The dipeptides of (L,L)-Glu-Cys and (L,L)-Lys-Cys were analyzed by ESI-MS and ^{1}H NMR before grafting. Gly-Cys or Lys-Cys was grafted onto the hydrophobic PBD segment of the amphiphilic block copolymer *via* the free radical addition between the thiol groups and the ene double bonds in PBD.[16] All chemical and solvents were purchased from Sigma-Aldrich.

Grafting of Gly-Cys or Lys-Cys onto PBD_n-b-PEO_m

The grafting procedure has been published elsewhere, and briefly, the reaction flask containing the polymer PBD_n-*b*-PEO_m, dipeptide, and 2,2 azoisobutyronitrile (AIBN) was degassed for 30 minutes. Dry solvent, 1-methyl-2-pyrrolidone (NMP) was then added. Molar ratio $[C=C]_0/[-SH]_0/[AIBN]_0$ = 1:1.5:0.33 was used to achieve a low grafting density of 30%. The resulting solution was heated to 70ºC and stirred for 48 hours under an argon atmosphere. AIBN was reinjected after 24 hours. After the reaction was complete, excess dipeptide was removed by dialysis. The product was freeze-dried and collected for ^{1}H NMR and Gel Permeation Chromatography (GPC) analysis.

Using Glu-Cys grafted hybrid molecule as an example, in ^{1}H NMR analysis, the characteristic signals of the grafted dipeptide were observed at δ = 1.9 ppm (-C**H**$_3$, a), 2.1-2.3 ppm (-C**H**$_2$-C**H**$_2$-, b) and 4.4-4.6 (-CO-C**H**(R)-NH-, c); the signal of the thioether linkage –CH_2SCH_2- (d) arise at δ ~ 2.7 and 2.9 ppm. Resonances at δ = 4.8-5.6 ppm indicate that the conversion of the PBD double bond did not come to completion. The quantitative analysis of signal intensities relative to that of PEO at δ = 3.6 ppm reveals that the hybrid molecules contains about 4 EC units and 10 unreacted butadiene units. GPC analysis using NMP as eluent showed a single narrow peak for PBD_{14}-*b*-PEO_{93}

precursor (solid line) and the hybrid molecule with Glu-Cys grafts (dashed line) respectively, indicating the narrow polydispersity of the PBD-b-PEO precursor has been preserved during the grafting process

Preparation of Complex Vesicles

Complex vesicles were prepared by mixing equal molar (0.68 mM) ratios of COO^- to NH_3^+ in water pH 7.2: PBD_{14}-4Glu + PBD_{14}-4Lys (1mg/mL), PBD_{14}-8Glu + PBD_{14}-8Lys (0.60 mg/mL), PBD_{14}-8Glu + **2** PBD_{14}-4Lys (0.6mg/mL and 1.0 mg/mL respectively), PBD_{40}-12Glu + **1.5** PBD_{14}-8Lys (0.48mg/mL and 0.6mg/mL respectively), PBD_{40}-12Glu + **3** PBD_{14}-4Lys (0.48 mg/mL and 1mg/mL respectively). Solutions were vortexed for 30 seconds followed by sonication for 10 minutes and allowed to equilibrate at room temperature overnight. To encapsulate FITC Dextran, a solution of FITC Dextran (MW 4000, 1mg/mL, pH 7.2) was used in place of water.

TEM imaging

Images of complex vesicles were obtained on a FEI TECNAI 20G Transmission Electron Microscope. Typically, 2 μL of complex vesicle solution was pipetted onto a 400 mesh, formvar coated copper grid (Electron Microscopy Sciences, Hatfield, PA) and plunged into liquid nitrogen. The sample was freeze dried overnight and then imaged at 5000 x magnification.

FT-IR spectroscopy studies

FT-IR spectra of complex vesicles were acquired on a Digilab (Cambridge, MA) FTS-7000 Fourier Transform Infrared spectrometer, equipped with a MCT detector, ZnSe crystal and continuously purging with dry filtered air. 40 μL of complex vesicle aqueous solution was applied directly to the crystal and allowed to dry. Interferograms were

collected at 4 cm^{-1} resolution and apodized wit a NB (Norton-Beer) function. Second derivative spectra of Amide I band were obtained with the use of a 9 point Savitsky-Golay algorithm from the Digilab software.

Release of FITC Dextran Release from Complex Vesicles

Complex vesicle solutions (3mL), prepared as described above, containing encapsulated FITC Dextran was injected into a dialysis cassette (MWCO 7000, 3 mL capacity, Thermo Scientific) and dialysized against 200 mL purified water, pH 7.2, for 6 hours to remove unencapsulated FITC Dextran. The release of FITC Dextran was determined by monitoring the absorbance at 480 nm using a Cary 100 UV-Vis spectrophotometer. To obtain samples for release kinetics, 100 μL samples were removed from the dialysis cassette every 12 hours and placed into a 4X2mm quartz microcuvette for absorbance readings. The solution was then injected back into the cassette. At the conclusion of the experiment, the total sample volume was measured to verify that there was no increase in volume ensuring that the observed decrease in FITC dextran concentration was not related to sample dilution.

3.5 References

1. Zana, R., *Dynamics of Surfactant Self-Assemblies: Micelles, Microemulsions, Vesicles and Lyotropic Phases* CRC Press: New York, 2005.

2. Wang, X.; Guerin, G.; Wang, H.; Wang, Y.; Manners, I.; Winnik, M. A., Cylindrical Block Copolymer Micelles and Co-Micelles of Controlled Length and Architecture. *Science* **2007,** 317, 644-647.

3. Cornelissen, J. J. L. M.; Fischer, M.; Sommerdijk, N. A. J. M.; Nolte, R. J. M., Helical Superstructures from Charged Poly(styrene)-Poly(isocyanodipeptide) Block Copolymers. *Science* **1998,** 280, 1427-1430.

4. Kukula, H.; Schlaad, H.; Antonietti, M.; Forster, S., The Formation of Polymer Vesicles or "Peptosomes" by Polybutadiene-block-poly(L-glutamate)s in Dilute Aqueous Solution. *J. Am. Chem. Soc.* **2002,** 124, 1658-1663.

5. Checot, F.; Lecommandoux, S.; Gnanou, Y.; Klok, H.-A., Water-soluble stimuli-responsive vesicles from peptide-based diblock copolymers. *Angew. Chem.* **2002,** 41, 1340-1343.
6. Li, Z.; Kesselman, E.; Talmon, Y.; Hillmyer, M. A.; Lodge, T. P., Multicompartment Micelles from ABC Mikroarm Stars in Water. *Science* **2004,** 306, 98-101.

7. Geng, Y.; Discher, D.; Justynska, J.; Schlaad, H., Grafting Short Peptides onto Polybutadiene-block-poly(ethylene oxide): A Platform for Self-assembling Hybrid Amphiphiles. *Angew. Chem.* **2006,** 45, 7478-7581.

8. Jain, S.; Bates, F. S., On the origins of morphological complexity in block copolymer surfactants. *Science* **2003,** 300, 460-464.

9. Krimm, S.; Bandekar, J., Vibrational Spectroscopy and Conformation of Peptides, Polypeptides and Proteins. *Adv. Protein Chem.* **1986,** 38, 181-364.

10. Miyazawa, T.; Blout, E. R., The Infrared Spectra of Polypeptides in Various Conformations: Amide I and II Bands1. *Journal of the American Chemical Society* **1961,** 83, (3), 712-719.

11. Singh, B. R., *Infrared Analysis of Peptides and Protiens Principles and Applications*. American Chemical Society: Washington, D.C., 2000; Vol. 750, p 204.

12. Surewicz, W. K.; Mantsch, H. H.; Chapman, D., Determination of protein secondary structure by Fourier transform infrared spectroscopy: a critical assessment. *Biochemistry* **1993,** 32, (2), 389-394.

13. Cai, S.; Singh, B. R., Identification of -turn and random coil amide III infrared bands for secondary structure estimation of proteins. *Biophysical chemistry* **1999,** 80, (1), 7-20.

14. Forster, S.; Kramer, E., Synthesis of PB- PEO and PI- PEO Block Copolymers with Alkyllithium Initiators and the Phosphazene Base t-BuP4. *Macromolecules* **1999,** 32, (8), 2783-2785.

15. Merrifield, B.; Maat, L., *Life during a golden age of peptide chemistry: the concept and development of solid-phase peptide synthesis*. American Chemical Society Washington, DC: 1993.

16. Geng, Y.; Discher, D. E.; Justynska, J.; Schlaad, H., Grafting Short Peptides onto Polybutadiene block poly (ethylene oxide): A Platform for Self Assembling Hybrid Amphiphiles. *Angewandte Chemie* **2006,** 118, (45), 7740-7743.

CHAPTER 4

DNA PACKAGING VIA COMBINATIVE SELF-ASSEMBLY

Haley, J.; Li, X.; Marshall, N.; Locklin, J. and Geng Y. *Molecular Biosystems*, **2008**, 4, 515-517

4.1 Abstract

A novel and verstatile DNA packaging approach was developed by grafting DNA-binding oligopeptides onto a polymer scaffold to combinatively self-assemble with DNA into compact nanostructures.

4.2 Introduction

The promise of human gene technology in advancing science and medicine is well recognized and vigorously pursued.[1-3] While genetically manipulating bacteria and primitive eukaryotic cells (*e.g.* yeast) is now well-established, the next level of genetic technology on human cells in the applications of gene therapy,[1] as well as cell reprogramming[2] and tissue engineering,[3] is facing far more complicated challenges. Among all of the challenging aspects, the development of a safe and efficient gene transfer vector that can effectively package/protect genes and transport them across all barriers into the cell nucleus is indeed the bottleneck.[4] Naked genes can not enter cells on their own, and are easily degraded by nucleases in biofluids. The conventional mechanical transfection techniques, *e.g.* electroporation, that work well on bacteria and yeasts, tend to cause poor viability in human cells.[5] Another popular transfection technique by the use of recombinant viral vectors, though highly efficient, is associated with innate immunogenicity and safety issues that are critical concerns in human gene technology.[4] Unlike viral vectors, synthetic vectors are free of those risks and have attracted a lot of attention in recent years. While tremendous progress has been made, development of synthetic vectors is still at a very early stage. So far, synthetic vectors are rather pristine compared to viral vectors and are typically associated with unsatisfyingly low transfection efficiency.[4] Significant knowledge gaps also exist in all

aspects of synthetic vector design: vector-gene complex formation, dissociation (*i.e.* gene release) mechanism, and biological interactions of the vector-gene complex with the host from transport, through internalization to transfection.

Intimately relating to synthetic gene vector development, condensation of DNA has also been of long-standing interest to the biophysics and molecular biology communities, as a model system to reveal the interactions underlying the gene packaging within cell nuclei, viruses and sperm cells. Natural oligo-amines, *e.g.* spermidine and spermine,[6, 7] small multivalent (valcency $\geq$ 3) cations (e.g. $Co(NH_3)_6^{3+}$),[8] synthetic polycations (*e.g.* polylysine, polyethylene imine),[9] as well as liposomes,[10] have been extensively explored as condensing agents to complex with negatively charged DNA *via* electrostatic interactions into various compact structures in dilute solutions, including spheroids, disks, toroids and rods. Those works have provided invaluable information on DNA packaging as well as insights for synthetic vector design.

Among recent progress, the groups of Kataoka and Kabanov have used block copolymers of polyethylene glycol-*b*-polylyine (PEG-*b*-PLL) to form polyion complex micelles with DNA, where the PLL electrostatically interacts with DNA to form the hydrophobic core, surrounded by the hydrophilic PEG corona.[11, 12] The stealthy PEG corona has proved to significantly improve the stability, solubility and biocompatibility of the DNA complex. Another interesting approach is to use synthetic oligopeptides that emulate the active nucleotide binding site for DNA condensation.[13] Oligopeptides can provide direct insights on DNA-protein interactions, and when compared to large whole proteins, have the major advantages of high efficiency in functionality, less antigenicity,

flexibility and ease in the sequence design and synthesis via solid phase peptide synthesis (SPPS).

Aiming to develop a promising synthetic gene vector, as well as to elucidate the gene packaging mechanisms in general, herein, we report a novel and versatile approach by grafting gene-binding oligopeptides onto a polymer scaffold to combinatively self-assembly with genes into compact nanostructures, Figure 4.1. The polymer scaffold creates a spatial clustering arrangement and multiplies the oligopeptide binding sites with DNA, and our initial studies on DNA condensation here demonstrate that the clustering of oligopeptides has led to much more effective DNA compaction than free oligopeptides, and that the clustering density has a profound influence on DNA packaging.

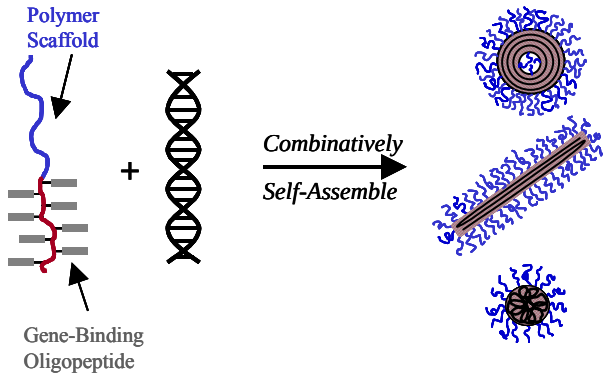

Figure 4.1 Schematic illustration of combinative polymer-peptide hybrids self-assembling with genes into compact nanostructures.

4.3 Results and Discussion

In this report, oligopeptides were grafted onto the hydrophobic segment – polybutadiene (PBD) – of the ampiphilic block copolymers of PEO-*b*-PBD. The gene binding oligopeptide grafted PBD segment is expected to complex with DNA to form the

core, and the PEO segment to form a protecting corona. The grafting proceeded *via* the modular free radical addition route that we recently reported.[14] By using cysteine as the terminal linker of the oligopeptide sequence, the thiol group of the cysteine reacts with the double bonds of PBD by the free radical addition reaction and "clicks" the desired oligopeptide sequence onto PEO-*b*-PBD, Figure 4.2.[14] Here, a simple gene-binding tripeptide sequence (L, L, L)-lysine-tryptophan-lysine (KWK), was synthesized by SPPS and used for grafting. It is known that KWK binds with DNA *via* two kinds of interactions: electrostatic interactions between the positively charged lysine residues and negatively charged phosphate DNA backbone, and the intercalation of aromatic tryptophan within DNA base pairs.[13] PEO_{75}-*b*-PBD_{25} with the weight fraction of PEO $w_{EO} \sim 0.7$, was used as the polymer scaffold. The free radical grafting has led to well-defined molecular architectures, sustaining the narrow molecular weight distribution of PEO-*b*-PBD precursor, synthesized by living anionic polymerization (polydispersity index ≤ 1.05). The grafting density can be controlled and tuned by changing the molar ratio between the thiol group and the PBD double bonds. In this communication, two combinative polymer-peptide hybrids with different grafting densities were synthesized: PEG_{75}-*b*-PBD_{25} with four peptide grafts, designated as **PP4**, and that with eight peptide grafts, designated as **PP8**.

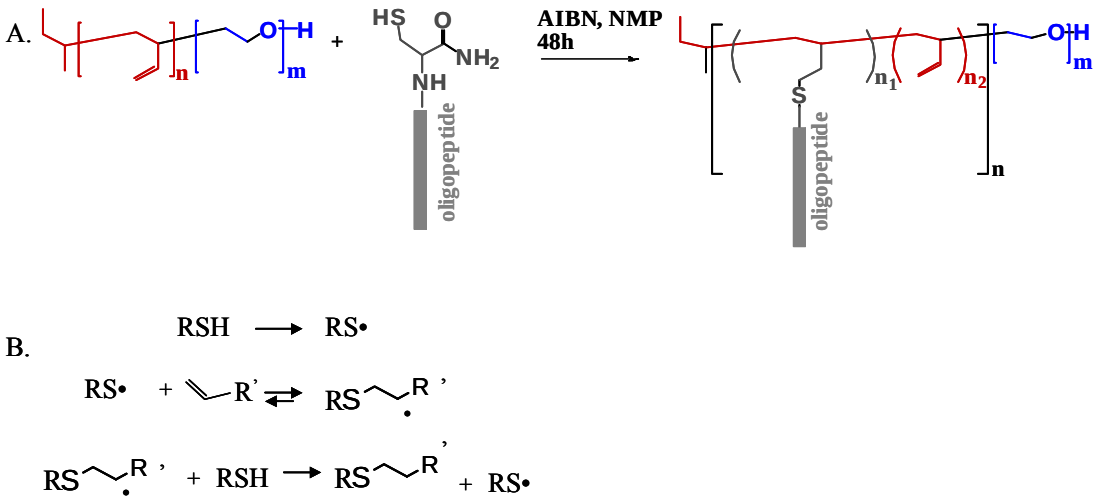

Figure 4.2 (A) Schematic representation and (B) the mechanism for grafting Cys-oligopeitpde onto PEG-*b*-PBD *via* free radical addition.

Long linear lambda phage DNA, λ-DNA, (double-stranded, 48 kbp, MW = 3 x 10^7 Da, contour length ~ 17 μm) in dilute aqueous solution (100 μg/mL DNA in 10 mM pH = 6.5 sodium cacodylate buffer containing 0.5 mM EDTA) was used for packaging studies. Complexes between DNA and KWK, **PP4** and **PP8** were prepared by simply mixing an equal volume of both components in the same buffer at room temperature. The final DNA concentration was set at 50 μg/mL throughout the studies in this report. The DNA-KWK, DNA-**PP4** and DNA-**PP8** complex structures were investigated by AFM on mica substrates. AFM is a well-established, reliable technique for studying DNA condensate structures, and it has been proven that absorbance of DNA condensates onto mica does not significantly change their structures.

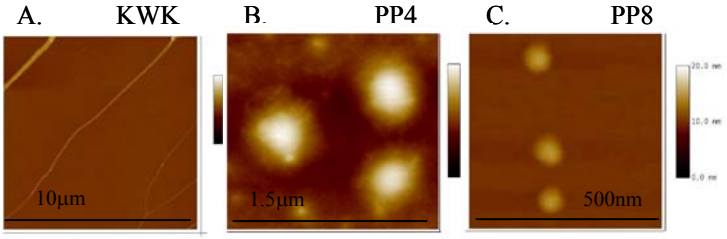

Figure 4.3 AFM imaging of DNA Complexes (A) KWK-DNA complex, (B) **PP4**-DNA complex, and (C) **PP8**-DNA complex in 10 mM sodium cacodylate buffer.

The free gene-binding tripeptide KWK is unable to induce λ-DNA compaction, even over a wide peptide concentration range. A typical DNA-KWK complex structure at 64 μM KWK visualized by AFM is shown in Figure 4.3A. No DNA compaction was observed. Instead, long extended thick bundles of DNA were found. The width of each bundle was measured to be between 5 to 10 nm. Considering an individual double stranded DNA is about 2 nm in width, the much thicker DNA bundles observed here indicate that each bundle was aggregated by at least two ds-λDNA. Upon Careful examination of some DNA bundles, single ds-λDNA (~ 2 nm width) can be seen to protrude from bundle stems, Figure 4.3A. Since KWK has only two lysines, with one at each end, it seems that this gemini-like dication tends to bridge DNA intermolecularly rather than inducing intramolecular compaction. This is consistent with Manning's electrolyte counterion theory that a counterion with higher than 3 valency is needed to induce DNA compaction.[15]

Grafting KWK onto the PEO-*b*-PBD scaffold has dramatically changed its complexation behaviour with DNA. Control experiments showed negligible interactions between DNA and the neutral amphiphilic PEO-*b*-PBD backbone with the linker cysteine

(where –SH is already converted into a thiol ether group) in dilute solutions. Therefore, for the polymer-KWK hybrids, **PP4** and **PP8**, their major interactions with DNA also originate from KWK. However, under the same stoichiometric KWK concentration at 64 μM, *i.e.* 16 μM **PP4** and 8 μM **PP8**, respectively, the polymer-KWK hybrids **PP4** and **PP8** are able to self-assemble with λ-DNA and condense the long DNA into compact structures, Figure 4.3B, C. For **PP4** with a lower density of KWK grafts, partial DNA compaction was observed by AFM, Figure 4.3B. Surrounding the compacted portion with an average size ~ 300 nm in diameter, a portion of uncompacted DNA molecule is visible in the periphery, Figure 4.3B. In comparision, **PP8** with twice as high grafting density is able to completely compact λ-DNA into much smaller nanostructures, Figure 4.3C. Statistical analysis demonstrated that such DNA-**PP8** complexes are all disk-like in shape and have rather narrow size distribution with an average diameter around 100 nm and height around 10 nm. This significant difference is probably due to that by clustering the oligopeptides, they can bind and bend/distort DNA in a more cooperative fashion into compact structures. With higher grafting density, the number of the oligopeptides being clustered by the polymer scaffold increases and they are brought to closer proximity, leading to more efficient DNA compaction. The disk-like DNA complex structure formation, instead of the more ordered toroids, may relate to the nature of KWK, which contains only two lysine residues separated by a bulky tryptophan spacer. The size of the PBD polymer scaffold may also exert some influence on the DNA complex formation. We speculate that by using different gene-binding oligopeptide sequences and a PBD-*b*-PEO scaffold with different degrees of

polymerization (*i.e.* molecular weight), different DNA complex structures can potentially be formed and tuned.

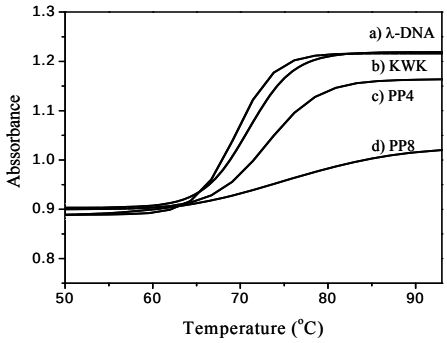

Figure 4.4 Melting profiles of DNA Complexes (a) 50mg/mL native λ-DNA, (b) DNA-KWK complex, (c) DNA-**PP4** complex, and (d) DNA-**PP8** complex in 10 mM sodium cacodylate buffer.

The stability of DNA-KWK, DNA-**PP4** and DNA-**PP8** complexes was investigated by DNA melting studies. Breakage of double-stranded DNA into single strands was monitored by an increase in the DNA absorbance at 260 nm, due to the disruption of hydrogen bonds between base pairs (i.e. hyperchromic effect). For native λ-DNA, T_m, the temperature at which 50% of ds-DNA dissociates, was determined to be 70°C, Figure 4.4a. For melting studies on DNA-KWK, DNA-**PP4** and DNA-**PP8** complexes, weak background absorbances have been subtracted to achieve accurate DNA absorbance measurements. By complexing with 64 μM KWK, T_m was only slightly shifted, showing no strong intramolecular stabilization on the double-stranded λ-DNA, Figure 4.4b. This is consistent with the AFM results, where only intermolecular DNA bridging by KWK but no DNA compaction was observed. In comparison, the DNA-**PP4**

complex where DNA was partially compacted showed a notable T_m shift to 75°C, Figure 4.4c. For the completely compacted DNA-**PP8** complex, a tremendously improved stability was shown. A much slower ds-DNA dissociation curve was observed, Figure 4.4d. Even by the upper limit of DNA melting studies in aqueous solution, 95°C, *i.e.* right below the boiling point of water, only a slight change in DNA absorbance was detected, suggesting that the majority of the double stranded DNA remained intact.

4.3 Conclusion

In conclusion, we have developed a novel and versatile combinative self-assembly approach for the packaging of genetic materials into stable, compact nanostructures. This approach is expected to provide new insights into how the spatial arrangement of gene-binding oligopeptides affects gene packaging, and serves as a promising new designing platform for synthetic gene vector development. For imminent future research, we are interested in exploring different gent-binding oligopeptide sequences, molecular architecture of the polymer scaffold, solution conditions (buffer, salt, pH) in order to gain further understanding and control over the combinative self-assembly behavior with genes.

4.4 Experimental

Materials

All chemicals were purchased from Sigma-Aldrich. KWK and CKWK were synthesized using standard Fmoc SPPS procedure with HOBT, HBTU and DIPEA couplings, followed by N-capping with acetic anhydride. Peptides were analyzed by ESI-MS and ^{1}H NMR before Grafting. Amphiphilic block copolymer PEO-*b*-PBD was synthesized by the well-established living anionic polymerization. The structure of PEO-

b-PBD was confirmed by NMR and its polydispersity (PDI) was determined to by Gel Permeation Chromatography to be ≤ 1.05.

λ-phage DNA 250 μg/mL stored in 10 mM Tris buffer/0.5mM EDTA was purchased from New England Biolabs. This DNA stock solution was dialyzed against 10 mM sodium cacodylate buffer (pH 6.5) containing 0.5 mM EDTA and further diluted to 100 μg/mL before use.

Grafting of Cysteine containing peptide to PEO-b-PBD

CKWK was grafted to PBD_{25}-*b*-PEO_{75} according to a procedure published elsewhere. Briefly, the reaction flask containing polymer (PBD_{25}-*b*-PEO_{75}), peptide (CKWK) and 2,2 azoisobutyronitrile (AIBN) was degassed for 30 minutes and then dry solvent, 1-methyl-2-pyrrolidinone (NMP), was added. Different molar ratios between $[C=C]_0$ and $[-SH]_0$ were used in order to achieve different grafting densities. $[C=C]_0/[-SH]_0/[AIBN]_0$ = 1:3:0.33 and 1:5:0.33 were used for **PP4** and **PP8** synthesis respectively. The resulting solution was heated to 70°C and stirred for 48 hours under argon atmosphere. AIBN was reinjected after 24 horus. After the reaction was complete, NMP was removed under vacuum. The crude product was re-dissolved in water and dialyzed against pure water to remove the unreacted peptides. The product was freeze-dried and collected for ^{1}H NMR and Gel Permeation Chromatography (GPC) analysis.

In ^{1}H NMR analysis on **PP4** and **PP8**, the characteristic signals of the grafted oligopeptide were observed at δ = 6.6-7.6 (tryptophan), and 8.1 ppm (NH); the signal of the thioether linkage $-CH_2-S-CH_2-$ arise at δ ~ 2.7 and 2.9 ppm. Resonances at δ = 4.8-5.6 ppm indicate that the conversion of PBD double bonds did not come to completion. The quantitative analysis of single intensities relative to that of PEG at δ ~ 3.6 ppm

reveals that **PP4** contains about 4 KWK units and 21 unreacted butadiene units, whereas **PP8** contains 8 KWK units and 17 unreacted butadiene units. GPC analysis showed a single narrow peak for PP4 and PP8 respectively, indicating the narrow polydispersity of the PBD-*b*-PEG scaffold has been preserved during the grafting process.

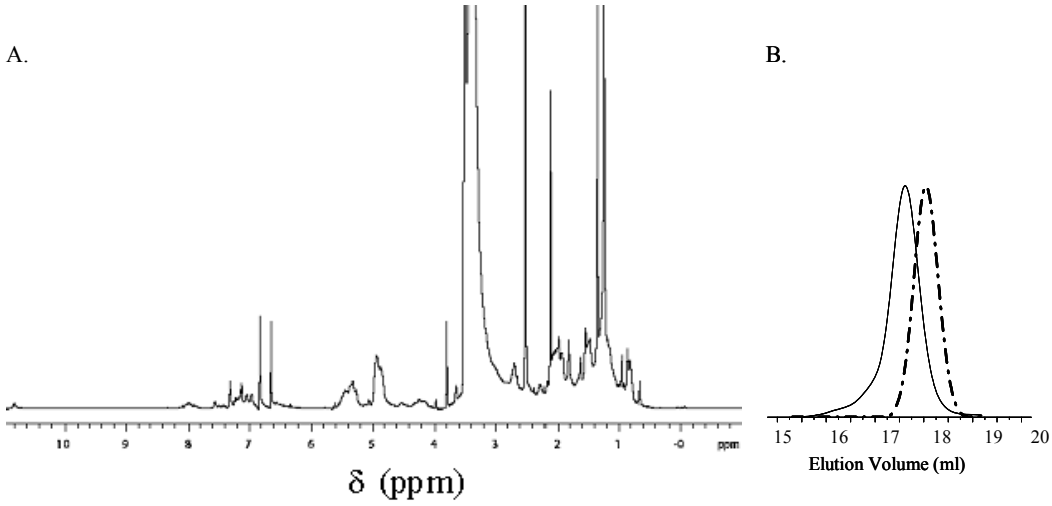

Figure 4.5 (A) Representative ^{1}H NMR spectrum (solvent: DMSO-d6) and (B) GPC chromatogram (eluent: NMP; solid line (PBD-*b*-PEO precursor, dashed line: **PP4**) of **PP4.**

Preparation of DNA complexes

DNA-KWK, DNA-**PP4** and DNA-**PP8** complexes were prepared by simply mixing of an equal volume of 100 μg/mL DNA and KWK, **PP4** and **PP8** with the desired concentrations in the 10 mM sodium cacodylate buffer. The mixture solution was vortexed for 30 seconds and allowed to equilibrate at room temperature for a few hours. The final DNA concentration was set at 50 μg/mL. For comparison purposes, the same final stoichiometric KWK concentration at 64 μM was used for the three complex

systems: 64 μM free KWK, 16 μM **PP4** that contains 16 x 4 = 64 μM KWK, and 8 μM **PP8** that contains 8 x 8 = 64 μM KWK.

Characterization of DNA complex structures by Atomic Force Microscopy

DNA complexes were deposited on freshly cleaved mica and then allowed to air dry. Tapping mode AFM imaging was performed on a Digital Instruments Nanoscope IIIa scanning probe microscope with a multimode head. Silicon probes (VistaProbes T300) with spring constant 40 N/m and resonant frequency 300 kHz was used to obtain all images.

DNA Melting Studies

DNA melting studies on native DNA and DNA complexes in 10 mM sodium cacodylate buffer were performed on a Carey 100 UV-Vis. DNA absorbance at 260 nm was monitored with temperature, slowly increasing from 25°C to 95°C at 1°C/minute heating rate. For DNA-KWK, DNA-**PP4** and DNA-**PP8** complexes, weak background absorbances from KWK, **PP4** and **PP8** were directly subtracted from the measurements, by using the corresponding KWK, **PP4** and **PP8** in 10 mM sodium cacodylate buffer as reference cells.

4.6 References

1. Mulligan, R. C., Gene transfer and gene therapy: principles, prospects, and perspective. *Etiology of Human Disease at the DNA Level* **1991**, 143–189.

2. Takahashi, K.; Tanabe, K.; Ohnuki, M.; Narita, M.; Ichisaka, T.; Tomoda, K.; Yamanaka, S., Induction of pluripotent stem cells from adult human fibroblasts by defined factors. *Cell* **2007,** 131, (5), 861-872.

3. Bonadio, J., Tissue engineering via local gene delivery. *Journal of Molecular Medicine* **2000,** 78, (6), 303-311.

4. Lehn, P.; Fabrega, S.; Oudrhiri, N.; Navarro, J., Gene delivery systems: Bridging the gap between recombinant viruses and artificial vectors. *Adv. Drug Deliv. Rev* **1998,** 30, 5-11.

5. Somiari, S.; Glasspool-Malone, J.; Drabick, J. J.; Gilbert, R. A.; Heller, R.; Jaroszeski, M. J.; Malone, R. W., Theory and in vivo application of electroporative gene delivery. *Molecular Therapy* **2000,** 2, (3), 178-187.

6. Bloomfield, V. A., DNA condensation. *Current Opinion in Structural Biology* **1996,** 6, (3), 334-341.

7. Gosule, L. C.; Schellman, J. A., Compact form of DNA induced by spermidine. *Science* **1976**, 333-335.

8. Hud, N. V.; Downing, K. H., Cryoelectron microscopy of lambda phage DNA condensates in vitreous ice: The fine structure of DNA toroids. *Proceedings of the National Academy of Sciences* **2001,** 98, (26), 14925-14930.

9. Laemmli, U. K., Characterization of DNA Condensates Induced by Poly (ethylene oxide) and Polylysine. *Proceedings of the National Academy of Sciences* **1975,** 72, (11), 4288-4292.

10. Radler, J. O.; Koltover, I.; Salditt, T.; Safinya, C. R., Structure of DNA-cationic liposome complexes: DNA intercalation in multilamellar membranes in distinct interhelical packing regimes. *Science* **1997,** 275, (5301), 810.

11. Kabanov, A. V.; Kabanov, V. A., DNA Complexes with Polycations for the Delivery of Genetic Material into Cells. *Bioconjugate Chemistry* **1995,** 6, (1), 7-20.

12. Kataoka, K.; Togawa, H.; Harada, A.; Yasugi, K.; Matsumoto, T.; Katayose, S., Spontaneous formation of polyion complex micelles with narrow distribution from antisense oligonucleotide and cationic block copolymer in physiological saline. *Macromolecules* **1996,** 29, (26), 8556-8557.

13. Smith, L. C.; Duguid, J.; Wadhwa, M. S.; Logan, M. J.; Tung, C. H.; Edwards, V.; Sparrow, J. T., Synthetic peptide-based DNA complexes for nonviral gene delivery. *Advanced Drug Delivery Reviews* **1998,** 30, (1-3), 115-131.

14. Geng, Y.; Discher, D. E.; Justynska, J.; Schlaad, H., Grafting Short Peptides onto Polybutadiene block poly (ethylene oxide): A Platform for Self Assembling Hybrid Amphiphiles. *Angewandte Chemie* **2006,** 118, (45), 7740-7743.

15. Manning, G. S., The molecular theory of polyelectrolyte solutions with applications to the electrostatic properties of polynucleotides. *Quarterly reviews of biophysics* **1978,** 11, (02), 179-246.

CHAPTER 5

EFFECT OF CLUSTERED PEPTIDE BINDING ON DNA CONDENSATION

Haley, J.; Kabiru, P. and Geng Y. *Molecular Biosystems*, **2010**, 6, 249-255

5.1 Abstract

DNA condensation *in-vitro* has been studied as a model system to reveal common principles underlying gene packaging in biology, and as the critical first step towards the development of non-viral gene delivery vectors. In this study, we use a bio-inspired approach, where small DNA-binding peptides are controllably clustered by an amphiphilic block copolymer scaffold to reveal the effect of clustered peptide binding on the energetics, size, shape and physical properties of DNA condensation *in-vitro*. This provides insights into the general architectural effect of gene-binding proteins on DNA condensation process. Moreover, the versatility afforded by regulating the clustering density and composition of peptides may provide a novel design platform for gene delivery application in the future.

5.2 Introduction

Condensation of long strands of DNA into compact, ordered structures is an important biological process for gene protection, storage and replication. This phenomenon has attracted tremendous interest to a broad spectrum of scientific communities. DNA condensation in-vitro has been pursued as a model system to study the phase transition phenemona of polyelectrolytes,[1] to reveal common principles underlying gene packaging in biology,[2, 3] and as the critical first step towards the development of non-viral gene delivery vectors.[4, 5] Historically, toroids—where loops of DNA double helix pack in hexagonal arrays—have attracted the most attention and are considered as the predominant *in-vitro* DNA condensate structure.[6-9] Occasionally, metastable rod-like DNA condensates have also been discovered and are attracting increasing interest in recent years.[10, 11]

A wide variety of materials have been explored as DNA condensing agents, ranging from the original small natural amines (*e.g.* spermidine and spermine)[6] and multivalent cations (e.g. $Co(NH_3)_6^{3+}$)[7] to much more complex materials, such as lipids,[12] crowding agents,[13] dendrimers,[14] peptides,[15, 16] polyamines,[17-20] and their corresponding block copolymers[21, 22]. For small natural amines and multivalent cations, the mechanism and pathway of their DNA condensation have been vigorously studied and are fairly well understood providing an invaluable foundation for later studies.[8, 23] However, other than certain viruses, most DNA condensation process in biological systems, especially in bacteria and eukaryotic cells, all involve much more complex DNA interactions with large molecules of proteins. Thus, relevant biological information that can be revealed by simple small condensing agents is rather limited. Moreover, simple agents are unlikely to provide sufficient stabilization and protection of DNA for practical applications. However, as condensing materials become more complex, elucidation of their complexation process with DNA becomes increasingly difficult. Polymeric condensing agents, for example, have attracted significant attention in recent years, due to their superior ability in compacting and stabilizing DNA, and to their chemical flexibility in functionalization towards improving gene delivery efficiency.[17-22] However, interactions between long polymer chains and DNA strands are much more complicated,[24] and the innate polydispersity of synthetic polymers further complicate the DNA complexation process. Lack of systematic understanding and precise control about their DNA condensation process represents a severe drawback.

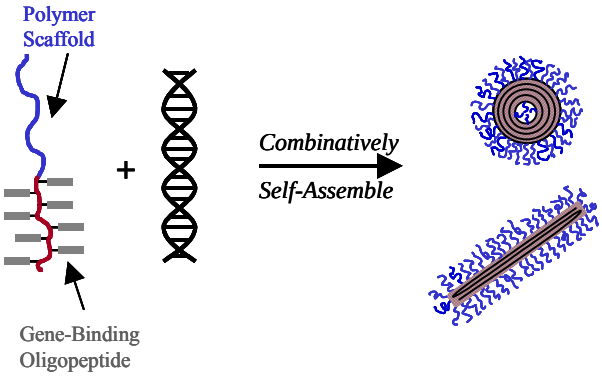

Figure 5.1 Combinative self-assembly of the block copolymer-peptide clustered hybrid with DNA into toroid and rod condensates.

We have recently developed a bio-inspired combinative self-assembly approach that can efficiently condense and package DNA in to nanoparticles.[25] Small oligopeptides that emulate the active nucleotide binding site of DNA compactions proteins can provide direct insights into DNA-protein interactions, and when compared to large whole proteins, have the advantages of high efficiency in functionality, less antigenicity, flexibility, and precision in the sequence design.[15] When grafted onto the hydrophobic segment of a block copolymer scaffold, a clustered spatial arrangement of the peptides is created towards DNA binding, Figure 5.1. Synthetic polymers have been used as scaffolds in the past to create multivalent ligands with controlled density, to probe the mechanism of receptor clustering at cell surface and cell signaling pathways.[26] In this report, we elucidate the effect of controlled peptide clustering on the energetics, size, shape, as well as physical properties of DNA condensation *in-vitro*. This provides insights into the general architectural effect of gene-binding proteins on DNA condensation and packaging processes. Moreover, the versatility afforded by regulating

the clustering density and composition of the peptides may provide a novel design platform for gene delivery applications in the future.

5.3 Results and Discussion

Model gene-binding oligopeptides, **KWK$_n$** (K = lysine, W = tryptophan), with different numbers of lysine residues (n = 2 or 4) were used for this study, and they were controllably grafted onto the hydrophobic polybutadiene segment of an amphiphilic poly(ethylene glycol)-*block*-polybutadiene (PEG_{93}-b-PBD_{14}) block copolymer scaffold at different grafting densities, *i.e.* either with four peptide grafts or eight peptide grafts, *via* an established modular peptide grafting route.[28] The peptide grafted polymer hybrids are designated as **PP** series, where **PP12** and **PP24** represent the polymer-peptide hybrids with four and eight **KWK$_2$** grafted, respectively and **PP20** and **PP40** with four and eight **KWK$_4$** grafted, respectively. Literature shows that **KWK$_n$** peptides bind to DNA through two kinds of interactions: electrostatic neutralization between the positively charged amino group of lysine (N) and the negatively charged phosphate DNA backbone (P), and the hydrophobic intercalation of aromatic tryptophan within the DNA base pairs.[27, 28] Such attractions between **KWK$_n$** peptides and DNA are expected to be the driving force for the complexation of the polymer-peptide hybrids with DNA, as control experiments reveal negligible interactions between DNA and the neutral block copolymer scaffold alone.[25]

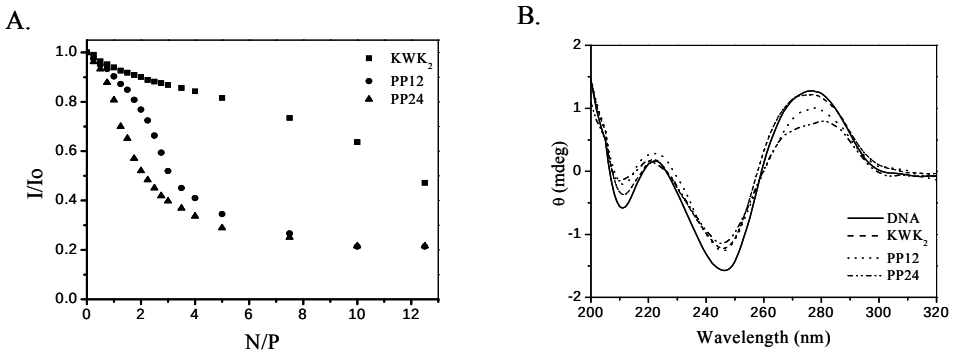

Figure 5.2 Characterization of the binding and conformational change of λ-DNA complexation with **KWK_2**, **PP12** and **PP24**. (A) EB displacement assay on DNA binding; (B) DNA conformation by CD analysis.

Five or more lysine residues are generally required in an oligopeptide sequence to condense DNA.[15, 16] With only three lysine residues **KWK_2** alone exhibited fairly low DNA binding affinity from the ethidium bromide (EB) displacement assay, Figure 5.2A. In the EB displacement assay, binding of an agent to DNA would displace the intercalated EB and subsequently quench the fluorescence caused by the EB-DNA complex. Figure 5.2A shows that free **KWK_2** can only weakly quench fluorescence over a wide range of N/P values. Even in large excess, at N/P =12, only 40% of quenching ($I/I_0 \sim 0.6$) could be achieved by free **KWK_2**. However, when **KWK_2** was clustered into proximity by the polymer PEG_{93}-*b*-PBD_{14} scaffold, **PP12** and **PP24** quenched the fluorescence much more efficiently at the same stoichiometeric N/P of free **KWK_2**, and both were able to achieve nearly complete quenching ($I/I_0 \leq 0.3$), Figure 5.2A. At higher grafting density, where more oligopeptides were clustered into closer proximity along the polymer scaffold, **PP24** – with eight peptides grafted – demonstrated more enhanced DNA binding than **PP12** – with four peptides grafted. It seems that the clustered

oligopeptide array gathered by the polymer scaffold can recognize the DNA double helix in a positive cooperative manner and thus can significantly strengthen the DNA binding. The surrounding overall hydrophobic environment generated by the PBD polymers may also contribute to the strengthened DNA binding effect.

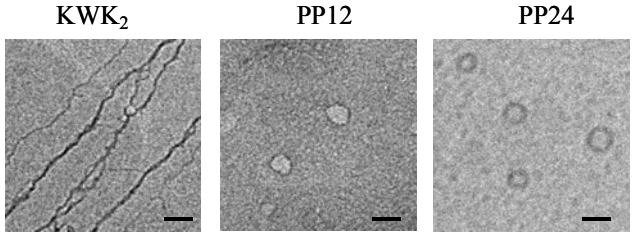

Figure 5.3 Representative TEM micrographs of λ-DNA condensates by **KWK_2**, **PP12** and **PP24** at N/P = 12. Scale bar is 50 nm.

Conformational changes in the DNA double helix induced by the binding of **KWK_2**, **PP12** and **PP24** were monitored by circular dichroism (CD), Figure 5.2B. The CD spectrum of native λ-DNA shows a typical B-form conformation, which is composed of four major peaks in the UV-Vis region: a negative 210 nm peak, a positive 220 nm peak, a negative 245 nm peak and a positive 280 nm peak.[29] Transition of the DNA conformation from the B-form to the less compact C-form, which is characterized by a decrease in the intensity of the positive 280 nm peak, is commonly found in condensed DNA systems, such as in virus heads and nucleosomes.[29, 30] With free **KWK_2**, negligible intensity change at the 280 nm peak was observed and the B-form of DNA conformation largely remained intact. **PP12** and **PP24**, on the other hand, provoked much more significant change in the 280 nm peak, indicating a partial B-to-C transition has occurred is such polymer-peptide clustered systems, and the higher the clustering density, the more

dramatic the conformational change. It seems that the clustered peptide-DNA binding can cooperatively distort and loosen the DNA double helix into the less compact C form, which facilitates DNA condensation.

Transmission electron microscopy (TEM) analysis reveals distinctly different DNA complexation phenomena between free **KWK_2** and it polymer clustered **PP12** and **PP24**, Figure 5.3. No DNA compaction, but rather exclusively extended DNA bundles, was observed for free **KWK_2**, even at a large excess of lysine at N/P = 12. The bundles are 10-20 nm thick and each contains 5-10 λ-DNA strands, considering the individual ds-DNA is ~ 2nm in width. With just three lysines, free **KWK_2** can not compact DNA, but its triple valency is able to bridge different DNA strands together. In sharp contrast, when **KWK_2** was clustered by the polymer scaffold, **PP12** and **PP24** were observed to condense DNA into toroidal structures, and the clustering density exhibited a strong effect on the condensation process. With low clustering density, **PP12** gave rise to ill-defined nucleation loops with an average large diameter of 80 nm at the same stoichiometeric N/P 12. However, no subsequent winding of DNA strands around the nucleation loops, *i.e.* toroid growth, was fostered, as floppy DNA strands surrounding the loops are clearly visible from the TEM images. As the peptide clustering density doubles in **PP24**, the toroid loop size was notably reduced and the subsequent toroid growth efficiently promoted. TEM analysis shows well-defined DNA toroids that have the average diameter of 50 nm and thickness of 20 nm at N/P = 12.

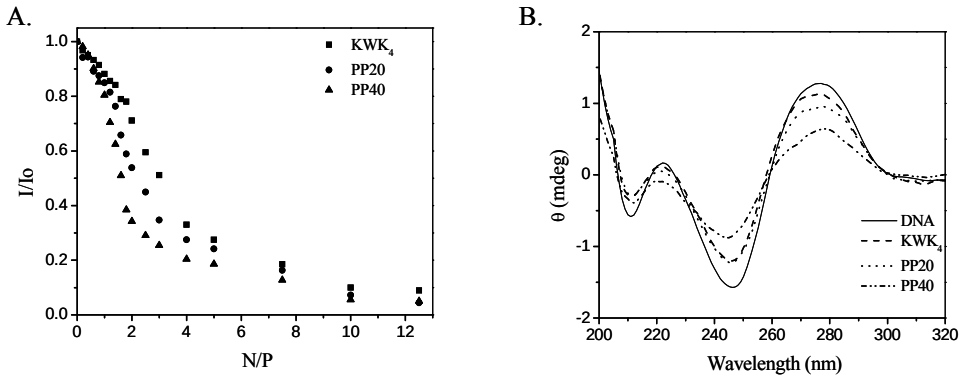

Figure 5.4 Characterization of the binding and conformational change of λ-DNA complexation with **KWK_4**, **PP20** and **PP40**. (A) EB displacement assay on DNA binding; (B) DNA conformation by CD analysis.

It is well known that the formation of DNA toroid condensates proceeds through two stages – the initial nucleation loop stage, followed by growth.[31] Looping of a semiflexible DNA chain is a spontaneous, diffusion-limited process, and the ease and size largely depend on the flexibility and bending energy of the DNA chain, as well as the ability of the condensing agents to anneal and stabilize the loop.[32] The cooperative, clustered binding of **KWK_2** seems to be able to significantly lower the bending energy of DNA and promote the formation of nucleation loops. With low grafting density, **PP12**, however, can not sufficiently reduce the DNA helix-helix association energy to foster the further winding of DNA strands around the loop. As the clustering density increases, **PP24** can not only overcome the extra strain associated with the smaller nucleation loops, it is also sufficient to promote the further growth of toroids. It appears that for oligopeptides with weak DNA affinity, clustered binding shifts the DNA compelxation process from intermolecular bridging to intramolecular toroidal compaction, and the

clustering density has a strong impact on the energetics and dimension of the DNA condensation process.

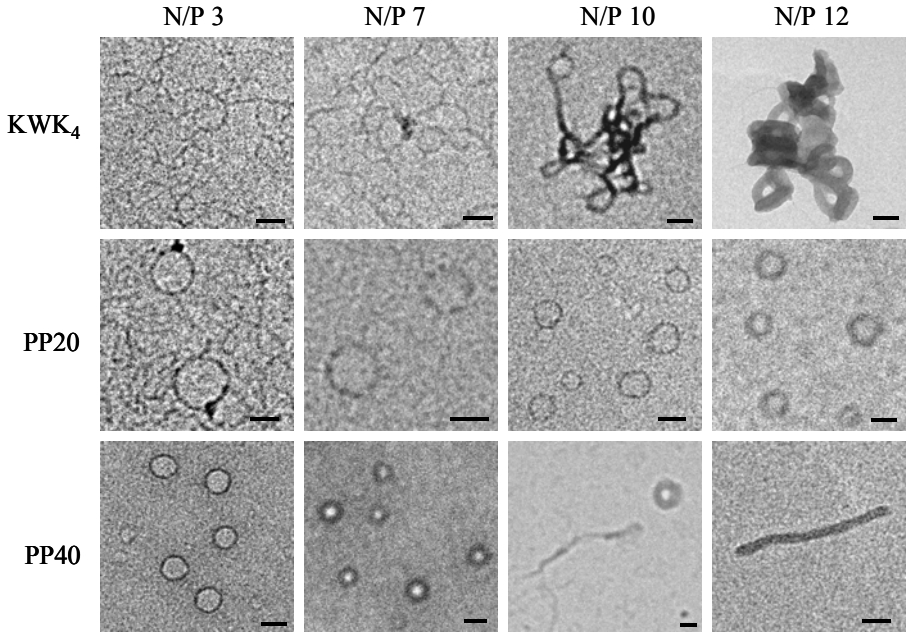

Figure 5.5 Representative TEM micrographs of λ-DNA condensates by **KWK_4**, **PP20** and **PP40** at increasing N/P from 3 to 12. Scale bar 50 nm.

To reveal the effect of clustered binding on DNA condensation for peptides with strong DNA affinity, **KWK_4** with five lysine residues and its corresponding polymer clustered hybrids, **PP20** – with four peptides grafted, and **PP40** – with eight peptides grafted, were studied respectively. Incorporation of more lysine residues is well known to enhance the binding between the peptide and DNA.[16] Indeed, EB displacement assay shows that **KWK_4** quenched the fluorescence much more efficiently than **KWK_2** and reached near complete binding as N/P increased to 10, Figure 5.4A. CD analysis also shows that the binding of **KWK_4** to DNA notably reduced the intensity of the 280 nm peak and induced a partial B-to-C conformational change in λ-DNA, Figure 5.4B. Like

KWK_2, clustering by the polymer scaffold nonetheless enhanced the DNA binding and provoked more pronounced B-to-C conformational change, and the higher the clustering density, the stronger the effect.

TEM studies confirmed that free **KWK_4** is able to condense DNA into compact structures, Figure 5.5. Intertwined aggregates of toroids were observed as the primary DNA condensate structure. It appears that initial low N/P values, **KWK_4** can simultaneously promote both intermolecular DNA aggregation and the formation of toroid nucleation loops, which progressively grew into intertwined full toroids. When **KWK_4** was clustered by the polymer scaffold, **PP20** produced discrete toroids without aggregation. Distinct nucleation loops with an average diameter of 70 nm were observed at N/P = 3, and higher N/P values further reduced the toroid loop size and promoted toroid growth. At N/P = 12, dispersed, well-defined toroids with average diameter of 45 nm and thickness of 15 nm were found as the exclusive DNA condensate structure. Compared to free **KWK_4**, which does not seem to differentiate intramolecular DNA compaction from the intermolecular DNA association process, the polymer-peptide clustered **PP20** must be able to lower the bending energy of DNA chains much more efficiently, so that it exclusively favors the intramolecular toroidal DNA condensation route. With higher clustering density in **PP40**, the difference in DNA condensation process becomes even more dramatic from the free **KWK_4**. **PP40** produces much smaller toroid loops with average diameter of 50 nm at N/P = 3, and fostered fast toroid growth to 25 nm in thickness at N/P = 7. Starting from N/P = 10, rod-like DNA condensate structures began to emerge, and upon reaching N/P = 12, a significant population (~50%) of well-defined rods with average length of 200 nm and width 15 nm

were observed. The rods were quite stable in solution as there was no apparent population change with time. This is surprising, considering studies with small condensing agents in literature suggest that DNA rod condensates are generally unstable, and would quickly convert to toroids with time. Controlling the morphology of DNA condensates between toroids and rods has been quite difficult,[11] and only in the presence of an alcohol solvent that destabilizes the DNA double helix, or with special bacterial chromatin proteins that can induce pronounced kinks in the DNA double helix, has higher populations of rods been reported.[10, 33] Here, the finding of a significant population of stable rods induced by **PP40** suggests that at sufficiently high density, the cooperative, clustered binding can sharply bend the DNA double helix into rod-forming kinks, as well as help stabilize the rods once formed. The entanglement nature of the polymer scaffold may also contribute to the stabilization of the rod DNA condensates. Thus, in the event of oligopeptides with strong DNA affinity, such as **KWK_4**, we show that peptide clustering by a polymer scaffold can alter the DNA condensation pathway from intertwined toroid aggregates to discrete toroid or rod DNA condensates. Controlled density plays a vital role in the clustering effect, which not only determines the size and dimension of DNA condensate structure, but also the shape transition from toroids to rods.

To evaluate the effect of the polymer scaffolded peptide clustering on physical properties of the resultant DNA condensates, melting and nuclease degradation studies were carried out to analyze their thermal and biological stability, respectively, Figure 5.6 In the melting study, dissociation of double-stranded DNA into single strands was monitored by an increase in absorbance of 260 nm, due to disruption of hydrogen bonds

between base pairs with raising temperature (*i.e.* hyperchromic effect). Figure 5.6A shows that compared to naked DNA, condensation with **KWK_4** notably shifted the DNA dissociation curve to higher T_m, the temperature at which 50% ds-DNA dissociates, and reduced the degree of change in absorbance, indicating enhanced DNA stabilization against double-strand breakage. When clustered by the polymer scaffold, **PP20** and **PP40** further stabilized DNA in comparison to free **KWK_4,** by shifting the DNA dissociation curve to even higher temperatures and more reduced absorbance changes, and the higher the clustering density, the more significant the enhancement. Even at the upper limit of DNA melting studies in aqueous solution, *i.e.* 95°C, which is just below the boiling point of water, the majority of the ds-DNA remained intact.

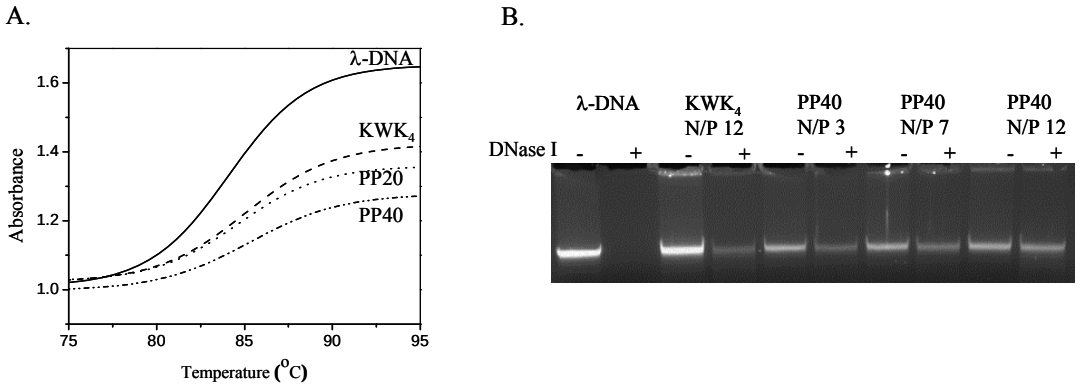

Figure 5.6 Stability of DNA complexes against thermal and biodegradation. (A) Melting profiles of native l-DNA and its complexes with **KWK_4**, **PP20** and **PP40**; (B) DNaseI protection assay (-) before treatment and (+) after treatment

DNA is also prone to nuclease degradation in biofluids, which represents a major challenge for gene delivery. To assess their resistance against DNase degradation, naked λ-DNA, DNA condensates with **KWK_4** and the polymer-peptide clustered **PP40**, were

incubated with DNaseI for 30 minutes and the integrity of the DNA before and after treatment was analyzed by agarose gel electrophoresis, Figure 5.6B. For naked λ-DNA, no intact DNA band could be detected after DNaseI treatment, indicating that the DNA has been completely degraded in to small fragments that are beyond the detection limit. For DNA-**KWK_4** condensates, even at high N/P =12, only a faint intact DNA band was observed after DNase treatment. Comparison between the DNA band intensity before and after DNase treatment shows that only a small fraction of DNA was preserved, and **KWK_4** itself does not provide sufficient protection for DNA. However, the polymer-peptide clustered **PP40** demonstrated much more enhanced DNA protection against nuclease degradation. As more **PP40** was used in DNA condensation, the intensity of the intact DNA band after treatment continuously increased with N/P, and at N/P=12, the DNA band before and after DNase treatment was measured to be nearly the same, suggesting that the integrity of the DNA has been largely preserved. We speculate that the superior protection of the block copolymer-peptide clustered hybrids originates from two aspects – highly efficient DNA compaction by the clustered peptides inside the core, and the surrounding dense, stealthy PEG shell that prevents the deposition and degradation of the nuclease. Apparently, the polymer-peptide clustered hybrids here have inherited all the general advantages in DNA stabilization and protection that are associated with polymeric systems, and the PEG shell can be further conjugated with a wide variety of functional groups to foster specific targeting, endosomal release and nuclear transport for future gene delivery applications.

5.4 Conclusions

In this study, we demonstrate that the peptide clustering can controllably alter the pathway and morphology of DNA condensation *in vitro*. Moreover, such peptide clustering by block copolymer scaffolds also significantly improves the DNA stability against breakage and DNase bio-degradation. The study here has comprehensively elucidated the general architectural effect of the clustered peptide binding on DNA condensation, as well as having provided a versatile new approach to tailor and optimize synthetic gene delivery vector design.

5.5 Experimental

Materials

λ-DNA in 10mM Tris buffer was purchased from New England Biolabs (Ipsich, MA). All chemicals and solvents were purchased from Sigma-Aldrich. Oligopetides were synthesized by the standard Fmoc Solid Phase Peptide Synthesis procedure, using HOBT, HBTU and DIPEA couplings, followed by N-capping with acetylation and C-capping with amidation. Each peptide was analyzed by ESI-MS and ^{1}H NMR before Grafting. Amphiphilic block copolymer PEG_{93}-*b*-PBD_{14}, where the subscripts denote the average number of repeating units, was prepared by the sequential living anionic polymerization of buta-1,3-butadiene and ethylene oxide.[34]

Grafting of model gene-binding KWKn peptides onto PEG-b-PBD

For grafting purpose, Cysteine that contains a thiol group was attached to **KWK_n** oligopeptides as the linker terminus. $CKWK_n$ were grafted to PEG_{93}-*b*-PBD_{14} according to a modular procedure published elsewhere, utilizing the free radical addition of the thiol group onto the double bonds of PBD.[25, 35] The grafting density, *i.e.* the percentage of the

PBD double bonds grafted with peptides, can be tuned by changing the molar ratio between the reacting thiol groups and double bonds, and the peptides are expected to be randomly linked along the PBD chain.[35]

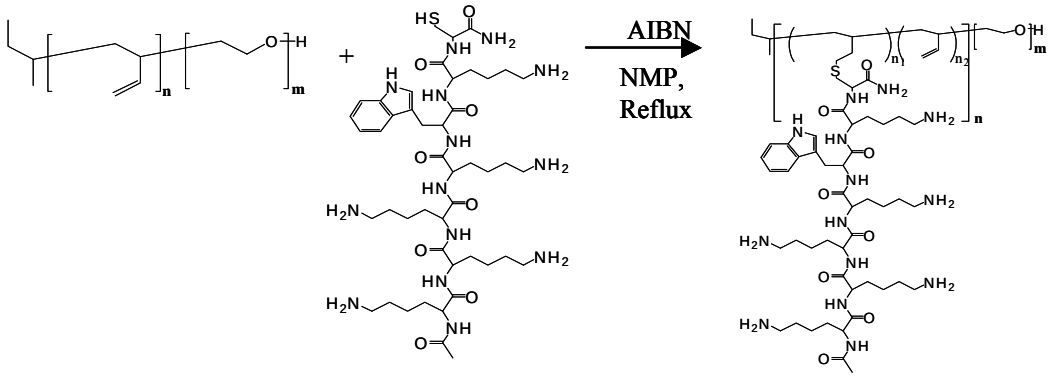

Figure 5.7 Grafting of oligopeptides onto the PEG-*b*-PBD via free radical addition route.

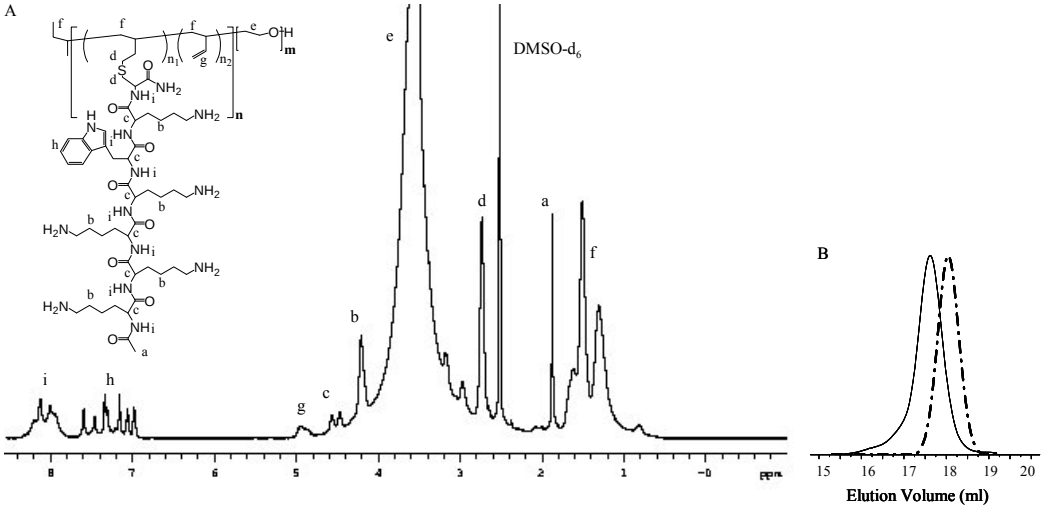

Figure 5.8 Characterization of the polymer-peptide hybrid by ^{1}H NMR and GPC. (A) Representative ^{1}H NMR (solvent: DMSO d6) of **PP40** and (B) GPC (eluent: NMP) of PEG-*b*-PBD precursor (solid line) and **PP40** (dashed line).

EtBr Displacement Assay

λ-DNA in Tris buffer (20ug/mL) was incubated with EtBr (0.8ug/mL) for 1 hour prior to analysis. The fluorescent intensity of the DNA-EtBr complex was measured using a Jobin Yvon FluoroMax-3 Fluorimeter (excitation: 520nm, emission: 590nm). Measured concentrated **KWK_n** or their polymer clustered hybrids was then titrated into the DNA-EtBr solution, and the corresponding fluorescence at different N/P was determined.

Circular Dichroism Analysis

CD spectra were recorded using Jasco J-715 spectropolarimeter, at the far-UV region (200-320 nm) and with a scanning speed of 50 nm/min. A total of four scans were accumulated, and temperature was maintained at 25^{o}C. DNA complexes with **KWK_n** or their polymer clustered hybrids in Tris buffer were set the concentration of 50 ug/ml and N/P 0.5 for the CD studies. Weak background absorbance from the buffer and condensing agents were directly subtracted from the measurements.

TEM Imaging

λ-DNA complexes with **KWK_n** and their polymer clustered hybrids were prepared by mixing an equal volume of DNA (10ug/mL) with the condensing agents at desired N/P in 1X TE buffer (10 mM Tris-Cl, 1 mM EDTA, pH 7.0). The complex solution was then vortexed for 30 seconds and allowed to equilibrate at room temperature for 2 hours. The complex sample was then deposited onto the glow discharged formvar coated copper grids and stained with 2% uranyl acetate for 1 minute. The grids were blotted and then air-dried for TEM imaging on a 200kV Tecnai 20 Transmission Electron Microscope at a magnification of 10,000X.

DNA Melting Study

Melting profiles of native λ-DNA and the DNA complexes with **KWK_n** or their polymer clustered hybrids (50 μg/ml, N/P 0.5) were obtained by monitoring their absorbance at 260nm with a Carey 100 UV-Vis Spectrophotometer. Samples were heated from 30°C to 95°C with a heating rate of 1°C/min. Weak background absorbance from the buffer and condensing agents were directly subtracted from the measurements.

DNaseI Degradation Assay

DNaseI (1 unit) in 10X digestion buffer was added to 0.02ml, 10ug/mL DNA and DNA complex samples (0.2ug DNA). The samples were incubated at 37°C for 15 minutes, followed by inactivation with 4uL of 25mM EDTA at room temperature for 10 minutes. Finally, 7.5uL of 100mg/mL heparin was added and incubated at room temperature for 2 hours to release DNA for gel electrophoresis analysis (0.8% agarose gel, 1X TAE running buffer, 0.5ug/mL ethidium bromide, 100V, 1hour).

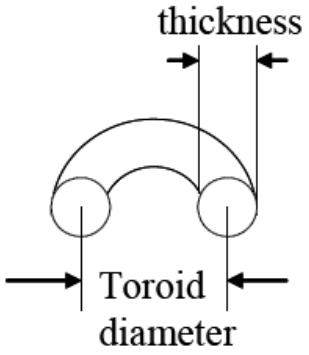

Figure 5.9 Definition of the diameter and thickness of toroids

5.6 References

1. Manning, G. S., The molecular theory of polyelectrolyte solutions with applications to the electrostatic properties of polynucleotides. *Quarterly reviews of biophysics* **1978,** 11, (02), 179-246.

2. Klimenko, S. M.; Tikchonenko, T. I.; Andreev, V. M., Packing of DNA in the head of bacteriophage T2. *Journal of Molecular Biology* **1967,** 23, (3), 523-533.

3. Cerritelli, M. E.; Cheng, N.; Rosenberg, A. H.; McPherson, C. E.; Booy, F. P.; Steven, A. C., Encapsidated conformation of bacteriophage T7 DNA. *Cell* **1997,** 91, (2), 271-280.

4. Luo, D.; Saltzman, W. M., Synthetic DNA delivery systems. *Nature biotechnology* **2000,** 18, (1), 33-37.

5. Mintzer, M. A.; Simanek, E. E., Nonviral vectors for gene delivery. *Chemical reviews* **2008,** 109, (2), 259-302.

6. Gosule, L. C.; Schellman, J. A., Compact form of DNA induced by spermidine. *Science* **1976**, 333-335.

7. Widom, J.; Baldwin, R. L., Cation induced toroidal condensation of DNA studies with Co (NH 3) 6 3þ. *Journal of Molecular Biology* **1980,** 144, 431-453.

8. Conwell, C. C.; Vilfan, I. D.; Hud, N. V., Controlling the size of nanoscale toroidal DNA condensates with static curvature and ionic strength. *Proceedings of the National Academy of Sciences* **2003,** 100, (16), 9296-9301.

9. Hud, N. V.; Downing, K. H.; Balhorn, R., A Constant Radius of Curvature Model for the Organization of DNA in Toroidal Condensates. *Proceedings of the National Academy of Sciences* **1995,** 92, (8), 3581-3585.

10. Arscott, P. G.; Ma, C.; Wenner, J. R.; Bloomfield, V. A., DNA condensation by cobalt hexaammine (III) in alcohol-water mixtures: dielectric constant and other solvent effects. *Biopolymers* **1995,** 36, (3), 345-64.

11. Vilfan, I. D.; Conwell, C. C.; Sarkar, T.; Hud, N. V., Time study of DNA condensate morphology: implications regarding the nucleation, growth, and equilibrium populations of toroids and rods. *Biochemistry* **2006,** 45, (26), 8174-8183.

12. Radler, J. O.; Koltover, I.; Salditt, T.; Safinya, C. R., Structure of DNA-cationic liposome complexes: DNA intercalation in multilamellar membranes in distinct interhelical packing regimes. *Science* **1997,** 275, (5301), 810.

13. Laemmli, U. K., Characterization of DNA Condensates Induced by Poly (ethylene oxide) and Polylysine. *Proceedings of the National Academy of Sciences* **1975,** 72, (11), 4288-4292.

14. Haensler, J.; Szoka Jr, F. C., Polyamidoamine cascade polymers mediate efficient transfection of cells in culture. *Bioconjugate chemistry* **1993,** 4, (5), 372-379.

15. Smith, L. C.; Duguid, J.; Wadhwa, M. S.; Logan, M. J.; Tung, C. H.; Edwards, V.; Sparrow, J. T., Synthetic peptide-based DNA complexes for nonviral gene delivery. *Advanced Drug Delivery Reviews* **1998,** 30, (1-3), 115-131.

16. Wadhwa, M. S.; Collard, W. T.; Adami, R. C.; McKenzie, D. L.; Rice, K. G., Peptide-Mediated Gene Delivery: Influence of Peptide Structure on Gene Expression. *Bioconjugate chemistry* **1997,** 8, 81-88.

17. Wagner, E.; Zenke, M.; Cotten, M.; Beug, H.; Birnstiel, M. L., Transferrin-polycation conjugates as carriers for DNA uptake into cells. *Proceedings of the National Academy of Sciences of the United States of America* **1990,** 87, (9), 3410.

18. Choi, Y. H.; Liu, F.; Park, J. S.; Kim, S. W., Lactose-poly (ethylene glycol)-grafted poly-L-lysine as hepatoma cell-targeted gene carrier. *Bioconjugate Chemistry* **1998,** 9, (6), 708-718.

19. Mislick, K. A.; Baldeschwieler, J. D.; Kayyem, J. F.; Meade, T. J., Transfection of folate-polylysine DNA complexes: evidence for lysosomal delivery. *Bioconjugate chemistry* **1995,** 6, (5), 512-515.

20. Zauner, W.; Ogris, M.; Wagner, E., Polylysine-based transfection systems utilizing receptor-mediated delivery. *Advanced drug delivery reviews* **1998,** 30, (1-3), 97-113.

21. Kataoka, K.; Togawa, H.; Harada, A.; Yasugi, K.; Matsumoto, T.; Katayose, S., Spontaneous formation of polyion complex micelles with narrow distribution from antisense oligonucleotide and cationic block copolymer in physiological saline. *Macromolecules* **1996,** 29, (26), 8556-8557.

22. Kakizawa, Y.; Kataoka, K., Block copolymer micelles for delivery of gene and related compounds. *Advanced Drug Delivery Reviews* **2002,** 54, (2), 203-222.

23. Bloomfield, V. A., DNA condensation by multivalent cations. *Biopolymers* **1997,** 44, (3), 269-282.

24. Nayvelt, I.; Thomas, T.; Thomas, T. J., Mechanistic Differences in DNA Nanoparticle Formation in the Presence of Oligolysines and Poly-L-lysine. *Biomacromolecules* **2007,** 8, (2), 477-484.

25. Haley, J.; Li, X.; Marshall, N.; Locklin, J.; Geng, Y., DNA packaging via combinative self-assembly. *Molecular BioSystems* **2008,** 4, (6), 515-517.

26. Cairo, C. W.; Gestwicki, J. E.; Kanai, M.; Kiessling, L. L., Control of multivalent interactions by binding epitope density. *J. Am. Chem. Soc* **2002,** 124, (8), 1615-1619.

27. Pörschke, D.; Ronnenberg, J., The reaction of aromatic peptides with double helical DNA. Quantitative characterisation of a two step reaction scheme. *Biophysical Chemistry* **1981,** 13, (4), 283-290.

28. Mascotti, D. P.; Lohman, T. M., Thermodynamics of single-stranded RNA and DNA interactions with oligolysines containing tryptophan. Effects of base composition. *Biochemistry* **1993,** 32, (40), 10568-10579.

29. Baase, W. A.; Johnson, W. C., Circular dichroism and DNA secondary structure. *Nucleic Acids Research* **1979,** 6, (2), 797.

30. Boettcher, C.; Endisch, C.; Fuhrhop, J. H.; Catterall, C.; Eaton, M., High-Yield Preparation of Oligomeric C-Type DNA Toroids and Their Characterization by Cryoelectron Microscopy. *JOURNAL-AMERICAN CHEMICAL SOCIETY* **1998,** 120, 12-17.

31. Hud, N. V.; Vilfan, I. D., TOROIDAL DNA CONDENSATES: Unraveling the Fine Structure and the Role of Nucleation in Determining Size. *Annu Rev Biophys Biomol Struct* **2005,** 34, 295-318.

32. Jun, S.; Bechhoefer, J.; Ha, B. Y., Diffusion-limited loop formation of semiflexible polymers: Kramers theory and the intertwined time scales of chain relaxation and closing. *EPL (Europhysics Letters)* **2003,** 64, 420.

33. Sarkar, T.; Conwell, C. C.; Harvey, L. C.; Santai, C. T.; Hud, N. V., Condensation of oligonucleotides assembled into nicked and gapped duplexes: potential structures for oligonucleotide delivery. *Nucleic Acids Research* **2005,** 33, (1), 143.

34. Forster, S.; Kramer, E., Synthesis of PB-PEO and PI-PEO block copolymers with alkyllithium initiators and phosphazene base t-BuP4. *Macromolecules* **1999,** 32, 2783-2785.

35. Geng, Y.; Discher, D. E.; Justynska, J.; Schlaad, H., Grafting short peptides onto polybutadiene-b-poly (ethylene oxide): a platform for self-assembling hybrid amphiphiles. *Angew Chem Int Ed* **2006,** 45, 7578–7581.

CHAPTER 6

ROLE OF DNA IN CONDENSATION AND COMBINATIVE SELF-ASSEMBLY

Haley, J. and Geng Y. *Chemical Communications*, **2010**, 46, 955-957

6.1 Abstract

We reveal the vital role of DNA topology and conformation in directing the combinative self-assembly and condensation pathway and morphology.

6.2 Introduction

The phenomenon of DNA condensation into nanostructures has long been studied as a model system to reveal the common principles underlying gene packaging in biology.[1] It is also the critical first step towards the development of artificial gene vectors, as studies show that the size and shape of DNA condensates strongly influence their transfection efficiency.[2-4] Moreover, condensation can be potentially used in the broader DNA nanotechnology. In recent years, intensive effort has focused on developing synthetic materials for DNA complexation and delivery.[5-7] Few studies, however, sought to elucidate the role that DNA itself may play in the condensation process.[8, 9] Although limited studies show that DNA topology and conformation can be recognized in complexation processes, the systematic functional role of DNA in determining the condensation pathway and morphology remains unclear.

We have recently developed a combinative self-assembly approach that can efficiently condense and package DNA.[10, 11] We use an amphiphilic block copolymer as a scaffold to create a clustered array of small gene-binding peptide grafts that emulate the active binding site of gene-compaction proteins.[10, 11] Such polymer-peptide hybrids are able to combinatively self-assemble with DNA molecules and condense DNA into nanostructures.[10, 11] This bio-inspired approach can not only reveal the insights into the relevant DNA condensation processes found in nature, but it can also provide a versatile design platform for developing artificial gene vectors as well as DNA-based multi-

component supramolecular assemblies. Previously, we have investigated the structural effect of the polymer-peptide hybrid on the DNA condensation process.[10, 11] In this study, we pursue a new direction and reveal the vital role of DNA itself in condensation and combinative self-assembly by systematically investigating how DNA topology and conformation affect the pathway and morphology of such processes,Figure 6.1.

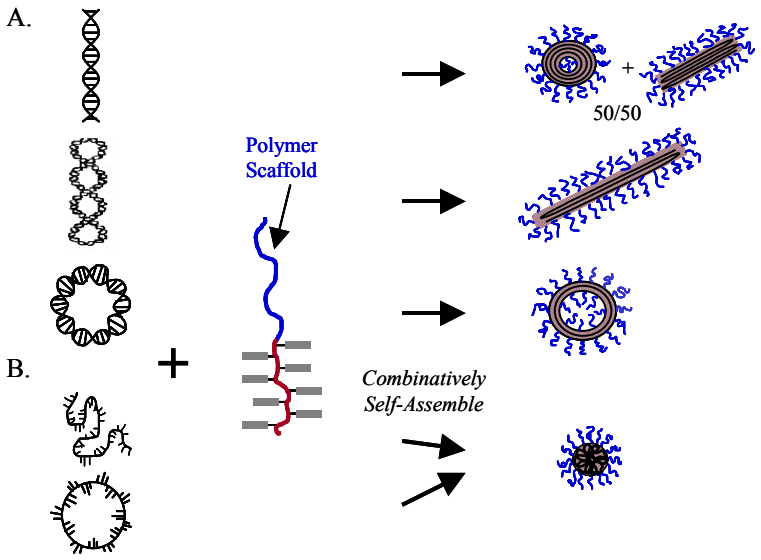

Figure 6.1 Condensation and packaging of various forms of ΦX174 DNA via the combinative self-assembly. (A) double-stranded linear, supercoiled and relaxed circular; (B) single-stranded linear and circular.

6.3 Results and Discussion

Model ΦX174 plasmid DNA (4K bp) in five different forms – double-stranded (ds) linear (*l*), negative-supercoiled (*sc*), and relaxed-circular (*rc*), as well as single-stranded (ss) linear and circular (*c*) – were used for this study. The distinct conformation of each DNA topology was directly visualized by AFM, Figure 6.2A. The semi-flexible linear ds-DNA (persistence length L_p ~ 50 nm, 150 bp) exhibited a typical worm-like

chain conformation with contour length of 1.5 μm, Figure 6.2A-Ia. In comparison, a tighter, writhed conformation was observed for the supercoiled ds-DNA, and an open circle conformation for the relaxed-circular ds-DNA, Figure 6.2A-Ib-c. Compared to ds-DNA, ss-DNA is much more flexible and contractile (L_p ~ 5 nm, 3 bp) and tend to coil into much tighter structures. Irregular triangular and globular structures of ~ 100 nm in size were observed for linear and circular ss-DNA respectively, Figure 6.1A-IIa, b.

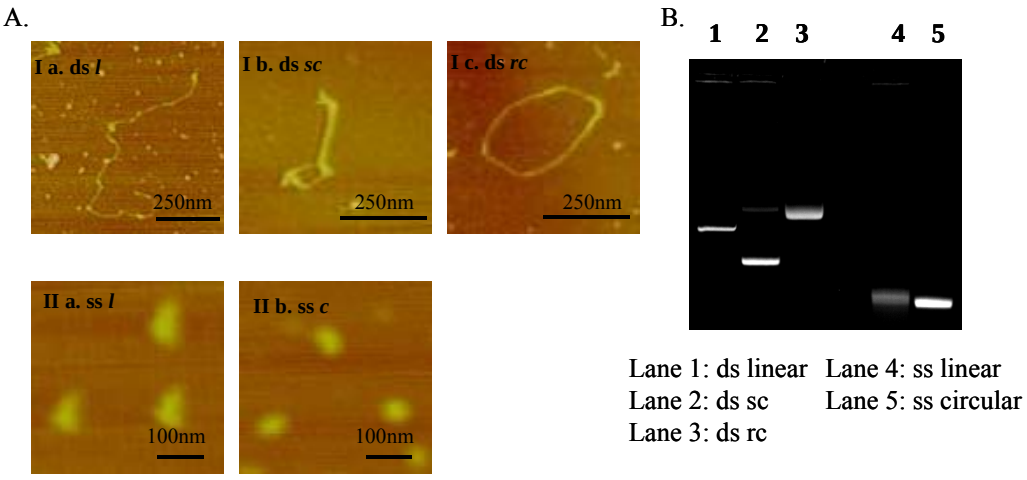

Figure 6.2 Characterization of various forms of ΦX174 DNA (A) AFM imaging and (B) Agarose Gel Electrophoresis

The conformational differences between the five forms of DNA were also reflected in the agarose gel electrophoresis experiments, Figure 6.2B, in which the mobility of DNA molecules is primarily determined by their radius of gyration.[12] For ds-DNA, the tightest supercoiled ds-DNA migrated the fastest (lane 2), whereas the open relaxed-circular ds-DNA with the biggest cross-section migrated the slowest (lane 3). For ss-DNA, both linear and circular (lane 4, 5) migrated much faster than ds-DNA due

to their much more compact conformations, and only trivial mobility differences were observed between the two forms of ss-DNA due to their similar small sizes.

Each form of ΦX174 DNA was then complexed with a representative polymer-peptide hybrid **PP40** to reveal the effect of DNA on the condensation process. **PP40** has eight gene-binding oligopeptides KWK_4 (K: lysine; W: tryptophan) grafted onto a polybutadiene-*block*-poly(ethylene oxide) scaffold, PBD_{14}-*b*-PEO_{93}, and can efficiently bind with DNA.[10, 11] Under the same complexation conditions at N/P = 3 (N: nitrogen; P: phosphorous), where binding of **PP40** with each DNA is complete, different condensation behavior was observed for different forms of DNA, Figure 6.3. Depending on the topology, ds-DNA preferably condenses into toroids or rods, whereas the highly flexible ss-DNA generates extremely small spherical nanoparticles.

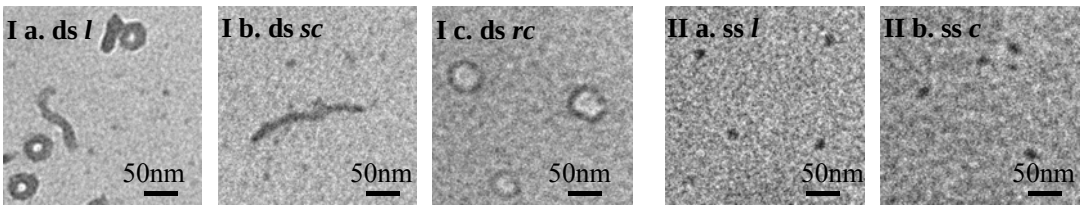

Figure 6.3 Representative TEM images of the five different forms of ΦX174 DNA condensates via the combinative self-assembly.

Statistical analysis on TEM images shows a near 50:50 mixture of toroids and rods for the linear ds-DNA condensates, Figure 6.3-Ia. The toroids have well-defined inner holes of 10 nm average diameter and 20 nm thickness, whereas the rods have similar width but 100 nm average length. It is known that semi-flexible ds-DNA strands pack in hexagonal arrays either in loops for toroids or in bundles for rods.[13] The equal population of toroids and rods for linear ds-DNA suggests that, when condensing with an

agent that can efficiently stabilize the sharp bends of ds-DNA in the rod formation (*e.g* **PP40**), packing of ds-DNA in rods and toroids is virtually isoenergetic and these two morphologies can coexist at equilibrium.[13] In comparison, negative-supercoiled ds-DNA predominantly condenses into rods that appear to be slightly thinner and longer than that of linear ds-DNA, Figure 6.3-Ib. This is likely because negative supercoiling unwinds the DNA double helix and facilitates sharp bending to occur, thus enhancing the ease of rod formation. Without negative-supercoiling, the relaxed-circular ds-DNA predominantly condenses into thin toroids with large holes instead, which have an average thickness of 8 nm and inner hole diameter of 35 nm, Figure 6.3-Ic. The notable differences between the relaxed-circular and linear ds-DNA toroids indicate that the topological strain associated with the enclosed circular ds-DNA has a significant impact on toroid formation. Toroids are known to form through two steps: spontaneous nucleation loop formation followed by toroidal growth, *i.e*. subsequent winding of DNA strands around the nucleation loop.[14] The nucleation loop size is sensitive to the flexibility of the DNA,[15] and we expect extra strain by circular ds-DNA can also alter the subsequent toroidal growth pathway. While linear ds-DNA can grow freely both outward and inward from the nucleationloop, with the inward growth diminishing the hole size,[14] the circular ds-DNA seems to prefer the less strained outward growth pathway, leading to thin toroids with large holes.

For highly flexible and contractile ss-DNA, packing into hexagonally ordered toroids or rods is clearly not energetically favored. Significant tightening from the initial 100 nm coiled structures to extremely small nanoparticle condensates of ~ 15 nm in size was observed for both linear and circular ss-DNA instead, Figure 6.3-IIa, b. Although at

equal N/P ratio, the number of polymer chains relative the ss-DNA would be half that of the ds-DNA, the tendency of ss-DNA to condense into small nanoparticles seems to be determined by its highly flexible and contractile nature, not by this polymer chain – DNA strand ratio difference. Even when more **PP40** was used and N/P ratio doubled, small nanoparticle condensates from ss-DNA were still observed.

6.4 Conclusion

In summary, we have elucidated the systematic functional role of DNA in directing the combinative self-assembly and condensation pathway and morphology. This discovery highlights the significance of the gene itself in the condensation process, and we expect that this will lead to new strategies for designing artificial gene vectors. Our results may also shed light on the diverse kinds of viral gene packaging found in nature. For example, the tendency of ss-DNA to condense into such small particles may well be correlated to the structure of ss-DNA viruses, such as adeno-associated virus, which is one of the smallest yet most infectious mammalian viruses. Moreover, exploring the role of DNA in combinative self-assembly should inspire new directions for fabricating multi-component supramolecular assemblies.

6.5 Experimental

Materials

The double stranded negative-supercoiled, relaxed-circular and single-stranded circular ΦX174 DNA, supplied in 1XTE buffer pH 8.0, were purchased from New England Biolabs. The 1XTE buffer was exchanged for 18.2 MΩ water using Qiagen QIAquick gel extraction kit. The quantity of the DNA was determined by

spectrophotometric analysis at 260 nm. DNA was diluted to a final concentration of 20 μg/mL in 18.2 MΩ water for further studies.

Obtaining the linear double-stranded DNA by linearization of the negative supercoiled ΦX174 plasmid DNA

Double-stranded supercoiled ΦX174 plasmid DNA was linearized with the restriction enzyme *SspI* and purified using Qiagen QIA quick gel extraction kit according to supplier's protocol. Briefly, 5 units of *SspI*/μg DNA in 1X NEBuffer were incubated at 37°C for 3 hours, followed by inactivation at 65°C for 30 minutes. Three volumes of Buffer ZC and one volume of isopropanol was added to the reaction mixture, placed in the spin column, centrifuged and washed with Buffer PE. Linearized DNA was eluted from the column with 18.2MΩ water. Full linearization of the DNA was determined by agarose gel electrophoresis (1.2% agarose, 100V, 60 minutes).

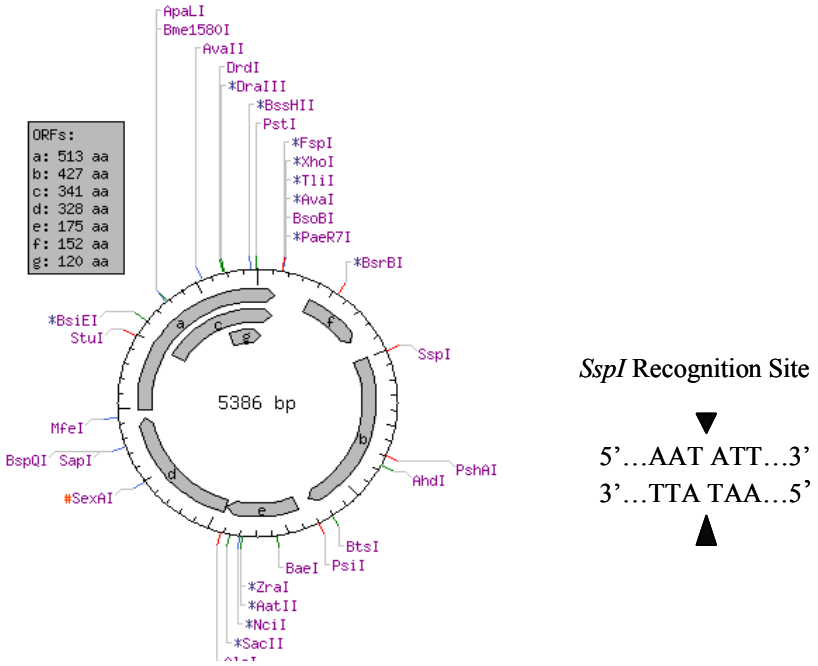

Figure 6.4 Linearization of ΦX174 plasmid DNA

Obtaining the linear single-stranded DNA by denaturation of the linear double-stranded DNA

Denaturation of the linear double-stranded DNA was performed by heating the DNA solution to 95°C for 4 minutes, followed by immediate incubation on ice. The degree of denaturation of the double-stranded linear ΦX174 RFI was assessed by agarose gel electrophoresis (1.2% agarose, 100V, 60 minutes). The quantity of double-stranded linear ΦX174 RFI and single-stranded linear ΦX174 RFI was determined by spectrophotometric analysis at 260 nm. The DNA was diluted to a final concentration of 20 μg/mL in 18.2 MΩ water for further studies.

Grafting of gene-binding oligopeptide onto PBD-b-PEO diblock copolymer

The amphiphilic diblock copolymer scaffold (PBD_{14}-*b*-PEO_{93}, subscripts denote the average number of repeating units) with a narrow molecular-weight distribution (M_n ~ 4900 g/mol) polydispersity index PDI = 1.05) was prepared by the well-establised sequential anionic polymerization of buta-1,3-diene and ethylene oxide. Thiol-containing Cystein (Cys) was attached to the gene-binding oligopeptide KWK_4 as the linker terminus for grafting purposes. Peptide $CKWK_4$ was synthesized using the standard Fmoc Solid Phase Peptide Synthesis procedure with HOBT, HBTU and DIPEA couplings, followed by N-capping with acetylation and C-capping with amidation. The synthesized peptides were analyzed by ESI-MS and ^1H NMR before grafting. $CKWK_4$ was then grafted to PBD_{14}-*b*-PEO_{93} to produce **PP40** according to the procedure published elsewhere, utilizing the free radical addition of the thiol group of cysteine to the double bonds of PBD. Characterization of **PP40** by NMR and SEC has been published elsewhere. Briefly, NMR analysis confirms that eight butadiene units of

PBD_{14}-*b*-PEO_{93} have been grafted with the $CKWK_4$ peptide in PP40 (M_n ~ 12,8000 g/mol), and SEC shows that PP40 has a similar narrow PDI as the PBD_{14}-*b*-PEO_{93} scaffold.

Agarose Gel Electrophoresis

Fifteen microliters of each DNA sample was loaded into a 1.2% agarose gel, and the electrophoresis was ran at 100V for 60 minutes in 40mM Tris-acetate, 1mM EDTA, pH 8 running buffer. Gels were stained with ethidium bromide (0.5 μg/mL, 60 minutes) and visualized with an UV transilluminator.

AFM Analysis

10 μg/mL of each DNA aqueous solution was mixed 1:1 with 20 mM Tris, 2 mM EDTA, 12.5 mM $MgCl_2$. AFM imaging was then performed using tapping mode at ambient temperature on a Dimension 3100 AFM (Veeco), equipped with Nanoscope III software (Digital Instruments, Santa Barbara, CA). Silicon probes (Veeco RTESP, spring constant 40 N/m, resonant frequency 100 Hz) were used to obtain all images.

TEM Analysis

Equal volumes of **PP40** (78 μM) and DNA (10 μg/mL) were mixed to obtain a final N/P ratio of 3 (N: nitrogen from positively charged lysine; P: phosphorous from the negatively charged DNA backbone). The DNA-**PP40** complexes were allowed to equilibrate at room temperature for 1 hour and then deposited onto glow discharged formvar coated copper grids. The complexes were then stained with 2% uranyl acetate for 1 minute, and the grids were blotted and air-dried. EM imaging was performed on a 200kV Tecnai 20 transmission electron microscope at a magnification of 10,000X.

Ethidium Bromide (EB) Displacement Assay

The degree of DNA condensation was determined as a function of the N/P ratio by an ethidium bromide displacement assay. In the EB displacement assay, binding of an agent to DNA would displace the intercalated EB and subsequently quench the fluorescence caused by the EB-DNA complex. Before measurement, DNA (20 μg/mL) was incubated with EB (0.8 μg/mL) for 1 hour. Concentrated **PP40** (78 μM) was then titrated into the DNA-EB solution. The fluorescence intensity of samples at different N/P ratios were excited at 520 nm, and the fluorescence was measured at 590 nm at 25°C, using a Jobin Yvon FluoroMax-3. Sample fluorescence was determined after subtracting the baseline fluorescence of EB in the absence of the DNA.

For each form of DNA, **PP40** continuously binds to DNA and quenches the fluorescence as N/P increases. Upon N/P = 3, **PP40** is able to achieve nearly complete quenching ($I/I_o \leq 3$), indicating complete binding between **PP40** and DNA

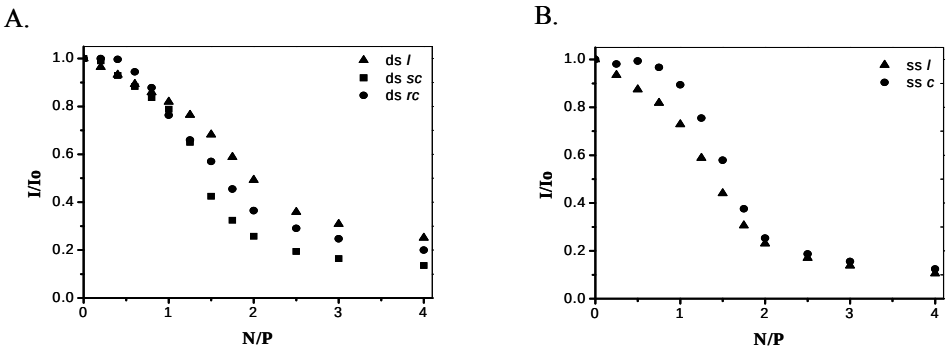

Figure 6.5 Binding of **PP40** with ΦX174 DNA's via EB displacement Assay. (A) ds ΦX174. (B) ss ΦX174. I_o = fluorescence intensity of DNA-EB complex without addition of PP40.

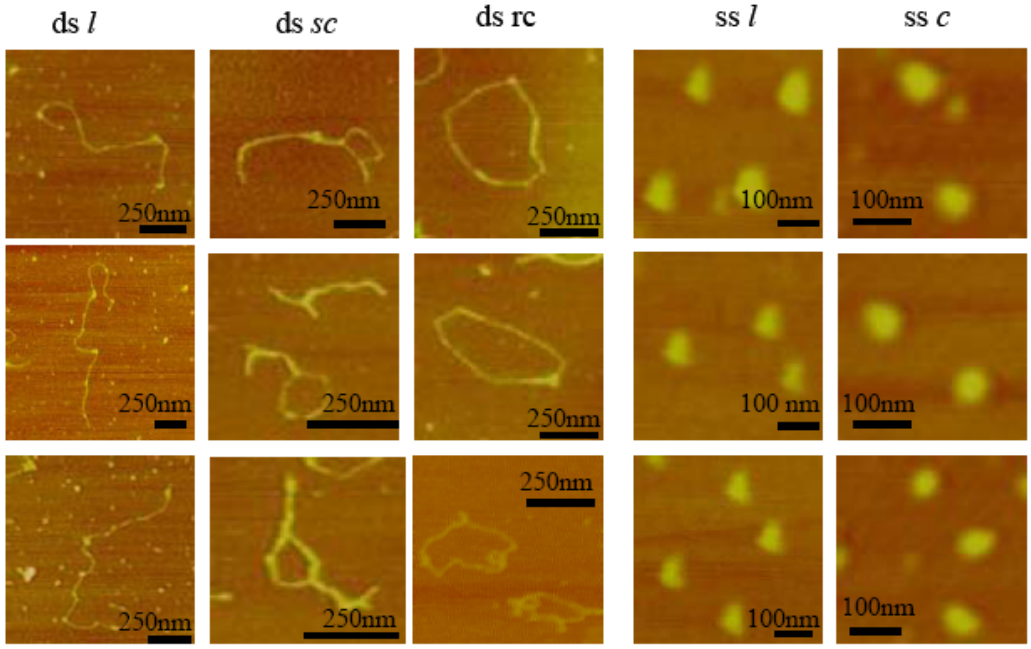

Figure 6.6 More representative AFM images of the five different forms of ΦX174 DNA

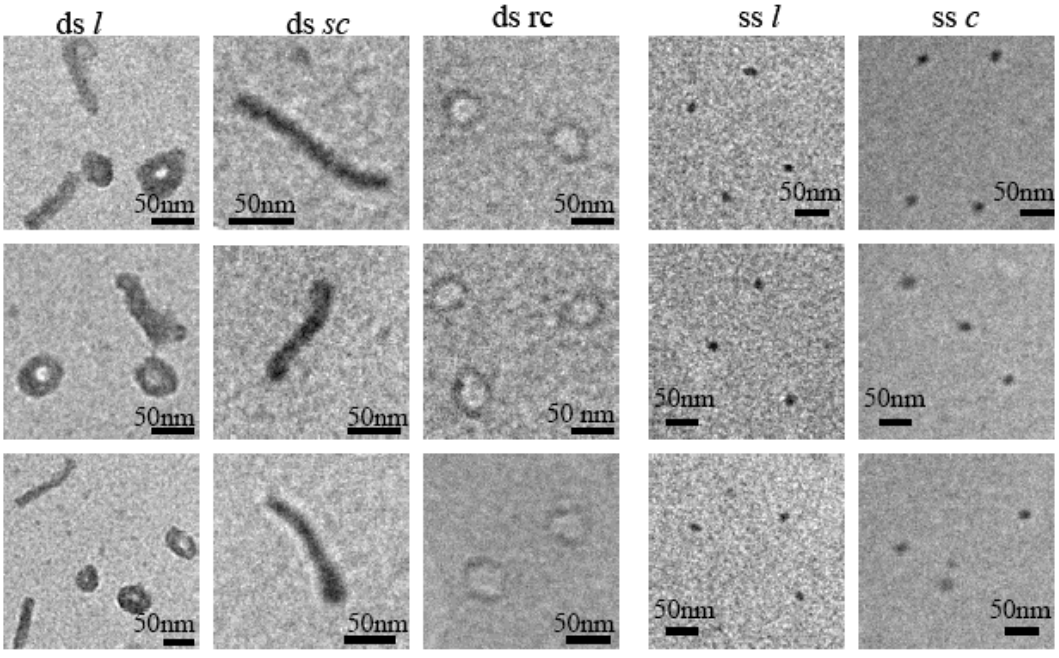

Figure 6.7 More representative TEM images of the five different forms of ΦX174 DNA condensates via the combinative self-assembly.

6.5 References

1. Gosule, L. C.; Schellman, J. A., Compact form of DNA induced by spermidine. *Nature* **1976,** 259, (5541), 333-335.

2. Luo, D.; Saltzman, W. M., Synthetic DNA delivery systems. *Nature biotechnology* **2000,** 18, (1), 33-37.

3. Molas, M.; Bartrons, R.; Perales, J. C., Single-stranded DNA condensed with poly-l-lysine results in nanometric particles that are significantly smaller, more stable in physiological ionic strength fluids and afford higher efficiency of gene delivery than their double-stranded counterparts. *BBA-General Subjects* **2002,** 1572, (1), 37-44.

4. Stanic, V.; Arntz, Y.; Richard, D.; Affolter, C.; Nguyen, I.; Crucifix, C.; Schultz, P.; Baehr, C.; Frisch, B.; Ogier, J., Filamentous condensation of DNA induced by pegylated poly-L-lysine and transfection efficiency. *Biomacromolecules* **2008,** 9, (7), 2048-2055.

5. Mintzer, M. A.; Simanek, E. E., Nonviral vectors for gene delivery. *Chemical reviews* **2008,** 109, (2), 259-302.

6. Breitenkamp, R. B.; Emrick, T., Pentalysine-grafted romp polymers for DNA complexation and delivery. *Biomacromolecules* **2008,** 9, (9), 2495-2500.

7. Srinivasachari, S.; Fichter, K. M.; Reineke, T. M., Polycationic -Cyclodextrin "Click Clusters": Monodisperse and Versatile Scaffolds for Nucleic Acid Delivery. *J. Am. Chem. Soc* **2008,** 130, (14), 4618-4627.

8. Bronich, T. K.; Nguyen, H. K.; Eisenberg, A.; Kabanov, A. V., Recognition of DNA Topology in Reactions between Plasmid DNA and Cationic Copolymers. *J. Am. Chem. Soc* **2000,** 122, (35), 8339-8343.

9. Arscott, P. G.; Li, A. Z.; Bloomfield, V. A., Condensation of DNA by trivalent cations. 1. Effects of DNA length and topology on the size and shape of condensed particles. *Biopolymers* **1990,** 30, (5-6), 619-30.

10. Haley, J.; Li, X.; Marshall, N.; Locklin, J.; Geng, Y., DNA packaging via combinative self-assembly. *Molecular BioSystems* **2008,** 4, (6), 515-517.

11. Haley, J.; Kabiru, P.; Geng, Y., Effect of clustered peptide binding on DNA condensation. *Molecular BioSystems* **2010,** 6, (1), 249-255.

12. Aaij, C.; Borst, P., The gel electrophoresis of DNA. *Biochimica et Biophysica Acta (BBA)-Nucleic Acids and Protein Synthesis* **1972,** 269, (2), 192-200.

13. Bloomfield, V. A., Condensation of DNA by multivalent cations: considerations on mechanism. *Biopolymers* **1991,** 31, (13), 1471-1481.

14. Conwell, C. C.; Vilfan, I. D.; Hud, N. V., Controlling the size of nanoscale toroidal DNA condensates with static curvature and ionic strength. *Proceedings of the National Academy of Sciences* **2003,** 100, (16), 9296-9301.

15. Jun, S.; Bechhoefer, J.; Ha, B. Y., Diffusion-limited loop formation of semiflexible polymers: Kramers theory and the intertwined time scales of chain relaxation and closing. *EPL (Europhysics Letters)* **2003,** 64, 420.

CHAPTER 7

CONCLUSION

Polymer-Peptide hybrids are a novel class of macromolecules that combine sophisticated functionality of biopolymers with synthetic versatility of synthetic polymers. In this work, polymer-peptide hybrids were synthesized utilizing a modular grafting procedure in which Cysteine-containing peptides are "clicked" on the hydrophobic segment of the amphiphilic polymer polybutadiene-*block*-poly(ethylene oxide) (PBD-*b*-PEO) via free radical addition of the thiol onto the double bonds. These polymer-peptide hybrids were then applied in two areas of research: tuning amphiphilic block copolymer self-assemblies with grafted charged peptides and combinative self-assembly with DNA.

A new twist to amphiphile design yielded angular supramolecular cone geometry, with a broken symmetry between the apex and the base. Such supramolecular cones demonstrated a surprising stickiness property at their base, which fostered their spontaneous higher-order self-assembly. The apex angle, length, as well as the stickiness of the cones can all be tuned by chemical manipulations and reveal the delicate balance of forces that govern the unusual sticky supramolecular cone formation.

Clustering of gene binding peptides onto the polymer scaffold can controllably alter the pathway and morphology of *in-vitro* DNA condensation and significantly improves the DNA stability against breakage and DNase bio-degradation. The studies here comprehensively elucidated the general architectural effect of the clustered peptide

binding on DNA condensation, as well as having provided a versatile new approach to tailor and optimize synthetic gene delivery vector design.

The systematic functional role of DNA in directing the combinative self-assembly and condensation pathway and morphology was also elucidated. This discovery highlights the significance of the gene itself in the condensation process, and opens the door to new strategies for designing artificial gene vectors. These results may also shed light on the diverse kinds of viral gene packaging found in nature. For example, the tendency of ss-DNA to condense into such small particles may well be correlated to the structure of ss-DNA viruses, such as adeno-associated virus, which is one of the smallest yet most infectious mammalian viruses. Moreover, exploring the role of DNA in combinative self-assembly should inspire new directions for fabricating multi-component supramolecular assemblies.

By varying the grafting density and peptide sequence, unique supramolecular assemblies can be observed in addition to precise control over the DNA condensation process.